Real-time motion of open quantum systems: Structure of entanglement, renormalization group, and trajectories

Evgeny A. Polyakov*
Russian Quantum Center, Skolkovo IC, Bolshoi Bulvar 30, Bld. 1, Moscow 121205, Russia

(Received 17 May 2021; revised 31 January 2022; accepted 1 February 2022; published 14 February 2022)

In this paper, we provide a complete description of the life cycle of entanglement during the real-time motion of open quantum systems. The quantum environment can have arbitrary (e.g., structured) spectral density. The entanglement can be seen constructively as a Lego: its bricks are the modes of the environment. These bricks are connected to each other via operator transforms. The central result is that during each infinitesimal time interval one new (*incoming*) mode of the environment gets coupled (*entangled*) to the open system, and one new (*outgoing*) mode gets irreversibly decoupled (*disentangled* from the future). Moreover, each moment of time, only a few *relevant* modes (three to four in the considered cases) are non-negligibly coupled to the *future* quantum motion. These relevant modes change (*flow* or *renormalize*) with time. As a result, the *temporal* entanglement has the structure of a matrix-product operator. This allows us to pose a number of questions and to answer them in this paper: What is the intrinsic quantum complexity of a real time motion? Does this complexity saturate with time or grow without bounds? How does one do the real-time renormalization group in a justified way? How do the classical Brownian stochastic trajectories emerge from the quantum evolution? How does one construct the few-mode representations of non-Markovian environments? We provide illustrative simulations of the spin-boson model for various spectral densities of the environment: semicircle, subohmic, ohmic, and superohmic.

DOI: 10.1103/PhysRevB.105.054306

I. INTRODUCTION

A major innovation brought by quantum mechanics is that a physical system can be in a superposition of its classical configurations. While the classical state is a point in phase space, the quantum state is a wave in the space of classical configurations [1]. All current experimental evidence suggests that the quantum theory works. Therefore, the superposition principle is expected to apply at all scales: from a single microscopic degree of freedom to one mole of any substance with $N_A \propto 10^{23}$ degrees of freedom. However, if we try to imagine the quantum state as a wave in the 10^{23}-dimensional space, then the quantum reality appears before us as an object of tremendous complexity. This complexity is reflected in the notion of a Hilbert space [2].

We believe it is obvious that the overwhelming part of this *potential* complexity is not realized in natural observable processes [3–5]. It is enough to review those tremendous difficulties that the experimenters face in their attempts to build a quantum computer [6,7]. This convinces us that there are rather effective mechanisms of how the quantum complexity decays during natural processes.

We can put it differently: It is expected that only a tiny fraction of the Hilbert space is relevant for the observable motion of quantum systems. Therefore, to reduce the complexity, we need some tools to identify this relevant subspace. We can call this the problem of efficient Hilbert space decimation. The motivation is twofold: conceptual and pragmatic. Conceptually, we want to understand the structure of quantum states and their evolution; we want to answer basic questions like the characterization of the boundary between the quantum and the classical reality. Pragmatically, we want to be able to calculate any property we are interested in.

The main idea of this paper is that the structure of entanglement can provide answers to all these questions. The whole point is to look at the entanglement constructively. We consider it like a Lego. The bricks of this Lego are the degrees of freedom (the modes) of the environment in some trivial (separable) state. The entanglement is built by connecting these bricks via some (non)unitary operators. If we know how the entanglement is built in real time from its bricks, we can keep track of them and rigorously consider such questions as, What is the quantum complexity of real-time motion? How does this complexity behave in time, whether it saturates or grows? How does one construct a few-mode approximation of the non-Markovian environment? What is even more important, if we know how the entanglement is built, then we know how to compute the properties of quantum state by *disassembling* the entanglement brick by brick. This is the renormalization group (RG) [8–13] in one of its most advanced forms.

As a specific example, we consider in this paper the model of a finite quantum system coupled to an infinite environment. This model plays an important role in quantum physics. Its practical significance is due to the large number of covered situations: behavior of mesoscopic degrees of freedom in physical chemistry and condensed matter [14] and models of quantum measurement and control [15–20]. At the same time,

*evgenii.poliakoff@gmail.com

the unique combination of simplicity and capability to exhibit many-body physics [21–24] makes it a paradigmatic model which is used to challenge and improve our perspective on quantum phenomena.

In this paper, we use the model of an open quantum system to study the life cycle of entanglement during the real-time evolution [25]. Suppose we couple the open system to the environment. Then it starts to emit quanta into the environment. Some of them will be reabsorbed, but a significant number of quanta will fly further and further into the environment, therefore entangling increasingly more modes of the environment. This leads to a combinatorial growth of the dimension of the joint wave function. Such a combinatorial growth of complexity is called the entanglement barrier [26] and it presents a significant obstacle both to interpretation and real-time computational methods.

In an attempt to make sense of the entanglement barrier, let us ask the question: What is the ultimate fate of the emitted quantum field? First, we expect that the emitted field becomes asymptotically decoupled from the *future* motion of an open system. For concreteness, let us assume that at some time moment t^* a certain mode ϕ_{out} of the environment becomes effectively and irreversibly decoupled. Then it is important how this mode is entangled to the rest of the environment. The mode ϕ_{out} can be entangled to those modes of the environment which were coupled to the open system before t^*. We say figuratively that ϕ_{out} is entangled to the past. However, ϕ_{out} cannot be significantly entangled to any mode ϕ_{in} which couples to the open system after t^*. This is because the entanglement can only be created via unitary evolution under coupling, which is effectively absent for ϕ_{out} after t^*. Therefore, we say figuratively that ϕ_{out} is not entangled to the future. Now suppose that we have succeeded in arranging the following two streams of modes: (i) the stream of incoming modes such that the mode $\phi_{\text{in}}(t)$ assigned to the time moment t couples to the open system only after t and (ii) the stream of outgoing modes such that the mode $\phi_{\text{out}}(t)$ assigned to the time moment t is irreversibly decoupled from the future motion after t. This system of modes leads to the entanglement structure depicted in Fig. 1.

From this picture, one sees that our entanglement Lego contains the two types of bricks: the incoming modes $\phi_{\text{in}}(t_p)$ and the outgoing modes $\phi_{\text{out}}(t_p)$. If we look at how the entanglement builds forward in time, we can observe that these two types of bricks play different roles. The incoming modes $\phi_{\text{in}}(t_p)$ are sequentially attached to the structure via the evolutions $\widehat{U}'_p$, thus increasing its complexity. At the same time, the outgoing modes $\phi_{\text{out}}(t_p)$ do not participate in the construction. Therefore, we can remove them by tracing them out as soon as they emerge. This is how we can disassemble the entanglement by continuously removing all such emerging idle bricks. The competition between the two processes, the attachment of $\phi_{\text{in}}(t_p)$, and the removal of $\phi_{\text{out}}(t_p)$, determines the final complexity of the structure. In Fig. 1, we have assumed that $\phi_{\text{in}}(t_p)$ and $\phi_{\text{out}}(t_p)$ occur with equal rates in time. Then, in each moment of time only a finite number of bricks (in Fig. 1, they are the vertical salmon-colored lines connecting the adjacent evolutions) are attached to the structure. The quantum complexity of real-time motion only survives in these bricks. The quantum complexity will saturate and become bounded

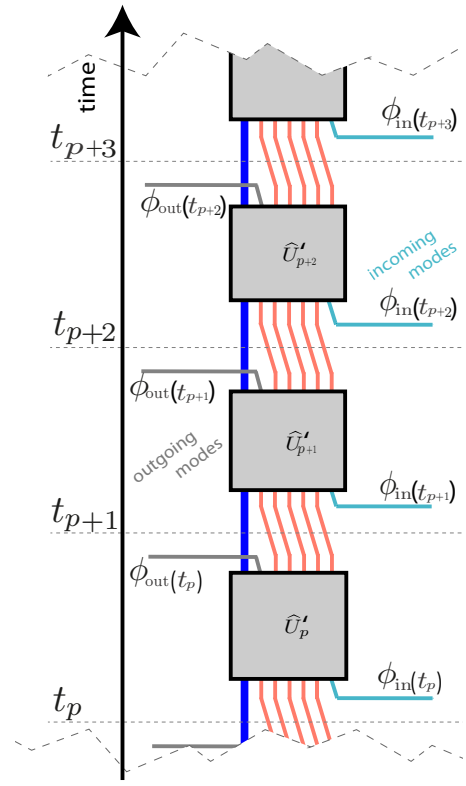

FIG. 1. The temporal structure of entanglement which follows from the existence of the streams of incoming and outgoing modes. The blue line depicts the quantum numbers of the open system. The evolution $\widehat{U}'_p$, which occurs during each infinitesimal time interval $[t_p, t_{p+1}]$ couples one additional incoming mode $\phi_{\text{in}}(t_p)$. The corresponding quantum numbers are denoted by the turquoise line. After that, one additional outgoing mode $\phi_{\text{out}}(t_{p+1})$ becomes irreversibly decoupled from the future evolution. Its quantum numbers are denoted by the gray line.

with time if the occupation of the coupled modes is bounded. In other words, the flux $j_{\text{in}}(t_p)$ of the quanta emitted by the open system should balance the flux $j_{\text{out}}(t_p)$ of the quanta leaking out to the outgoing modes.

The structure in Fig. 1 yields a few-mode representation of the bath. If we consider the reduced joint state of the open system and the coupled modes, then all the effects of the environment on the system will be taken into account. In this paper, we verify this idea by considering the model of an open quantum system in an environment with subohmic, ohmic, superohmic, and semicircle (waveguide) spectral density.

The structure in Fig. 1 indicates that time plays the role of a flow parameter of some RG: the movement in time is accompanied with the emergence of degrees of freedom which are unentangled to the future flow. In the language of RG, they are called the irrelevant degrees of freedom. Such degrees of freedom are iteratively traced out while computing the flow. Here we mean the modern variants of RG, like the entanglement renormalization (ER) [8–11]. In this paper, we propose a numerical implementation of the real-time RG which follows from Fig. 1. We verify the idea by a calculation for the environment with a semicircle spectral density.

The second thing we expect to eventually happen is that the emitted field becomes observed. For example, one can imagine that the environment is filled with observers at an extremely low density, so when the emitted field hits the observer, it has already effectively decoupled from the open system. These observers can perceive, e.g., the signal of displaced vacuum of the environment (i.e., they observe some global classical background of the environment). Such a signal is expected to be a superposition of the stochastic vacuum noise and some deterministic motion due to interaction with the open system [27]. Because of the entanglement structure in Fig. 1, such a measurement does not disturb the future quantum evolution: the trace over the outgoing modes can be represented as a stochastic average over the ensemble of their measurement signals. In Fig. 1, this corresponds to replacing each occurring gray line with some classical noise. Then we immediately conclude that there exist two kinds of entanglement: (i) the entanglement which is coupled to the future quantum motion—it appears to be a genuinely quantum phenomenon—and (ii) the *outgoing* entanglement which is irreversibly decoupled from the future quantum motion [and which is carried by the outgoing modes $\phi_{\text{out}}(t_p)$]. The latter kind of entanglement is equivalent to the stochastic ensemble of classical signals. This fact has both pragmatic and conceptual consequences. Pragmatically, we can efficiently simulate/analyze the outgoing entanglement via the Monte Carlo sampling of the signal realizations. The resulting procedure, the RG for quantum trajectories, is presented in this paper. Conceptually, we conjecture that the outgoing entanglement is the carrier of classical reality. We verify the idea by a calculation for the environment with a subohmic spectral density.

In the following sections, we develop this picture up to numerical schemes by proposing a *measure of average coupling to the future*.

This paper is structured as follows. We place our ideas into the current research context in Sec. II. The model of an open quantum system and its environment are introduced in Sec. III. Then, in Sec. IV, we study how the emitted field decouples from its source. We encourage the reader to pay special attention to Figs. 4 and 11, which describe the physical mechanism of how the stream of incoming modes and irreversibly decoupled (outgoing) modes emerge in real time. We verify our ideas by providing the calculations for the subohmic/ohmic/superohmic and semicircle environments. The reader interested in the justification of the real-time RG should pay attention to Sec. IV C and to the discussion of Figs. 8 and 9. The Schrodinger equation for the model of an open quantum system is reformulated in terms of the incoming and outgoing modes in Sec. V. As a result, in Fig. 17 we obtain the entanglement structure of Fig. 1. In Sec. VI, the outgoing modes are traced out in real time as soon as they occur: this is the RG for density matrix. We verify this idea by a calculation for the semicircle spectral density (waveguide environment). In Sec. VI F, Fig. 25, we present a calculation which supports our conjecture that there is a balance between the fluxes of incoming and outgoing quanta, i.e., the complexity of real-time motion is expected to saturate. In Sec. VII, we consider the Markovian limit of our RG procedure. In Sec. VIII, we implement another alternative for the RG procedure: to measure the irrelevant modes in real time as soon as they occur. We verify this by a calculation for the environment with a subohmic spectral density. Our approach is compared with a state-of-the-art tensor network method (TEMO [28]). In Sec. IX, we introduce the measure of temporal entanglement. We conclude in Sec. X. There are also four appendices where we provide some implementation details of our RG procedures.

II. RELATION TO OTHER APPROACHES

Ultimately, our approach is to find such a quantum circuit (Fig. 1) which shows how the entanglement is built along the flow (which is the real time in our case) from some set of uncoupled degrees of freedom. This promotes the viewpoint of entanglement as some kind of Lego. Its bricks are the uncoupled degrees of freedom. These bricks are stuck together by applying (non)unitary operations. The merit of this viewpoint is that the observable properties of the resulting complex many-body states can be computed by gradually disassembling this Lego brick by brick.

Actually, this viewpoint is close in spirit to the ideas of ER [8–11]. However, we extend ER in the following two aspects:

First, ER studies of how the entanglement is arranged over the increasing length scales. In other words, for ER the relevant degrees of freedom are those which contribute to the low-energy (infrared) properties. While this is appropriate for the description of low-temperature equilibrium properties, it becomes unjustified in the case of real-time evolution. During the real-time motion, the widely separated energy scales may become coupled, e.g., after a sudden quench of parameters. We avoid this problem since in our approach the relevant degrees of freedom are exactly those which have a nonnegligible coupling to the future evolution.

The second difference is how our circuit model is derived. Below we introduce the metric $I_2[\phi;\tau]$ which measures how much the given mode ϕ at a given time moment τ is coupled to the future motion. This way, we rigorously identify the modes ϕ_{out} which are irreversibly irrelevant (decoupled) because their metric $I_2[\phi_{\text{out}};\tau]$ is below a certain threshold. Therefore, we prove our entanglement model. This should be contrasted to the reasoning behind ER which is more heuristic, e.g., by matching the structure of a tensor network against the expected entanglement scaling laws [29]. The main justification of ER comes from the corpus of the numerical calculation results.

In literature, there are many other formal ways to describe the evolution of open systems. They can be divided into the following four groups. The first group isthe methods which do not rely on the structure of entanglement. They are the master equations [14,30] and their stochastic unravelings [31–34], path integrals with influence functionals [35–40], equivalent chain representations [41], pseudomodes [42,43], and Markovian embeddings [44].

The second group of methods consists of the straightforward extensions of the Wilson RG ideas (e.g., the logarithmic discretization of energy scales, the focus on the infrared limit) to the real time case: impurity numerical RG [24]. These methods make the (often unjustified) assumption that

the real-time structure of entanglement is similar to the equilibrium case.

The third group of methods relies on the tensor network models of quantum states and evolution [28,45–47], usually within the framework of the influence functional formalism. The language of tensor networks is suitable for the description of the structure of entanglement [48]. However, in these methods the main focus is to employ the linear algebra methods (e.g., singular value decomposition (SVD)) to compress the numerical representation of quantum states. They neither reveal nor exploit the life cycle of entanglement in real time.

The final group consists of methods which are derived from different principles but which, in our opinion, turn out to implicitly exploit some aspects of the structure described in Fig. 1. These are the non-Markovian quantum state diffusion [27,49,50] and stochastic Schrodinger equations [51–54]; various variants of the approach of hierarchical equations of motion [55–61].

III. MODEL OF OPEN QUANTUM SYSTEM

Here we describe the model for which we implement our ideas in this paper: the open quantum system. The latter is defined by a Hamiltonian $\widehat{H}_{\rm s}$. The system is coupled to bosonic environment via some operator $\widehat{s}$. The environment is harmonic with a Hamiltonian $\widehat{H}_{\rm b}$:

$$\widehat{H}_{\rm b} = \int_0^{+\infty} d\omega \widehat{a}^\dagger(\omega)\widehat{a}(\omega). \tag{1}$$

Here the environment's degrees of freedom are $[\widehat{a}(\omega), \widehat{a}^\dagger(\omega')] = \delta(\omega - \omega')$. The environment is coupled to the open system via some site operator

$$\widehat{b} = \int_0^{+\infty} d\omega c(\omega)\widehat{a}(\omega). \tag{2}$$

The coupling constant is related to the spectral density $J(\omega) = \pi|c(\omega)|^2$. The total Hamiltonian of the joint system is

$$\widehat{H}_{\rm sb} = \widehat{H}_{\rm s} + \widehat{s}^\dagger\widehat{b} + \widehat{s}\widehat{b}^\dagger + \widehat{H}_{\rm b}. \tag{3}$$

In the interaction picture with respect to the free environment, we have

$$\widehat{H}_{\rm sb}(t) = \widehat{H}_{\rm s} + \widehat{s}\widehat{b}^\dagger(t) + \widehat{s}^\dagger\widehat{b}(t), \tag{4}$$

where

$$\widehat{b}(t) = \int_0^{+\infty} d\omega c(\omega)\widehat{a}(\omega)e^{-i\omega t}. \tag{5}$$

For convenience, we assume that initially at $t = 0$ the environment is in its vacuum state $|0\rangle_{\rm b}$, so the initial joint state is

$$|\Phi(0)\rangle_{\rm sb} = |\phi_0\rangle_{\rm s} \otimes |0\rangle_{\rm b}, \tag{6}$$

where $|\phi_0\rangle_{\rm s}$ is the initial state of the system. The vacuum initial condition can be easily generalized to a finite temperature state of the environment [27,62]. Here the subscripts b, s, and sb designate belonging to the Hilbert space of the open system $\mathcal{H}_{\rm s}$, the Fock space $\mathcal{F}_{\rm b}$ of the environment, and the joint space $\mathcal{H}_{\rm s} \otimes \mathcal{F}_{\rm b}$ of the open system and environment, correspondingly.

IV. HOW THE QUANTUM FIELD GRADUALLY DECOUPLES FROM ITS SOURCE

In this section, we find the incoming and outgoing modes from Fig. 1. The entanglement is generated by coupling. Therefore, the analysis of the entanglement structure is essentially the analysis of the decoupling mechanism. We consider the superspositions of single-quantum states which are emitted by the open system and describe the mechanism behind their irreversible decoupling which was proposed in Refs. [27,63]. Later in the next section, we apply this mechanism to the full many-quanta case.

A. Physical mechanism of decoupling

During its evolution, the open system emits and absorbs quanta in the environment. There are several important asymmetries between the emission and absorption processes which we discuss and exploit here.

Parametrization of the emitted quantum field

The Fock space of the environment Eq. (1) is infinite. The important nontrivial fact is that the Fock space of the quantum field which can be emitted by open system is dramatically smaller. Indeed, since the open system sits at one local site $\widehat{b}^\dagger$ of the environment, clearly it cannot resolve the full Fock space of the environment. The spatiotemporal resolution of the emitted field is determined by the spectral properties of $\widehat{b}^\dagger(t)$.

Formally, from the Hamiltonian Eq. (4) it is seen that at a time moment t the quanta are emitted via $\widehat{b}^\dagger(t)$. Let us assume that the evolution happens during the time interval $[0, t]$, starting from the initial state $|\Phi(0)\rangle_{\rm sb}$, Eq. (6). One can imagine that this time interval consists of a sequence of N time moments $\tau_0, \tau_1 \ldots, \tau_p, \tau_{p+1}, \ldots, 0 \leqslant \tau_p \leqslant t$, $p = 0 \ldots N$, which are equally spaced at an infinitesimal interval dt. Then, at each time moment τ_p the new quanta are created via $\widehat{b}^\dagger(\tau_p)$. This means that the wave function $|\Phi(t)\rangle_{\rm sb}$ can only depend on $\widehat{b}^\dagger(\tau_0), \ldots \widehat{b}^\dagger(\tau_p), \ldots \widehat{b}^\dagger(\tau_N)$. We may write it in the following form:

$$|\Phi(t)\rangle_{\rm sb} = \sum_{n_0=0}^{\infty} \cdots \sum_{n_N=0}^{\infty} \frac{1}{\sqrt{n_0! \ldots n_N!}} \times |\phi(n_0 \ldots n_N)\rangle_{\rm s} \otimes \widehat{b}^{\dagger n_0}(\tau_0) \ldots \widehat{b}^{\dagger n_N}(\tau_N)|0\rangle_{\rm b}. \tag{7}$$

We can visualize the resulting evolution by imagining it as a tape recorder, Fig. 2: the time is like a tape which moves with a constant speed [64]. This tape is divided into discrete cells, one cell for each time moment τ_p. Then the open system is like a read/erase head. At time moment τ_p the head writes new quanta into the τ_pth cell of the tape. At the same time, the head can erase quanta from any past cell τ_q, $\tau_q \leqslant \tau_p$, with the amplitude

$$[\widehat{b}(\tau_p), \widehat{b}^\dagger(\tau_q)] = \frac{1}{\pi}\int_0^{+\infty} d\omega J(\omega) e^{-i\omega(\tau_p - \tau_q)} = M(\tau_p - \tau_q), \tag{8}$$

where $M(\tau_p - \tau_q)$ is the so-called memory function of the environment. This equation follows from Eq. (5) and from the commutation relation $[\widehat{a}(\omega), \widehat{a}^\dagger(\omega')] = \delta(\omega - \omega')$. The past

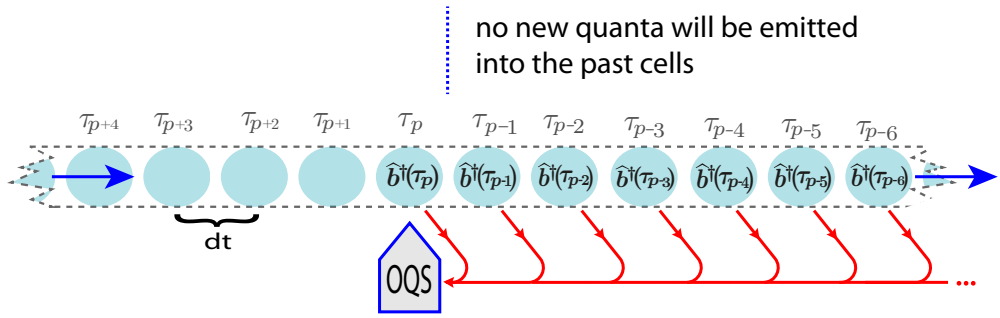

FIG. 2. We may think of time as a stream of infinitesimally close time moments $\tau_0, \tau_1, \ldots, \tau_p, \tau_{p+1}, \ldots$. The time moves with constant speed in one direction (the blue arrows) like a tape inside a tape recorder (or a *Turing machine*). Each time moment τ_p corresponds to a cell of the tape (the light turquoise circles). Then the open system acts like a write/erase head. At the time moment τ_p, the head is located in front of the corresponding cell. The head writes new quanta strictly to the cell τ_p [which is denoted by $\hat{b}^\dagger(\tau_p)$]—it is a local operation. At the same time, the erasing of quanta is a causal but long-range operation: the quanta can be erased from an arbitrarily distant past cell τ_r, with a slowly decaying amplitude $M(\tau_p - \tau_q)$ (red arrows). Erasing is the only way for the past cells to interact with the future motion. What is important is that in this representation the complexity of the emitted quantum field grows gradually. For example, after one infinitesimal time step, the Fock space of the emitted field is spanned by only one mode $\hat{b}^\dagger(\tau_0)$.

cells may be entangled with each other and with the head (open system), as follows from Eq. (7).

We see that in this picture both the creation and the absorption of quanta are causal processes: the future cells with $\tau_q > \tau_p$ are empty and uncoupled from the open system. They couple to the evolution one by one as the tape moves in front of the head. We call them the *stream of incoming modes*. They are the bricks of the Lego from which the entanglement is being built in real time.

The first important asymmetry is that the new quanta can be written in the present and future cells, with $\tau_q \geqslant \tau_p$, whereas no new quanta are created in the past cells with $\tau_q < \tau_p$. The past cells are coupled to the future motion only via the annihilation of quanta.

The second important asymmetry is that the creation of new quanta is a local operation, whereas the annihilation of quanta is a long-range operation, since the memory function $M(t)$ always has inverse-power law tails [27,63]. Indeed, since the physical spectral function $J(\omega)$ cannot have negative-frequency components, it should go to zero as a certain power of ω: $\omega^{p_0}\theta(\omega)$, where θ is a Heaviside function and $p_0 > 0$. This leads to a tail $\propto (\pm it)^{-p_0-1}$ in the large-t asymptotic behavior of $M(t)$. Moreover, every frequency ω_k, where $J(\omega_k + \delta\omega)$ has a discontinuous part $\delta\omega^{p_k}\theta(\pm\delta\omega)$, leads to an additional tail $\propto e^{-i\omega_k t}(\pm it)^{-p_k-1}$ in $M(t)$. These discontinuities can be, e.g., the band edges. Such tails were called the memory channels in Refs. [27,63].

For illustration, let us consider the widely used model of the environment with a spectral density:

$$J(\omega) = \frac{\alpha\omega_c}{2}\left[\frac{\omega}{\omega_c}\right]^s \exp\left(-\frac{\omega}{\omega_c}\right). \tag{9}$$

It covers many types of environments by varying the parameter s: the subohmic ($0 \leqslant s < 1$), ohmic ($s = 1$), and superohmic ($s > 1$). This spectral density corresponds to the memory function

$$M(t) = \frac{\alpha\omega_c^2}{2\pi}\frac{\Gamma(s+1)}{(1+it\omega_c)^{s+1}}, \tag{10}$$

which has a tail $\propto \tau^{-s-1}$ due to the discontinuity at the frequency $\omega = 0$. Another example is the waveguide environment (in the Schrodinger picture),

$$\hat{H}_b = \sum_{j=1}^{\infty}\{h\hat{a}_{j+1}^\dagger\hat{a}_j + h\hat{a}_j^\dagger\hat{a}_{j+1} + \varepsilon\hat{a}_j^\dagger\hat{a}_j\}, \tag{11}$$

with the open system being coupled to the first site $\hat{a}_1$. In the interaction picture with respect to $\hat{H}_b$, we get $\hat{b}(t) \equiv \hat{a}_1(t) = \exp(it\hat{H}_b)\hat{a}_1\exp(-it\hat{H}_b)$. Such an environment has a finite band of energies $[\varepsilon - 2h, \varepsilon + 2h]$, and the memory function is

$$M(t) = e^{-i\varepsilon t}\frac{J_1(2ht)}{ht} \propto t^{-\frac{3}{2}}e^{-i(\varepsilon-2h)t} + t^{-\frac{3}{2}}e^{-i(\varepsilon+2h)t}, \tag{12}$$

where now we have two tails, one tail per band edge at the frequencies $\omega_1 = \varepsilon - 2h$ and $\omega_2 = \varepsilon + 2h$.

This long-range character of $M(t)$ is a problem because it leads to a large number of past cells which are entangled and significantly coupled to the future motion. As a result, the complexity of real-time motion accumulates combinatorially fast and becomes prohibitive.

To solve this problem, let us consider the amplitude of the annihilation process. Suppose that by the time moment τ_p one quantum was emitted. Its state $|\phi\rangle_b$ is a superposition of the cell-write events:

$$|\phi\rangle_b = \{\phi_0\hat{b}^\dagger(\tau_0) + \ldots + \phi_{p-1}\hat{b}^\dagger(\tau_{p-1})\}|0\rangle_b. \tag{13}$$

Here, for the moment we neglect the degrees of freedom of the open system (in the next section, Sec. V, we derive the full equations of motion). Now suppose that in the future the open system points to some cell $\tau_{p'}$, with $\tau_{p'} > \tau_p$. Then it will erase this quantum state Eq. (13) with the amplitude

$$\mathcal{A}_{p'p}[\phi] = \sum_{r=0}^{p-1} M((p'-r)dt)\phi_r. \tag{14}$$

We see that the quanta in the past cells are coupled to the future via the convolution with $M(t)$. Now we recall that for the distant past the memory function $M(t)$ behaves as a superposition of its tails $M_k(t) = e^{-i\omega_k t}(\pm it)^{-p_k-1}$. Every such tail has

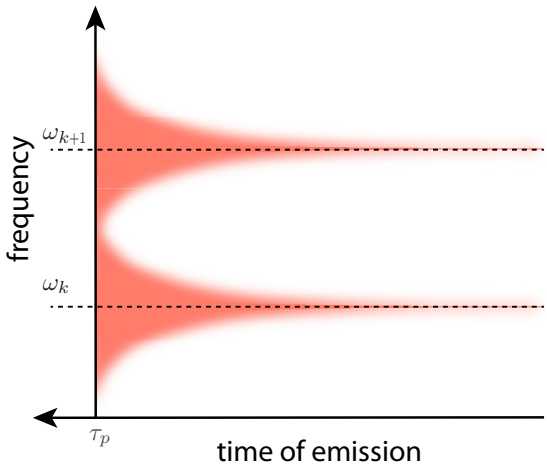

FIG. 3. The emitted quantum field is coupled to the future motion only via convolution with the memory function, Eq. (14). As a result, the spectral content of the emitted quanta is completely decoupled from the future motion, except a progressively small vicinity (salmon-colored area) of the singular frequencies $\omega_k, \omega_{k+1}, \ldots$ where the spectral function $J(\omega)$ has discontinuities. These singular frequencies may be, e.g., the boundaries of energy bands or other sharp features of the spectral density.

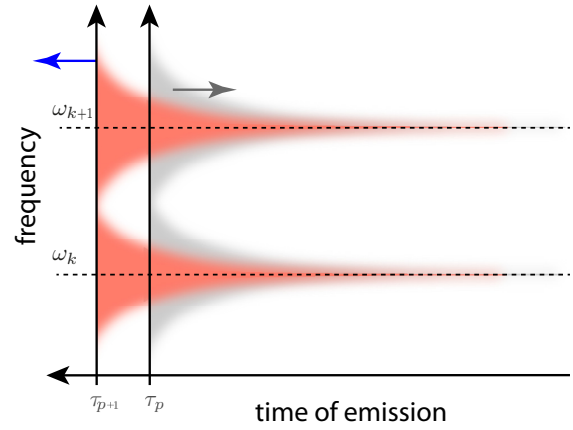

FIG. 4. When the real-time evolution is propagated forward one time step (blue arrow), from τ_p to τ_{p+1}, the emitted quantum field is shifted one step further into the past (gray arrow). Then the frequency scales $\Delta(t)^{-1}$ slightly shrink. As a result, each propagation step yields new spectral content (gray area) which is *irreversibly* decoupled from the future motion. The gray area should correspond to some continuously emerging *outgoing* modes of the environment.

the property that its local spectrum gradually becomes more and more narrowed to the frequency ω_k as the time argument t is increased. Equivalently, one may say that as t is increased, there is an increasingly large timescale $\Delta(t)$ over which the tail $M_k(t)$ can be considered as being effectively constant. Therefore, starting from t every spectral component of ϕ outside the frequency range $\approx[\omega_k - \Delta(t)^{-1}, \omega_k + \Delta(t)^{-1}]$ will be averaged to zero by convolving with $M(t)$ in Eq. (14). Physically, this means that in the remote past, the spectral content of the emitted quanta is completely decoupled from the future motion, except a progressively small vicinity of these singular frequencies ω_k, see Fig. 3.

The analysis above convinces us that as the time proceeds, new modes of the environment should continuously emerge which are effectively decoupled from the future motion, see Fig. 4. We call these the *stream of outgoing modes*. We will construct them formally in the following section.

Now suppose we succeeded in constructing the degrees of freedom which represent the different spectral areas in Fig. 4, namely, the cells from Fig. 2 are treated as independent quantum degrees of freedom. Then the frame is changed (via a unitary transform, Fig. 5) so instead of the past cells we have (i) the cells which are significantly coupled to the future (*the relevant modes*, from the salmon-colored area in Fig. 4) and (ii) the cells which are effectively and irreversibly decoupled from the future (the outgoing modes, from the gray area in Fig. 4), see Fig. 6. We expect that this way the coupling to the past will become short ranged, and the complexity of the real-time motion will become bounded. This is because the decoupled past modes can be traced out as we demonstrate below.

B. How to find the outgoing modes

In this section, we implement the intuition of Fig. 3: We find the modes which are significantly coupled to the future motion (lie inside the salmon-colored area) and those which are irreversibly decoupled (lie outside the salmon-colored area).

Let us again assume that by the time moment τ_p there is a single-quantum state of the tape Eq. (13). Recall that $\mathcal{A}_{p'p}[\phi]$ from Eq. (14) is the amplitude to annihilate this quantum at a later time moment $\tau_{p'}$. We introduce the shorthand bra-ket notation for Eq. (14),

$$\mathcal{A}_{p'p}[\phi] = (p'|M|\phi), \tag{15}$$

where matrix M is the discretized memory function $M_{lr} = M((l-r)dt)$, with $l, r \geqslant 0$. The set of amplitudes $\phi_0, \ldots, \phi_{p-1}$ is considered as a semi-infinite vector ϕ_r, $r \geqslant 0$, with $\phi_r = 0$ for $r \geqslant p$. This vector is denoted in the bra-ket notation as $|\phi)$. The notation $(p|\phi)$ means the amplitude on the cell τ_p: $(p|\phi) = \phi_p$.

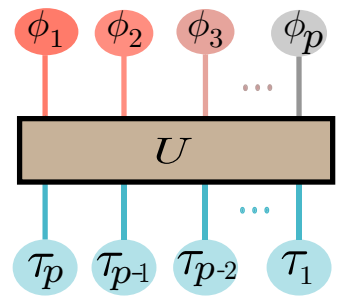

FIG. 5. If we find the degrees of freedom (the modes) which correspond to the coupled and decoupled spectral components of the emitted quantum field, then we can switch to the basis $\phi_1, \phi_2, \ldots$ of such modes by applying a suitable unitary transform U to the past cell degrees $\tau_1, \tau_2, \ldots, \tau_p$ of freedom of the time tape. The new cells ϕ_k are numbered in the decreasing order of their significance for the future evolution. Their color match the color of the spectral areas in Fig. 4.

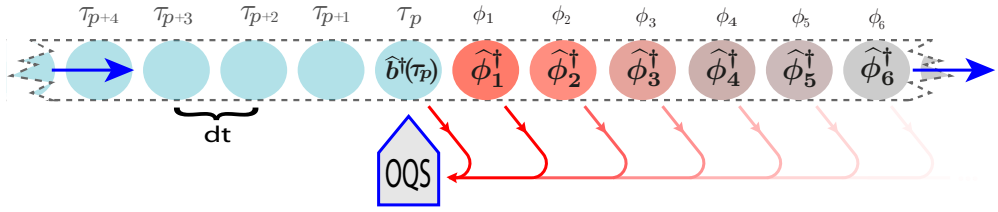

FIG. 6. In the basis of the modes ϕ_k whose significance for future motion rapidly decreases, the coupling to the past is expected to become short ranged.

To estimate the significance of ϕ for the future quantum motion, we can evaluate the average intensity of annihilation processes over all future time moments,

$$I_q[\phi;\tau_p] = \sum_{p'=p}^{\infty} (|(p'|M|\phi)|^q)^{\frac{1}{q}}/(\phi|\phi)^{\frac{1}{2}}, \tag{16}$$

with some parameter $q > 0$. The quantity $I_q[\phi;\tau_p]$ is the power mean of $\mathcal{A}_{p'p}[\phi]$ over the time interval $[\tau_p, \infty)$. Here the denominator in Eq. (16) removes the trivial dependence on normalization of ϕ. It is natural to expect that the mode ϕ_1 which makes the largest average contribution to the future annihilation processes is the most important for the future motion. Such a mode can be found by maximizing $I_q[\phi;\tau_p]$. The second-most important mode ϕ_2 can be found by maximizing $I_q[\phi;\tau_p]$ subject to the orthogonality constraint $(\phi_1|\phi_2) = 0$. Repeating iteratively this process by maximizing $I_q[\phi;\tau_p]$ subject to the constraint of orthogonality to all the previously found modes, we find the *fastest decoupling basis* of modes $\phi_1 \ldots \phi_p$.

Let us recall the intuitive picture of Fig. 3. The annihilation amplitude Eq. (15) has the convolutional form. The intensity $I_q[\phi;\tau_p]$ is the average magnitude of such convolutions which are shifted to future times. Therefore, we expect that the modes which maximize $I_q[\phi;\tau_p]$ correspond to the salmon-colored spectral area in Fig. 3. The modes which yield the least significant contribution to $I_q[\phi;\tau_p]$ lie outside the salmon-colored spectral area of Fig. 3.

In this paper, we consider the case of a root mean square intensity $I_2[\phi;\tau_p]$. In this case, the intensity assumes the form

$$I_2^2[\phi;\tau_p] = (\phi|K(p)|\phi), \tag{17}$$

where the matrix $K(p)$ is

$$K(p)_{r'r} = \sum_{p'=p}^{\infty} M^*\big((p'-r')dt\big)M[(p'-r)dt], \tag{18}$$

$0 \leqslant r, r' < p$. Then the fastest decoupling basis $\phi_1 \ldots \phi_p$ is given by the eigenvectors of $K(p)$,

$$K(p)|\phi_k) = \lambda_k|\phi_k), \tag{19}$$

where $k = 1, 2, \ldots$, and we sort the eigenvalues $\lambda_k(p)$ in the descending order.

1. Example calculations: Some tests of the ideas

As illustration, we present in Fig. 7 the plot of normalized eigenvalues $\lambda_k(p)/\lambda_1(p)$ for the cases of subohmic ($s = 0.5$), ohmic ($s = 1.0$) and superohmic ($s = 2.0$) environments, Eq. (10), for the time moment $t_p = pdt = 100$. One observes that the average coupling of these eigenvectors to the future evolution decays exponentially fast.

If the intuition of Fig. 3 is valid, then the oscillations of the eigenvectors ϕ_k should rapidly slow down so the spectral content of ϕ_k remains in the progressively small vicinity of the only singular frequency $\omega = 0$. In Fig. 8, we present the plots of ϕ_{10} for the cases of subohmic ($s = 0.5$), ohmic ($s = 1.0$), and superohmic ($s = 2.0$) environments. It is seen that the scale of their oscillations is almost constant on the logarithmic scale of times τ_r, which supports our intuition.

A more stringent test of our intuition is to compute the most important mode ϕ_1 for the waveguide memory function Eq. (12). If Fig. 3 is valid, and if the first eigenvalues of $K(p)$ indeed sample the salmon-colored spectral area, than the tails of ϕ_1 should behave as a superposition of $e^{+i(\varepsilon-2h)t}$ and $e^{+i(\varepsilon+2h)t}$. In Fig. 9, we present the plot of ϕ_1 for the waveguide with $\varepsilon = 1$ and $h = 0.05$.

Taking into account the exponentially fast decoupling of the modes ϕ_k, we can keep the first m modes $\phi_1, \ldots \phi_m$ as the relevant modes, and consider the remaining modes $\phi_{m+1}, \phi_{m+2}, \ldots$ as the outgoing modes. The latter are *irreversibly* decoupled, which is supported by the following

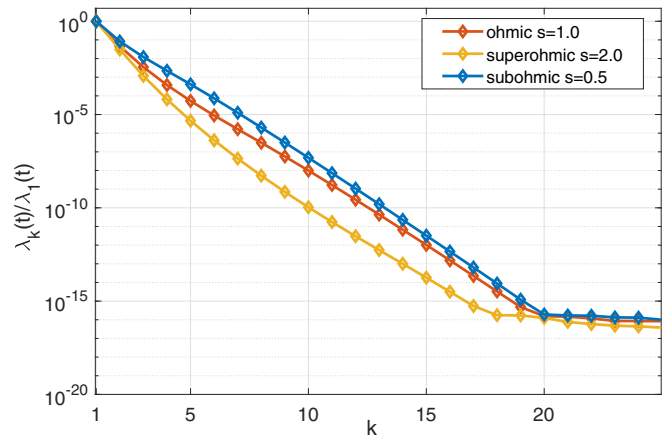

FIG. 7. The average contribution of the modes ϕ_k of the fastest decoupling basis to the future evolution decays exponentially fast. Here the cases of subohmic ($s = 0.5$), ohmic ($s = 1.0$), and superohmic ($s = 2.0$) environments are considered for the time moment $t_p = pdt = 100$ and $dt = 0.01$. The saturation on the level of 10^{-16} is due to roundoff errors.

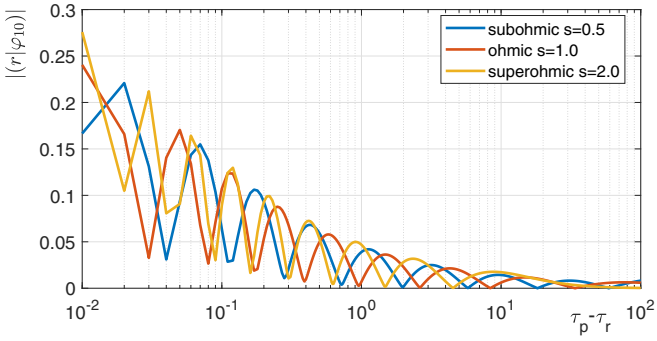

FIG. 8. Plot of the fastest decoupling basis function $|(r|\phi_{10})|$ vs $\tau_p - \tau_r$ for $t_p = pdt = 100$, for the cases of subohmic ($s = 0.5$), ohmic ($s = 1.0$), and superhomic ($s = 2.0$) environments. Observe that we plot with respect to the time of delay $\tau_p - \tau_r$ between the present τ_p and the past τ_r. The scales of their oscillations are approximately constant on the logarithmic scales of delay times.

property of the average intensity:

$$I_q[\phi;\tau_{p'}] \leqslant I_q[\phi;\tau_p] \quad \text{for} \quad \tau_{p'} \geqslant \tau_p, \tag{20}$$

which follows from its definition Eq. (16).

C. Implications for the renormalization group: The choice of relevant space

Looking at the fastest decoupling basis modes in Fig. 8, we notice the emergent logarithmic scale when the only singular frequency is $\omega = 0$. This logarithmic scale is a characteristic feature of the RG methods [65]. The interesting difference is that traditional (equilibrium-inspired) RG methods perform the logarithmic discretization of the energy band, whereas in our case it is the time behavior which scales logarithmically. However, the core principle is the same: (i) there is a flow and (ii) as we proceed along the flow, only the low-energy behavior remains to be relevant, see Fig. 10. In equilibrium-inspired RG methods, the flow is the decreasing characteristic energy cutoff. In our case, the flow is the aging (moving to the past in time) of the emitted field, and the relevant low-energy behaviour is the progressively small vicinity of the singular frequencies in spectral function $J(\omega)$, as in Fig. 3.

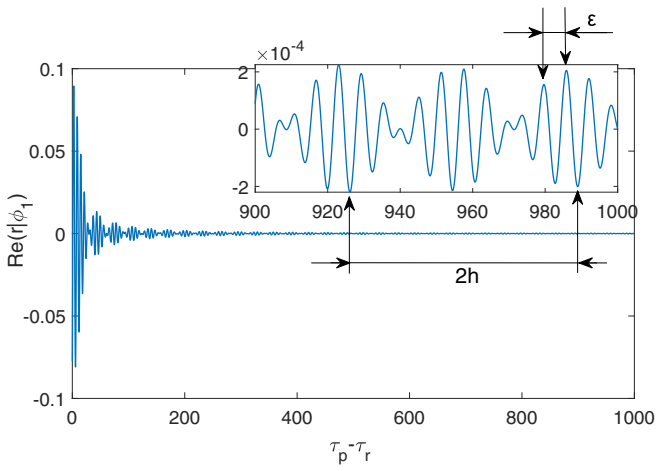

FIG. 9. Plot of the most important mode ϕ_1 for the waveguide memory function Eq. (12) with $\varepsilon = 1$ and $h = 0.05$. It is seen on the inset that the tail ϕ_1 behaves like a supersposition of oscillations with the frequencies $\varepsilon - 2h$ and $\varepsilon - 2h$. This supports the intuition of Fig. 3 that the coupled spectral content of the quanta emitted in the past shrinks to the singular frequencies of the spectral function.

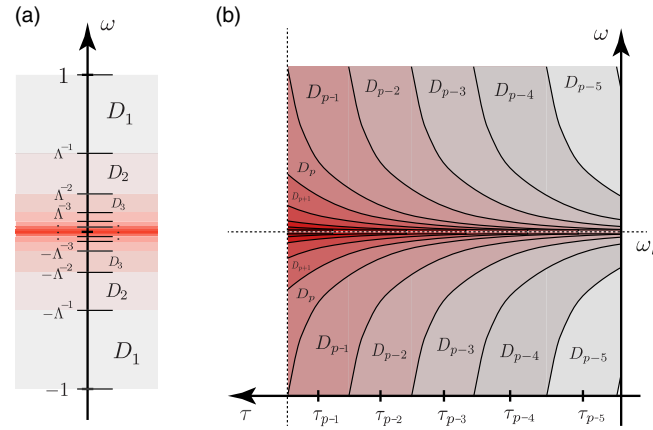

FIG. 10. Comparison between the traditional equilibrium-inspired and the real-time renormalization groups (RG). (a) In the traditional RG, we have initial energy interval $[-1, 1]$ (in some arbitrary units). Then one makes assumption that only the low energy behavior is relevant for the problem at hand. The logarithmic discretization of the energy interval is introduced with $\Lambda > 1$. We obtain an infinite sequence of energy shells $D_1 = [-1, -\Lambda^{-1}] \cup [\Lambda^{-1}, 1]$, $\ldots, D_k = [-\Lambda^{-k+1}, -\Lambda^{-k}] \cup [\Lambda^{-k}, \Lambda^{-k+1}], \ldots$. The RG flow is obtained by sequentially tracing out the degrees of freedom in shells $D_1, D_2, \ldots D_k, \ldots$. (b) In the real-time RG, the relevant degrees of freedom are contained in the progressively small vicinity of each singular frequency ω_k where the spectral density $J(\omega)$ has sharp features (e.g., band edges). Thus we obtain the sequence of *phase-space* shells $D_{p-1}, D_p, D_{p+1}, \ldots$. The shell D_k contains the spectral content which decouples from future evolution after the time moment τ_k, see Fig. 4. Each shell D_k carries a degree of freedom $\phi_{\text{out}}(k)$, which are constructed in Sec. IV D. These $\phi_{\text{out}}(k)$ are traced out in Sec. VI and collapsed to classical noise in Sec. VIII.

D. The emergence of outgoing modes in real time

In this section, we implement the intuition of Figs. 4 and 10: We construct the stream of outgoing modes. That is, for each infinitesimal motion $\tau_p \to \tau_{p+1}$, we identify the new mode $\phi_{\text{out}}(p)$ of the environment that has just become irreversibly decoupled (which belongs to the gray area in Fig. 4 and to the shell D_p in Fig. 10).

We construct the stream of outgoing modes by induction. Suppose we have chosen to keep no more than m relevant modes. This is how we demarcate the boundary of the salmon-colored area in Fig. 3. This means that for τ_p with $p \leqslant m - 1$, all the modes are relevant since the matrix $K(p)$ has no more than m eigenvalues. This is the basis for our inductive construction.

Now suppose that at a time moment τ_p, $p \geqslant m - 1$, we know the relevant modes $\phi_1(p), \ldots, \phi_m(p)$, and (zero or more) outgoing modes $\phi_{\text{out}}(p-1), \phi_{\text{out}}(p-2), \ldots, \phi_{\text{out}}(m)$, see Fig. 11(a). At time moment τ_p, the open system (the

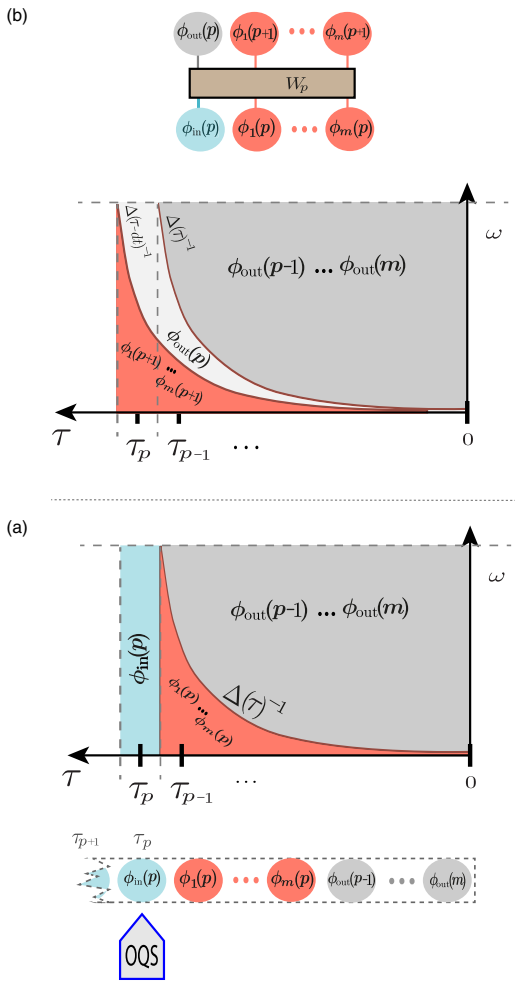

FIG. 11. (a) At a time moment τ_p, the open system gets coupled to the new incoming mode $\phi_{\rm in}(p)$. Since this mode is localized (in τ), it has a broadband spectrum (the vertical light turquoise spectral area). The past cells are represented by the relevant modes $\phi_1(p), \ldots, \phi_m(p)$, which carry the coupled part of the emitted quantum field [salmon-colored spectral area, under the decreasing scale $\Delta(\tau)^{-1}$]. There are also outgoing modes $\phi_{\rm out}(p-1), \phi_{\rm out}(p-2), \ldots, \phi_{\rm out}(m)$, which represent the irreversibly decoupled part of the emitted quantum field (the gray spectral area). (b) After the propagation to the next time moment $\tau_p \to \tau_{p+1}$, the incoming mode $\phi_{\rm in}(p)$ becomes one of the past cells. Then the scale $\Delta(\tau)^{-1}$ shifts to the left, $\Delta(\tau)^{-1} \to \Delta(\tau - dt)^{-1}$, as described in Fig. 4. This leads to the emergence of a new decoupled spectral content (light gray area). This spectral content is represented by a new outgoing mode $\phi_{\rm out}(p)$. The latter is found via a unitary transform W_p, Eq. (21), to the frame of the new relevant modes $\phi_1(p+1), \ldots, \phi_m(p+1)$.

write/erase head in our tape model) points to cell τ_p. This cell represents one incoming mode $\phi_{\rm in}(p)$ which is localized on this cell: $(r|\phi_{\rm in}(p)) = \delta_{rp}$, with δ being the Kronecker delta.

The inductive step in our construction is to consider what happens after the propagation to the next time moment $\tau_p \to \tau_{p+1}$. The incoming mode $\phi_{\rm in}(p)$ becomes one of the past cells (the write/erase head moves one position to the left). As a result, by time moment τ_{p+1} we have the following $m+1$ modes: $\phi_1(p), \ldots, \phi_m(p)$ and $\phi_{\rm in}(p)$. Our task is to transform these modes into the new m relevant modes $\phi_1(p+1), \ldots, \phi_m(p+1)$ and one new outgoing mode $\phi_{\rm out}(p)$,

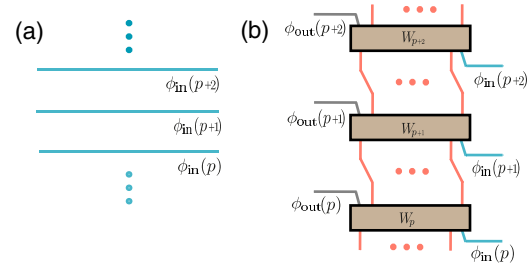

FIG. 12. (a). The tape model of real-time evolution assigns an incoming mode $\phi_{\rm in}(p)$ to each time moment τ_p. (b). The iterative construction of the m most relevant modes changes the structure of modes: Now we have the two streams of incoming $\phi_{\rm in}(p)$ (turquoise lines) and outgoing modes $\phi_{\rm out}(p)$ (gray lines) and also the relevant modes $\phi_1(p) \ldots \phi_m(p)$ (salmon-colored lines), which represent the corresponding spectral areas of Figs. 4 and 11.

$$\begin{bmatrix} \phi_1(p+1) \\ \vdots \\ \phi_m(p+1) \\ \phi_{\rm out}(p) \end{bmatrix} = W_p \begin{bmatrix} \phi_1(p) \\ \vdots \\ \phi_m(p) \\ \phi_{\rm in}(p) \end{bmatrix}, \tag{21}$$

via some unitary transform W_p. Here W_p acts as ordinary matrix on the column entries, e.g., $\phi_k(p+1) = \sum_l (W_p)_{kl}\phi_l(p) + (W_p)_{k,m+1}\phi_{\rm in}(p)$. To determine W_p, we choose the fastest decoupling basis. As the fastest decoupling basis, we take the eigenvectors of $K(p+1)$ in the space spanned by $\phi_1(p), \ldots, \phi_m(p)$ and $\phi_{\rm in}(p)$. The matrix elements of $K(p+1)$ in this subspace are

$$\widetilde{K}(p+1) = \begin{bmatrix} K_{\rm rr} & K_{\rm ri} \\ K_{\rm ri}^\dagger & K_{\rm ii} \end{bmatrix}, \tag{22}$$

where the blocks of the matrix are the scalar $K_{\rm ii} = (\phi_{\rm in}(p)|K(p+1)|\phi_{\rm in}(p)) = K(p+1)_{pp} = \sum_{p'=1}^{\infty} |M(p'dt)|^2$, the vector $(K_{\rm ri})_q = (\phi_{\rm in}(p)|K(p+1)|\phi_q(p))$, and the matrix $(K_{\rm rr})_{qq'} = (\phi_q(p)|K(p+1)|\phi_{q'}(p))$. This matrix has dimension $(m+1)\times(m+1)$. Therefore, if we diagonalize it and sort the $m+1$ eigenvectors in the descending order of their eigenvalues,

$$\widetilde{K}(p+1) = U \begin{bmatrix} \lambda_1 & & 0 \\ & \ddots & \\ 0 & & \lambda_{m+1} \end{bmatrix} U^\dagger, \tag{23}$$

we obtain $W_p = U^T$ for Eq. (21).

Iterating this inductive step, we construct the entire stream of outgoing modes $\phi_{\rm out}(p)$; see Fig. 12.

V. EQUATIONS OF MOTION IN TERMS OF INCOMING, OUTGOING, AND RELEVANT MODES

In this section, we give a precise meaning to Fig. 1. In the previous section, the treatment was on the level of superposition of single-quantum states of the environment. Here we derive the complete quantum equations of motions, which fully take into account the many-body correlations between the open quantum system and the environment.

We remind you that our goal is to find a minimum number of degrees of freedom which contain everything what is significant for the motion at future time moments. We want to stay in the small relevant subspace (spanned by these degrees of freedom) all the time. However, during each infinitesimal time interval the quantum amplitudes leak outside this space (due to the environment dispersion). In other words, at least one new degree of freedom gets entangled. To keep the minimal number of relevant modes, we need to find some degree of freedom (outgoing mode) which can be traced out. This latter degree of freedom should be independent and decoupled from everything. Otherwise, the real-time motion will become corrupted on large times. We conclude that we need to attach an independent degree of freedom to each infinitesimal time moment. Otherwise, there will be nothing to trace out and the number of coupled modes will grow with time. Therefore, in this section we develop a formalism which treats the infinitesimal time cells as independent degrees of freedom. The model of open quantum system Eq. (52) is mapped to the representation of independent time cells (tape model) in an exact and rigorous way. Then we derive how the outgoing modes can be traced out in a virtually exact way.

Observe the merit of the proposed picture of time cells. In the Schrodinger (spatial) picture, the spread of entanglement and decoupling happens simultaneously in the far degrees of freedom. Therefore, it is difficult to distinguish between these processes. However, we want to know how to separate them because we hope to find a balance between these processes. In contrast, in the model of time cells, Figs. 6 and 12, these two processes are clearly distinguished and the balance conjecture is easily formulated and checked.

A. Fock space for the tape cells

Each cell τ_p of the time tape (the light turquoise circles in Figs. 2, 5, and 6) is considered as independent bosonic degree of freedom with its own creation operator $\widehat{\psi}_p^\dagger$, $[\widehat{\psi}_q, \widehat{\psi}_p^\dagger] = \delta_{qp}$. The operator $\widehat{\psi}_p^\dagger$ creates a quantum in the mode $\phi_{\rm in}(p)$. Recalling Fig. 2, this implies that we map the creation operator $\widehat{b}^\dagger(\tau_p)$ to $\widehat{\psi}_p^\dagger$:

$$\widehat{b}^\dagger(\tau_p) \to \widehat{\psi}_p^\dagger. \tag{24}$$

As a result, the tape has its own vacuum $|0\rangle_{\rm t}$ and the tape Fock space $\mathcal{F}_{\rm t}$ is spanned by applying $\widehat{\psi}_p^\dagger$'s to $|0\rangle_{\rm t}$. This Fock space is formally different from that $\mathcal{F}_{\rm b}$ defined by the original model in Eq. (4). However, the quantum mechanics permits many different formal representations of a physical system, provided that the observable properties are invariant. For the latter, it is enough to conserve the commutation relation Eq. (8), which is ensured by the mapping

$$\widehat{b}(\tau_l) \to \sum_{r=0}^{l} M_{lr}\widehat{\psi}_r, \tag{25}$$

were we again employ the matrix M with elements $M_{lr} = M((l-r)dt)$. Now the tape model and the original model Eq. (4) are in one-to-one correspondence. For example, the states are mapped between these models as

$$\begin{aligned}&\widehat{\psi}_0^{\dagger n_0}\dots\widehat{\psi}_{p-1}^{\dagger n_{p-1}}|\phi(n_0,\dots n_{p-1})\rangle_{\rm s}\otimes|0\rangle_{\rm t}\\ \longleftrightarrow\ &\widehat{b}^{\dagger n_0}(\tau_0)\dots\widehat{b}^{\dagger n_{p-1}}(\tau_{p-1})|\phi(n_0,\dots n_{p-1})\rangle_{\rm s}\otimes|0\rangle_{\rm b}.\end{aligned} \tag{26}$$

Here $|\phi(n_0,\dots n_{p-1})\rangle_{\rm s}$ is a wave function of the open system which is not affected by the mapping. The vacuum initial condition for the tape model becomes $|\Phi(0)\rangle_{\rm st} = |\phi_0\rangle_{\rm s}\otimes|0\rangle_{\rm t}$.

B. The Hamiltonian for the tape model

The Hamiltonian for the tape model is obtained by applying the mapping rules Eqs. (24) and (25) to the original Hamiltonian Eq. (4):

$$\widehat{H}_{\rm sb}(\tau_p) \to \widehat{H}_{\rm st}(\tau_p) = \widehat{H}_{\rm s} + \widehat{s}\widehat{\psi}_p^\dagger + \widehat{s}^\dagger\sum_{r=0}^{p} M_{pr}\widehat{\psi}_r. \tag{27}$$

Observe that in the tape model, the real-time evolution happens in discrete time steps via jumps from one cell τ_p to the neighboring one τ_{p+1}. Of course, we want this discrete evolution to approximate the continuous one from the original model Eq. (4). It is desirable that the global propagation error is stable and vanishing as $dt \to 0$. The latter can be achieved by employing the implicit midpoint rule as a propagator,

$$\begin{aligned}|\Phi(t_{p+1})\rangle_{\rm st} = |\Phi(t_p)\rangle_{\rm st} - idt\widehat{H}_{\rm st}(\tau_p)\tfrac{1}{2}\{|\Phi(t_{p+1})\rangle_{\rm st}\\ + |\Phi(t_p)\rangle_{\rm st}\} + O(dt^3),\end{aligned} \tag{28}$$

where now we specify that the tape cells are located at the midpoint times: $\tau_p = (p+\frac{1}{2})dt$. This equation is solved for $|\Phi(t_{p+1})\rangle_{\rm st}$ by iterations with the initial guess $|\Phi(t_{p+1})\rangle_{\rm st} = |\Phi(t_p)\rangle_{\rm st}$. Here the Hamiltonian $\widehat{H}_{\rm sb}(\tau_p)$ corresponds to the head (open system) being coupled to the cell τ_p. Then the midpoint rule forces us to think that the Hamiltonian $\widehat{H}_{\rm sb}(\tau_p)$ generates the evolution from the wave function $|\Phi(t_p)\rangle_{\rm st}$ at the time moment $t_p = pdt$ to the wave function $|\Phi(t_{p+1})\rangle_{\rm st}$ at the next time moment $t_{p+1} = (p+1)dt$. This ensures the global error of $O(dt^2)$. The time moment t_p corresponds to the notation of Fig. 1.

The wave function $|\Phi(t_p)\rangle_{\rm st}$ depends on the modes $\widehat{\psi}_0^\dagger,\dots,\widehat{\psi}_{p-1}^\dagger$. During each propagation step of Eq. (28), it entangles one additional mode $\widehat{\psi}_p^\dagger$ [which corresponds to $\phi_{\rm in}(p)$], see Fig. 13. This is the usual growth of complexity which we overcome in this paper.

C. Partial trace

To completely define the tape model, we need to discuss how to compute the trace over the cell degrees of freedom. Suppose we compute the reduced density matrix for the open system via the partial trace over the environment,

$$\widehat{\rho}_{\rm s}(t_p) = {\rm Tr}_{\rm b}\{|\Phi(t_p)\rangle_{\rm sb\ sb}\langle\Phi(t_p)|\}, \tag{29}$$

where $|\Phi(t_p)\rangle_{\rm sb}$ is the wave function of the original model Eq. (4). The effect of ${\rm Tr}_{\rm b}$ is that each $\widehat{a}^\dagger(\omega)$ from the ket $|\Phi(t_p)\rangle_{\rm sb}$ becomes paired with $\widehat{a}(\omega)$'s from the bra ${}_{\rm sb}\langle\Phi(t_p)|$ at the same frequency. This follows from the commutation

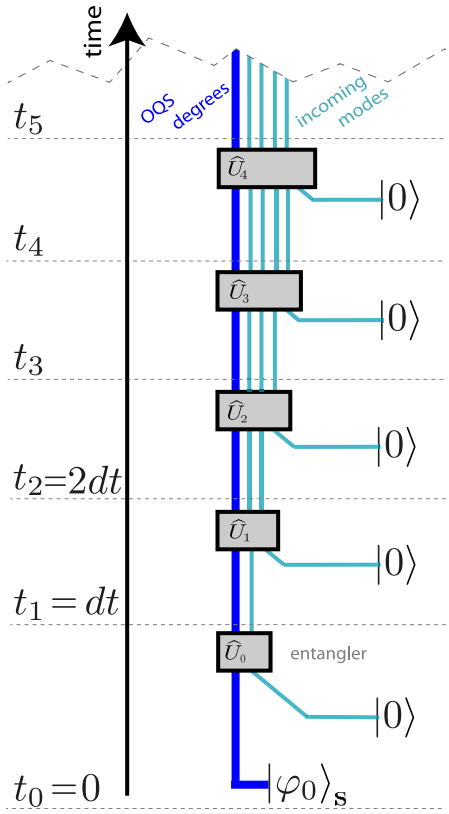

FIG. 13. In the tape model of the open system, the evolution happens between the discrete time moments $t_0 = 0, t_1 = dt, \ldots t_p = pdt, \ldots$. After propagation from t_p to t_{p+1}, one new incoming mode $\phi_{\rm in}(p)$ (turquoise line) corresponding to cell τ_p becomes entangled to the open system (blue line). The evolutions $\widehat{U}_p$ happen under the midpoint rule Eq. (28).

relations $[\widehat{a}(\omega), \widehat{a}^\dagger(\omega')] = \delta(\omega - \omega')$. We can rewrite the partial trace Eq. (29) in such a form that all the pairings become explicit:

$$\widehat{\rho}_{\rm s}(t_p) = {}_{\rm b}\langle 0| \Big\{ e^{\int_0^{+\infty} d\omega \widehat{a}^\dagger(\omega)\widehat{a}(\omega)} \times : |\Phi(t_p)\rangle_{\rm sb\,sb}\langle\Phi(t_p)| :\Big\}_A |0\rangle_{\rm b}. \tag{30}$$

Here the notation $\{: \ :\}_A$ means that the creation/annihilation operators coming from the Taylor expansion of the *pairing function* $\exp\int_0^{+\infty} d\omega \widehat{a}^\dagger(\omega)\widehat{a}(\omega)$ are antinormally ordered around the term $|\Phi(t_p)\rangle_{\rm sb\,sb}\langle\Phi(t_p)|$. The ordering of the latter term is not affected (which is indicated by placing it between : :). Observe that when we order the Taylor expansion of the pairing function, we regard its constituent creation/annihilation operators as commuting. The expressions Eqs. (29) and (30) are equal because they describe the same set of pairings between the $\widehat{a}^\dagger(\omega)$'s from the ket $|\Phi(t_p)\rangle_{\rm sb}$, and the $\widehat{a}(\omega)$'s from the bra ${}_{\rm sb}\langle\Phi(t_p)|$. The operation ${}_{\rm b}\langle 0| \cdot |0\rangle_{\rm b}$ denotes the projection of density matrix to the subspace of zero quanta in the environment. This operation does not affect the open system.

When defining the trace for the wave function $|\Phi(t_p)\rangle_{\rm st}$ of the tape model, we should take into account that each pairing between $\widehat{\psi}_r$ and $\widehat{\psi}_s^\dagger$ is possible due to the commutator

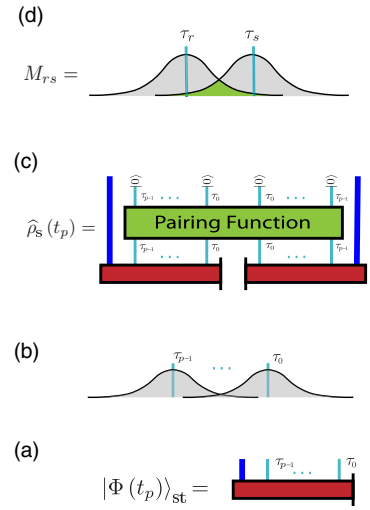

FIG. 14. (a) It is very desirable to consider the wave function as depending on quantum numbers of each infinitesimal time moment (turquoise lines). This approach is natural for analyzing how the entanglement gradually develops in real time. Especially, it is interesting to track how it is happening *continuously*: what gets entangled and disentangled each infinitesimal time moment. We succeed in deriving equations of motion which treat the infinitesimal time cells as independent degrees of freedom: see Eqs. (27) and (28). (b) Nevertheless, there are no time-local states in quantum mechanics. Due to the commutation relation Eq. (8), each time cell τ_k contributes to the observables at another time moment t like a wave packet $M^{1/2}_{\tau_k t}$ with long-range tails. Here $M^{1/2}_{\tau_k t} = (2\pi)^{-\frac{1}{2}} \int_0^{+\infty} d\omega e^{-i\omega(\tau_k - t)} \sqrt{J(\omega)}$. (c) We reconcile the dynamical locality and the observable nonlocality by introducing the pairing function. This effectively smears the time cells in time during the partial trace operation. The resulting density matrix $\widehat{\rho}_{\rm s}(t_p)$ depends only on quantum numbers of the open system (blue lines). (d) The elementary pairing M_{rs} corresponds to the overlap (green area) between the wave packets of the two quanta at τ_r and τ_s: $M_{rs} = \int_{-\infty}^{+\infty} M^{1/2}_{\tau_r t} M^{1/2*}_{\tau_s t} dt$.

$[\widehat{b}(\tau_r), \widehat{b}^\dagger(\tau_s)] = M_{rs}$:

$$\widehat{\rho}_{\rm s}(t_p) = {}_{\rm t}\langle 0| \Big\{ e^{\sum_{rs=0}^{p-1} \widehat{\psi}_r^\dagger M_{rs} \widehat{\psi}_s} : |\Phi(t_p)\rangle_{\rm st\,st}\langle\Phi(t_p)| :\Big\}_A |0\rangle_{\rm t}. \tag{31}$$

This is how the partial trace is performed in the tape model. The conceptual meaning of the pairing function is that the time-cell degrees of freedom yield a nonlocal contribution to the observables in quantum mechanics, see Fig. 14.

D. Propagation of wave function in terms of incoming, outgoing, and relevant modes

The initial condition for the propagation is $|\Phi(0)\rangle_{\rm st} = |\phi_0\rangle_{\rm s} \otimes |0\rangle_{\rm t}$. There are two regimes of propagation: $t_p < t_m$ and $t_p \geqslant t_m$.

As discussed in Sec. IV D, while $t_p < t_m$, all modes $\widehat{\psi}_0^\dagger \ldots \widehat{\psi}_{p-1}^\dagger$ are relevant: $\phi_{\rm in}(1) \equiv \phi_1(p-1), \ldots, \phi_{\rm in}(p-1) \equiv \phi_{p-1}(p-1)$. Therefore, the propagation from $|\Phi(t_p)\rangle_{\rm st}$ to $|\Phi(t_{p+1})\rangle_{\rm st}$ is done via the application of the midpoint rule Eq. (28). As a result, before time moment t_m the entanglement develops according to Fig. 13.

The situation changes for $t_p \geqslant t_m$. The wave function $|\Phi(t_p)\rangle_{\rm st}$ depends on the relevant modes $\phi_1(p-1) \ldots \phi_m(p-$

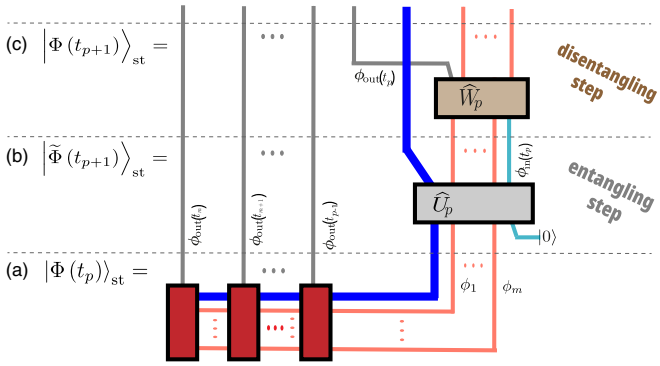

FIG. 15. The circuit model of how the wave function is propagated during one time step in three stages: (a) At a time moment t_p, the wave function $|\Phi(t_p)\rangle_{\rm st}$ depends on the occupations of outgoing modes $\phi_{\rm out}(k) \equiv \phi_{\rm out}(t_k)$, $k = m \dots p-1$ (gray lines) and of relevant modes $\phi_k \equiv \phi_k(p)$, $k = 1 \dots m$ (salmon lines). Also it depends on the quantum numbers of the open system (blue line). Observe the matrix-product-like structure of the wave function. This follows from the facts that (i) only m modes are significantly coupled to the future and (ii) each time step one outgoing mode is produced. (b) The discrete-time Hamiltonian Eq. (32) is applied via the midpoint rule Eq. (28), which approximates the evolution $\widehat{U}_p$. As a result, one incoming mode (turquoise line) gets entangled to the state. (c) The frame is changed actively via $\widehat{W}_p$ to produce one decoupled mode (gray line). Observe that $\widehat{U}_p$ and $\widehat{W}_p$ constitute the newly formed additional block of the matrix product structure of $|\Phi(t_{p+1})\rangle_{\rm st}$, see Fig. 16.

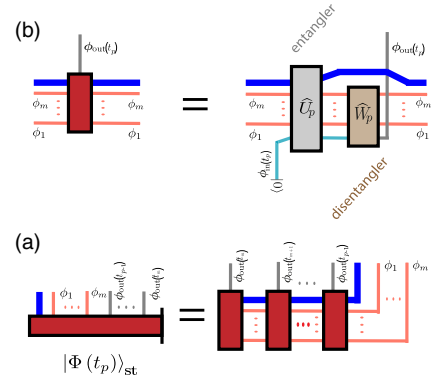

FIG. 16. (a) In the frame of relevant/outgoing modes, the real-time wave function $|\Phi(t_p)\rangle_{\rm st}$ has the structure of a matrix-product-state. (b) Each block (tensor) is a product of the entangling and disentangling transforms

1) via their creation operators $\widehat{\phi}_1^\dagger(p-1) \dots \widehat{\phi}_m^\dagger(p-1)$. Also, $|\Phi(t_p)\rangle_{\rm st}$ depends on zero or more outgoing modes $\phi_{\rm out}(p-1) \dots \phi_{\rm out}(m)$ via their creation operators $\widehat{\phi}_{\rm out}^\dagger(p-1) \dots \widehat{\phi}_{\rm out}^\dagger(m)$, see Fig. 15(a). Here each line represents the occupation number of the corresponding mode. The salmon-colored lines $\phi_k \equiv \phi_k(p-1)$, $k = 1 \dots m$, correspond to the relevant modes which are populated via the creation operators $\widehat{\phi}_k^\dagger(p-1)$. The blue line denotes the quantum numbers of the open system. The gray lines are the outgoing modes.

The propagation begins with the *entangling step*: when the discrete-time Hamiltonian $\widehat{H}_{\rm st}(\tau_p)$ Eq. (27) is applied, Fig. 15(b). We express the Hamiltonian in terms of the incoming mode $\widehat{\psi}_p^\dagger$, the relevant modes $\widehat{\phi}_k^\dagger(p)$, and the irrelevant modes $\widehat{\phi}_{\rm out}^\dagger(p)$,

$$\widehat{H}_{\rm st}(\tau_p) = \widehat{H}_{\rm s} + \widehat{s}\widehat{\psi}_p^\dagger + \widehat{s}^\dagger M(0)\widehat{\psi}_p + \widehat{s}^\dagger \sum_{i=1}^{\min(p,m)} M_i(p)\widehat{\phi}_i(p) + \widehat{s}^\dagger \sum_{i=m+1}^{p-1} M_{{\rm out}i}(p)\widehat{\phi}_{\rm out}(i), \tag{32}$$

where the coupling to the relevant modes is

$$M_i(p) = \sum_{r=0}^{p-1} M_{pr}\phi_i(p)_r, \tag{33}$$

and the coupling to the irrelevant modes is $M_{{\rm out}i}(p) = \sum_{r=0}^{p-1} M_{pr}\phi_{\rm out}(t_i)_r$. Up to now, the treatment was *exact* (in the limit $dt \to 0$). Here we make an approximation for the first time: The coupling between the incoming mode and the irrelevant modes [the last line of Eq. (32)] is discarded, so we have

$$\widehat{H}_{\rm st}(\tau_p) = \widehat{H}_{\rm s} + \widehat{s}\widehat{\psi}_p^\dagger + M(0)\widehat{\psi}_p + \widehat{s}^\dagger \sum_{i=1}^{\min(p,m)} M_i(p)\widehat{\phi}_i(p). \tag{34}$$

Below we will use this form of the Hamiltonian.

After the propagation $\widehat{U}_p$ via the rule Eq. (28), the resulting wave function $|\widetilde{\Phi}(t_{p+1})\rangle_{\rm st}$ still depends on the old relevant modes $\widehat{\phi}_k^\dagger(p)$. The wave function $|\widetilde{\Phi}(t_{p+1})\rangle_{\rm st}$ also entangles one additional incoming mode $\widehat{\psi}_p^\dagger$ [the turquoise line going up from Fig. 15(b)]: hence the name entangling step.

The propagation is finished by the *disentangling step*: we change to the basis of new relevant modes $\widehat{\phi}_k^\dagger(p+1)$, Fig. 15(c),

$$|\Phi(t_{p+1})\rangle_{\rm st} = \widehat{W}_p|\widetilde{\Phi}(t_{p+1})\rangle_{\rm st}, \tag{35}$$

where the *disentangler* $\widehat{W}_p$ is given by

$$\widehat{W}_p = \exp(i[\widehat{\phi}_1^\dagger \dots \widehat{\phi}_m^\dagger \widehat{\psi}_p^\dagger]h(p)[\widehat{\phi}_1 \dots \widehat{\phi}_m \widehat{\psi}_p]^T), \tag{36}$$

and the Hermitian $(m+1) \times (m+1)$ matrix $h(p) = i \ln W_p$, with the unitary matrix W_p defined in Eq. (21). Observe that in Eq. (35) we apply the active form of the frame-change transformation Eq. (36). As a result, the relevant modes lose their time dependence, $\widehat{\phi}_k^\dagger(p) \equiv \widehat{\phi}_k^\dagger$, $k = 1 \dots m$. The resulting wave function $|\Phi(t_{p+1})\rangle_{\rm st}$ has the same structure as $|\Phi(t_p)\rangle_{\rm st}$, namely, it has the same matrix-product-state structure as in Fig. 15(a). Each block in this structure is formed by a pair of entangler-disentangler transforms, Fig. 16.

Observe that as the result of $\widehat{W}_p$, one additional outgoing mode $\phi_{\rm out}(p)$ is produced in the wave function $|\Phi(t_{p+1})\rangle_{\rm st}$. The coupling of $\phi_{\rm out}(p)$ to the future is negligible by construction, so $\phi_{\rm out}(p)$ will not become entangled to the future incoming modes: hence the name disentangling step.

The iterative application of these propagation steps leads to the circuit model presented in Fig. 17.

E. Decoupling of the pairing function

Let us recall that when computing the observables, we need to apply the pairing function Eq. (31). It introduces an additional nonlocal coupling between the future and the

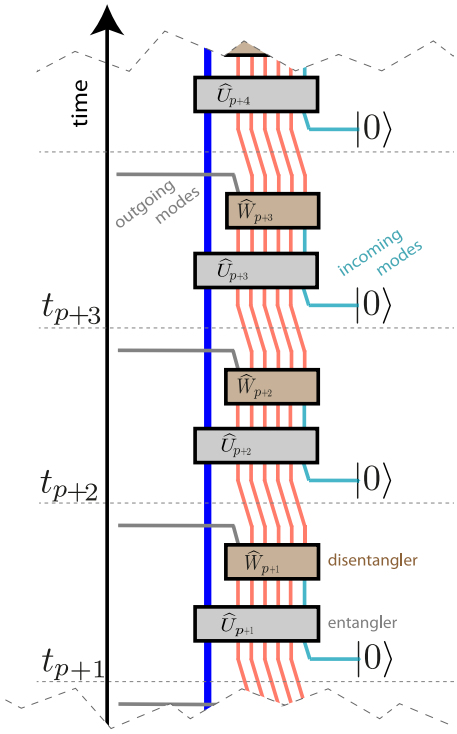

FIG. 17. The circuit model of real-time evolution of open quantum system. At each time step t_p, one new incoming mode $\phi_{\rm in}(p) \equiv \phi_{\rm in}(t_p)$ gets entangled to the open system via the Hamiltonian evolution $\widehat{U}_p$. Afterward, one new irreversibly decoupled mode $\phi_{\rm out}(p) \equiv \phi_{\rm out}(t_p)$ gets *disentangled* via the active change of frame $\widehat{W}_p$. Observe that the product $\widehat{W}_p\widehat{U}_p$ is equal to $\widehat{U}'_p$ from Fig. 1.

past cell modes. One might wonder if this would spoil the entanglement structure described in Figs. 15–17. The answer is no. The coupling in the pairing function has the same form of the convolutional annihilation process that was thoroughly analyzed in Sec. IV. Therefore, in the frame of the incoming/outgoing/relevant modes, we can neglect the pairings between the outgoing and the future incoming modes, Fig. 18, analogously to transition from Eq. (32) to Eq. (34). Below we ensure this by explicit calculation.

1. Change of frame in the pairing function

The pairing function in Eq. (31) is written in terms of the original incoming modes $\psi_k^\dagger$. Let us change to the frame of incoming/outgoing/relevant modes in the pairing function. Suppose that these frames are related as

$$\begin{bmatrix} \phi_1(p) \\ \vdots \\ \phi_m(p) \\ \phi_{\rm out}(m) \\ \vdots \\ \phi_{\rm out}(p-1) \end{bmatrix} = U \begin{bmatrix} \phi_{\rm in}(0) \\ \vdots \\ \phi_{\rm in}(p-1) \end{bmatrix}, \tag{37}$$

where the unitary matrix U is the cumulative effect of the disentanglers: $U = W_p W_{p-1} \dots W_m$. The creation operators are related in the same way,

$$\widehat{\boldsymbol{\phi}}^\dagger \equiv \begin{bmatrix} \widehat{\phi}_1^\dagger \\ \vdots \\ \widehat{\phi}_m^\dagger \\ \widehat{\phi}_{\rm out}^\dagger(m) \\ \vdots \\ \widehat{\phi}_{\rm out}^\dagger(p-1) \end{bmatrix} = U \begin{bmatrix} \widehat{\psi}_0^\dagger \\ \vdots \\ \widehat{\psi}_{p-1}^\dagger \end{bmatrix}, \tag{38}$$

where $\widehat{\boldsymbol{\phi}}^\dagger$ is shorthand for the column vector of creation operators. Its components $\widehat{\boldsymbol{\phi}}_1^\dagger \dots \widehat{\boldsymbol{\phi}}_m^\dagger$ refer to $\widehat{\phi}_1^\dagger \dots \widehat{\phi}_m^\dagger$ correspondingly, and $\widehat{\boldsymbol{\phi}}_{m+1}^\dagger \dots \widehat{\boldsymbol{\phi}}_{m+p}^\dagger$ refer to $\widehat{\phi}_{\rm out}^\dagger(m) \dots \widehat{\phi}_{\rm out}^\dagger(p-1)$ correspondingly. The inverse transforms are given by $U^\dagger$. We have for the pairing function,

$$\begin{aligned} \sum_{rs=0}^{p-1} \widehat{\psi}_r^\dagger M_{rs} \widehat{\psi}_s &= \sum_{rs=0}^{p-1} U_{ru}^\dagger \widehat{\boldsymbol{\phi}}_u^\dagger M_{rs} U_{sv}^T \widehat{\boldsymbol{\phi}}_v \\ &= \sum_{uv}^{p-1} \widehat{\boldsymbol{\phi}}_u^\dagger \widetilde{M}_{uv}(p) \widehat{\boldsymbol{\phi}}_v, \end{aligned} \tag{39}$$

where the matrix $\widetilde{M}$ has the block structure which reflects the pairings between the relevant and outgoing modes:

$$\widetilde{M}(p) = \begin{bmatrix} M_{\rm rr} & M_{\rm ro} \\ M_{\rm ro}^\dagger & M_{\rm oo} \end{bmatrix}. \tag{40}$$

Here $M_{\rm rr}$ generate the pairings between the relevant modes: $(M_{\rm rr})_{rs} = (\phi_r(p)|M|\phi_s(p))$, $(M_{\rm oo})_{rs} = (\phi_{\rm out}(r)|M|\phi_{\rm out}(s))$ generates the pairings between the outgoing modes, and $(M_{\rm ro})_{rs} = (\phi_r(p)|M|\phi_{\rm out}(s))$ defining the pairings between the relevant-outgoing modes.

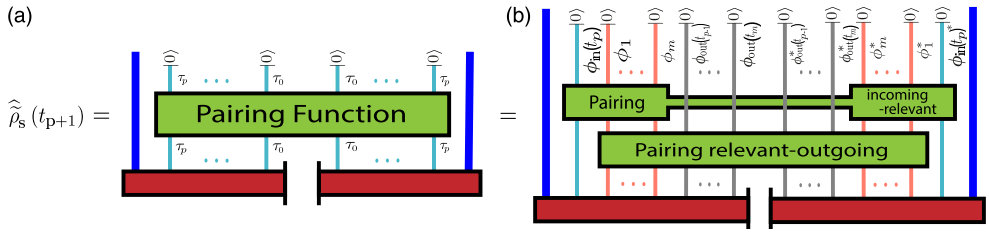

FIG. 18. (a) When evaluating observables or taking the partial trace, the pairing function introduces additional nonlocal coupling between the time cells. This coupling has the same convolutional form as the annihilation processes considered in Sec. IV. (b) Therefore, in the frame of incoming/relevant/outgoing modes, the couplings (i.e., pairings) between the past outgoing modes and the future incoming modes are still negligible. This is the foundation of our approach. The pairing function decouples into the two separate parts: pairings involving relevant-outgoing modes and the pairings involving incoming-relevant modes.

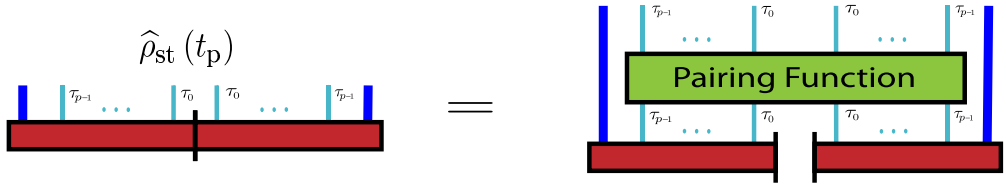

FIG. 19. The joint density matrix $\widehat{\rho}_{\rm st}(t_p)$ for the open system (blue lines) and the time cells (turquoise lines) is defined by applying the pairing function to $|\Phi(t_p)\rangle_{\rm st\,st}\langle\Phi(t_p)|$.

2. Negligible pairings between the past outgoing and the future incoming modes

Now suppose we have a new incoming mode $\phi_{\rm in}(p)$ with the creation operator $\widehat{\psi}_p^\dagger$. It will yield additional terms in the pairing function:

$$\widehat{\psi}_p^\dagger M(0)\widehat{\psi}_p + \sum_{s=0}^{p-1}\{\widehat{\psi}_p^\dagger M_{ps}\widehat{\psi}_s + \widehat{\psi}_s^\dagger M_{sp}\widehat{\psi}_p\}$$
$$= \widehat{\psi}_p^\dagger M(0)\widehat{\psi}_p + \widehat{\psi}_p^\dagger\left\{\sum_i M_i(p)\widehat{\phi}_i + \sum_i M_{{\rm out}i}(p)\widehat{\phi}_{\rm out}(i)\right\}$$
$$+ \text{c.c.} \tag{41}$$

The last term in the second line, $M_{{\rm out}i}(p)\widehat{\phi}_{\rm out}(i)$, can be discarded by construction of the streams of outgoing modes. Therefore, when taking the partial trace over the time cells, we can assume that there are no pairings between the past outgoing and the future incoming modes, and the described above structure of entanglement, Fig. 17, is preserved.

VI. TRACING OUT THE OUTGOING MODES: RENOMALIZATION GROUP FOR DENSITY MATRICES

In this section, we implement the idea that the idle bricks in Fig. 1 can be removed as soon as they emerge. In the conventional RG approach, we trace out the irrelevant degrees of freedom as soon as they appear. Therefore, in this section we introduce the joint density matrix $\widehat{\rho}_{\rm rel}(t_p)$ of the open system and of the relevant degrees of freedom of the environment as a partial trace over the irrelevant degrees. After that, an iterative propagation procedure is derived for $\widehat{\rho}_{\rm rel}(t_p)$.

A. The convention of growing Fock space

We consider the case of the vacuum initial condition for the environment. In this case, the incoming modes are always in vacuum. Then the notation will be more concise if we assume that the wave function $|\Phi(t_p)\rangle_{\rm st}$ is defined on a growing Hilbert space $\mathcal{H}_{\rm s}\otimes\mathcal{F}_{\rm t}(p)$ of the open system, the present and the past tape cells. Namely, at $t_0 = 0$ there are no cells at all, so $\mathcal{F}_{\rm t}(0) = \oslash$, and the initial condition is just $|\Phi(0)\rangle_{\rm st} = |\phi_0\rangle_{\rm s}$. After each propagation $t_p \to t_{p+1}$, one additional incoming mode $\psi_p^\dagger$ gets coupled, and the Fock space is enlarged: $\mathcal{F}_{\rm t}(p+1) = \mathcal{F}_{\rm t}(p)\otimes\{\text{space spanned by }\psi_p^\dagger\}$. Below we follow this convention.

B. Density matrix in the time domain

We recall the formula Eq. (31) for the partial trace over the time cells. We can rewrite it as

$$\widehat{\rho}_{\rm s}(t_p) = {}_{\rm t}\langle 0|\widehat{\rho}_{\rm st}(t_p)|0\rangle_{\rm t}, \tag{42}$$

where we introduce the joint density matrix for the open system and the time cells,

$$\widehat{\rho}_{\rm st}(t_p) = \left\{e^{\sum_{rs=0}^{p-1}\widehat{\psi}_r^\dagger M_{rs}\widehat{\psi}_s} : |\Phi(t_p)\rangle_{\rm st\,st}\langle\Phi(t_p)| :\right\}_A, \tag{43}$$

see also Fig. 19. This density matrix is Hermitian and positive semidefinite. The latter follows from the fact that $|\Phi(t_p)\rangle_{\rm st\,st}\langle\Phi(t_p)|$ is positive semidefinite, and the action of the pairing function is a completely positive map since it has the sandwich form required by the Stinespring factorization theorem. Indeed, each elementary pairing has the form

$$\sum_{rs} M_{rs}\widehat{\psi}_s : \ldots : \widehat{\psi}_r^\dagger = \int_{-\infty}^{+\infty} d\tau\widehat{K}(\tau) : \ldots : \widehat{K}^\dagger(\tau), \tag{44}$$

where $\widehat{K}(\tau) = \sum_s M^{1/2}_{\tau\tau_s}\widehat{\psi}_s$, and $M^{1/2}_{\tau\tau'} = (2\pi)^{-\frac{1}{2}}\int_0^{+\infty} d\omega e^{-i\omega(\tau-\tau')}\sqrt{J(\omega)}$ is the wave packet of a single emission event from Fig. 14.

However, the density matrix $\widehat{\rho}_{\rm st}(t_p)$ need not be normalized in the conventional sense, $\mathrm{Tr}\widehat{\rho}_{\rm st}(t_p) \neq 1$. Instead, its vacuum part is always normalized:

$$\mathrm{Tr}\{{}_{\rm t}\langle 0|\widehat{\rho}_{\rm st}(t_p)|0\rangle_{\rm t}\} = 1. \tag{45}$$

This follows from the fact that density matrix of open system is normalized, $\mathrm{Tr}\widehat{\rho}_{\rm s}(t_p) = 1$, and that the partial trace over the environment involves the vacuum projection in the tape model, Eq. (31). Let us remind that we have derived the trace formula Eq. (31) from the formal requirement that all the commutators are conserved, see Secs. V A and V C. However, later, in Sec. VIII B, we find a physical interpretation of this relation: partial trace Eq. (31) and the normalization Eq. (45) can be interpreted as a result of vacuum fluctuations of the classical background of the environment.

C. Definition of the relevant density matrix

Here we define the relevant density matrix $\widehat{\rho}_{\rm rel}(t_p)$, and in the next section we discuss how it can be computed. To introduce the relevant density matrix $\widehat{\rho}_{\rm rel}(t_p)$, we first switch to the frame of incoming/relevant/outgoing modes in the definition Eq. (43) of $\widehat{\rho}_{\rm st}(t_p)$, Fig. 20(a). This change of frame was described in Sec. V E 1. After that, all the outgoing modes which have emerged by time moment t_p are projected

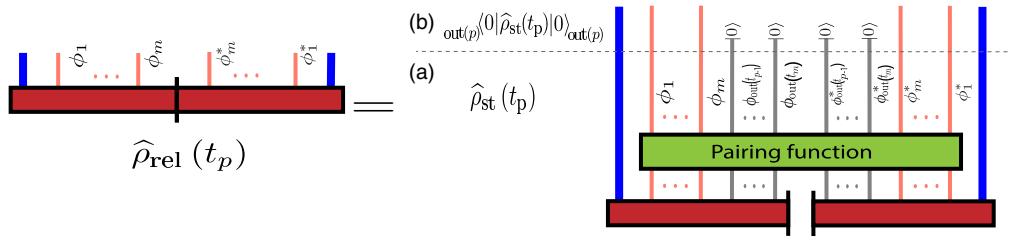

FIG. 20. Renormalization group method amounts to tracing out the the irrelevant degrees of freedom as they emerge during the flow. This results in the density matrix $\widehat{\rho}_{\rm rel}$ which is the joint reduced state of relevant degrees of freedom and open system. This matrix is defined in two steps: (a) we take the joint density matrix of open system and time cells $\widehat{\rho}_{\rm st}(t_p)$ in the frame of relevant/outgoing modes, (b) then we project to the vacuum all the outgoing modes which have emerged by time moment t_p.

to vacuum, Fig. 20(b),

$$\widehat{\rho}_{\rm rel}(t_p) = {}_{{\rm out}(p)}\langle 0|\Big\{ e^{\sum_{rs=0}^{p-1}\widehat{\psi}_r^\dagger M_{rs}\widehat{\psi}_s} \times :|\Phi(t_p)\rangle_{\rm st\ st}\langle\Phi(t_p)|:\Big\}_A |0\rangle_{{\rm out}(p)}, \tag{46}$$

where

$$|0\rangle_{{\rm out}(p)} = |0\rangle_{\phi_{\rm out}(p-1)}\otimes\ldots\otimes|0\rangle_{\phi_{\rm out}(m)} \tag{47}$$

is the joint vacuum of the outgoing modes $\phi_{\rm out}(m)$, $\ldots$, $\phi_{\rm out}(p-1)$ which have emerged by time moment t_p. The operation ${}_{{\rm out}(p)}\langle 0|\cdot|0\rangle_{{\rm out}(p)}$ in Eq. (46) denotes the projection of density matrix to the subspace of zero quanta in the outgoing modes $\phi_{\rm out}(m),\ldots,\phi_{\rm out}(p-1)$. This operation does not affect the other degrees of freedom. Actually, this projection restricts the growing Fock space $\mathcal{F}_{\rm t}(p)$ to the subspace $\mathcal{F}_{\rm rel}$ spanned by the relevant modes $\phi_1\ldots\phi_m$. The reduced density matrix for the open system is obtained via the projection

$$\widehat{\rho}_{\rm s}(t_p) = {}_{\rm rel}\langle 0|\widehat{\rho}_{\rm rel}(t_p)|0\rangle_{\rm rel}, \tag{48}$$

where here and below, under $|0\rangle_{\rm rel}$ we designate the joint vacuum for the relevant modes $\widehat{\phi}_1^\dagger,\ldots,\widehat{\phi}_m^\dagger$.

D. Propagation of density matrix

Given an environment with a spectral density $J(\omega)$, one computes its memory function $M(t-t')$. Then the incoming/outgoing/relevant modes and disentanglers W_p are found according to the algorithm of Sec. IV D. This needs to be done once for a given $J(\omega)$.

The initial condition for the propagation is $\widehat{\rho}_{\rm rel}(0) = |\phi_0\rangle_{\rm s\,s}\langle\phi_0|$, since there are no relevant modes at $t_0=0$.

Now suppose we have $\widehat{\rho}_{\rm rel}(t_p)$, which is an operator acting in $\mathcal{H}_{\rm s}\otimes\mathcal{F}_{\rm rel}$, Fig. 21(a). The first step of propagation is the *entangling step*, Fig. 21(b). Here the Hamiltonian $\widehat{H}_{\rm st}(\tau_p)$ of Eq. (34) is applied. We use the following three facts: First, since $\widehat{H}_{\rm st}(\tau_p)$ is not Hermitian, the bra state ${}_{\rm st}\langle\Phi(t_p)|$ evolves under $\widehat{H}_{\rm st}^\dagger(\tau_p)$, whereas the ket state $|\Phi(t_p)\rangle_{\rm st}$ evolves under $\widehat{H}_{\rm st}(\tau_p)$. Second, the Hamiltonian $\widehat{H}_{\rm st}(\tau_p)$ can be commuted to the left of the pairing function in Eq. (46). Analogously, the Hamiltonian $\widehat{H}_{\rm st}^\dagger(\tau_p)$ can be commuted to the right of the pairing function. Third, the Hamiltonian $\widehat{H}_{\rm st}(\tau_p)$ entangles one additional incoming mode $\widehat{\psi}_p^\dagger$. Therefore, the Fock space is enlarged from $\mathcal{F}_{\rm rel}$ to $\mathcal{F}_{\rm rel+i}$ due to the states generated by $\widehat{\psi}_p^\dagger$. The the density matrix $\widehat{\rho}_{\rm rel}(t_p)$ is embedded into the space $\mathcal{H}_s\otimes\mathcal{F}_{\rm rel+i}$ as $\widehat{\rho}_{\rm rel+i}(t_p) = \widehat{\rho}_{\rm rel}(t_p)\otimes|0\rangle_{\varphi_{\rm in}(p)\varphi_{\rm in}(p)}\langle 0|$.

It propagates as

$$\widehat{\rho}^{(1)}_{\rm rel+i}(t_{p+1}) = \widehat{\rho}_{\rm rel+i}(t_p) - idt\big\{\widehat{H}_{\rm st}(\tau_p)\widehat{\rho}^{(1/2)}_{\rm rel+i}(t_p) - \widehat{\rho}^{(1/2)}_{\rm rel+i}(t_p)\widehat{H}^\dagger_{\rm st}(\tau_p)\big\}, \tag{49}$$

where $\widehat{\rho}^{(1/2)}_{\rm rel+i}(t_p) = \frac{1}{2}(\widehat{\rho}^{(1)}_{\rm rel+i}(t_{p+1}) + \widehat{\rho}_{\rm rel+i}(t_p))$. This propagation corresponds to the operators $\widehat{U}_p$ and $\widehat{U}_p^\dagger$ in Fig. 21.

Observe that $\widehat{\rho}^{(1)}_{\rm rel+i}(t_{p+1})$ entangles one additional incoming mode $\widehat{\psi}_p^\dagger$, and the pairing function in Eq. (46) does not yet contain the pairings for this mode. As follows from Fig. 18 and Sec. V E, only the pairings of the incoming mode with itself and with the relevant modes should be included. Therefore, the second step is the *pairing update*, Fig. 21(c):

$$\widehat{\rho}^{(2)}_{\rm rel+i}(t_{p+1}) = \big\{e^{\widehat{\psi}_p^\dagger M(0)\widehat{\psi}_p + (\widehat{\psi}_p^\dagger\sum_i M_i(p)\widehat{\phi}_i + {\rm c.c.})} : \widehat{\rho}^{(1)}_{\rm rel+i}(t_{p+1}) :\big\}_A. \tag{50}$$

During the propagation, the pairing update is the only operation which can make the density matrix impure. This is the non-Markovian analog of the jump $L\widehat{\rho}L^\dagger$ terms in the Markovian Lindblad dissipator [30,66].

In the third step of propagation, the *disentangling step*, Fig. 21(d), we apply the disentangler $\widehat{W}_p$ to convert the incoming mode $\widehat{\psi}_p$ into the new outgoing mode $\widehat{\phi}_{\rm out}(p)$:

$$\widehat{\rho}^{(3)}_{\rm rel+o}(t_{p+1}) = \widehat{W}_p\widehat{\rho}^{(2)}_{\rm rel+i}(t_{p+1})\widehat{W}_p^{-1}. \tag{51}$$

Here we change the subscript from rel+i to rel+o to make explicit the fact that (i) we start with the Fock space spanned by the relevant modes $\widehat{\phi}_1^\dagger\ldots\widehat{\phi}_m^\dagger$ and one incoming mode $\widehat{\psi}_p^\dagger$ and (ii) after the disentangler transform, we end with the Fock space spanned by the relevant modes $\widehat{\phi}_1^\dagger\ldots\widehat{\phi}_m^\dagger$ and one outgoing mode $\widehat{\phi}_{\rm out}^\dagger(p)$.

The last step, *the oblivion*, Fig. 21(e), is to discard the quantum content of this irrelevant mode:

$$\widehat{\rho}_{\rm rel}(t_{p+1}) = {}_{\phi_{\rm out}(t_p)}\langle 0|\widehat{\rho}^{(3)}_{\rm rel+o}(t_{p+1})|0\rangle_{\phi_{\rm out}(t_p)}. \tag{52}$$

As a result, we return to the smaller Fock space $\mathcal{F}_{\rm rel}$. Then the propagation procedure is repeated for the next time moment t_{p+1}.

These four steps, Eqs. (49)–(52) constitute one complete iteration of the real-time RG flow. They can be implemented numerically in a Fock space of the tape cells (see Fig. 22), see Appendix A, which is truncated in the maximal total occupation of the modes. The pairing update

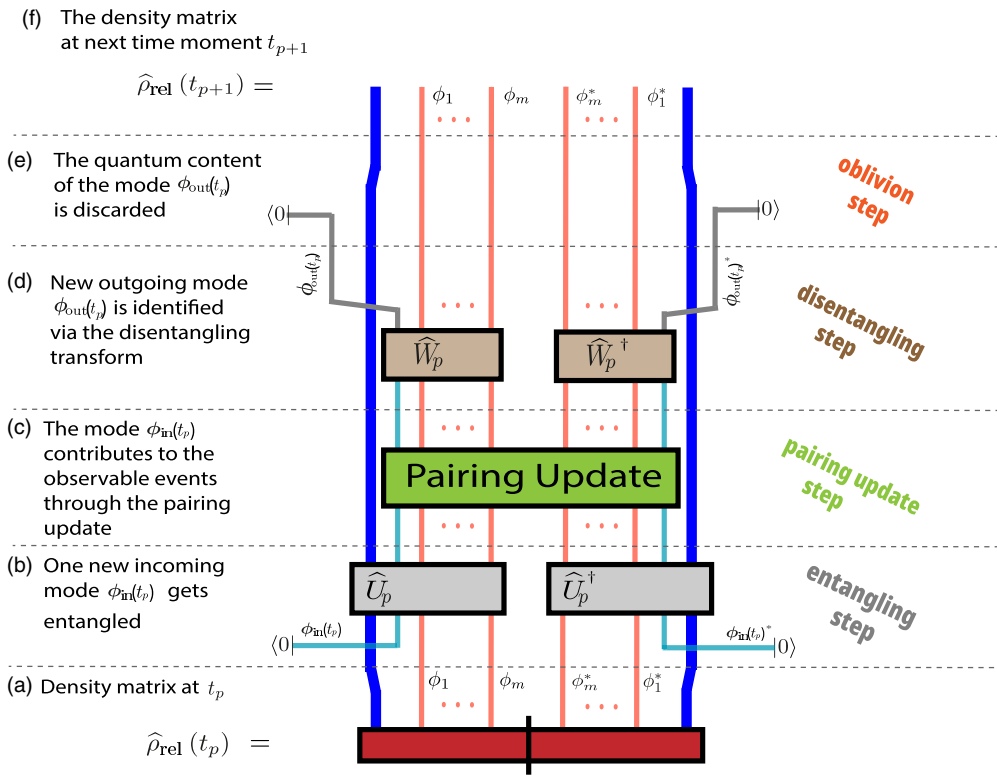

FIG. 21. The life cycle of entanglement in course of real time evolution. It directly maps to the numerical recipe of the renormalization group for density matrices.

Eq. (50) is inexpensive since we can truncate it to second order, see Appendix B. The disentangler Eq. (52) can be efficiently implemented using Lanczos-like algorithms: see Appendix C.

E. Example calculation

In Fig. 23, we present the results of calculation of the RG for density matrices for the system of a driven qubit coupled to the waveguide Eq. (11) with $\varepsilon = 1$ and $h = 0.05$. We have $\widehat{H}_{\rm s} = \widehat{\sigma}_+\widehat{\sigma}_- + 0.1\cos t$, and $\widehat{s} = \widehat{\sigma}_-$. We conduct a series of simulations with one ($m = 1$), two ($m = 2$), three ($m = 3$), and five ($m = 5$) relevant modes. The convergence is achieved when only the states of no more than two quanta were kept in the tape Fock spaces $\mathcal{F}_{\rm t}(p)$, $\mathcal{F}_{\rm rel}$, $\mathcal{F}_{\rm rel+i}$, $\mathcal{F}_{\rm rel+o}$. It is seen that the simulation already converges for the three ($m = 3$) relevant modes. In Fig. 24, we compare the converged result with the numerically exact solution of the Schrodinger equation. The Schrodinger equation was solved in the truncated Hilbert space of the model Eq. (11). The truncation was done by keeping the first $\widetilde{m}$ lattice sites $\widehat{a}_1^\dagger \ldots \widehat{a}_{\widetilde{m}}^\dagger$ and by keeping all the Fock states $\widehat{a}_1^{\dagger n_1} \ldots \widehat{a}_{\widetilde{m}}^{\dagger n_{\widetilde{m}}}|0\rangle_{\rm b}$ with maximal total occupation $n_1 + \ldots + n_{\widetilde{m}} \leqslant \widetilde{n}$. The numbers $\widetilde{m}$ and $\widetilde{n}$ were increased until the convergence of observables on the considered time interval: this occurs for $\widetilde{m} = 14$ and $\widetilde{n} = 7$. Our RG procedure yields a benefit in comparison with the bare solution of the Schrodinger equation: three modes versus fourteen and two quanta versus seven. The physical explanation is that among the fourteen modes only three are non-neglibigly coupled to the future motion, and their occupation is rather small, so two quanta are enough.

F. Balance of complexity

As we discussed in the Introduction, the quantum complexity is expected to saturate if the rates of occurrences of incoming and outgoing modes are equal and the incoming and outgoing fluxes are also equal. Here we discuss these questions on the example of the driven qubit in the waveguide from the previous section.

1. Rates of occurrences of incoming and outgoing modes

As seen from Fig. 22, the rates of outgoing modes are not always equal to the rates of incoming modes. On the time interval $[0, t_m]$, every incoming mode becomes relevant: no outgoing modes are produced at all. During this initial period, the dimension of the relevant space grows linearly with time. However, due to the fastest decoupling property, Fig. 7, when the dimension becomes equal to m, the contribution of new relevant modes becomes exponentially small. The relevant space saturates. We can keep the dimension fixed to m and start to produce the outgoing modes with the rate equal to the rate of incoming modes.

2. Balance of fluxes

For the same system of a driven qubit in the waveguide, we check the proposed conjecture that the flux of the quanta emitted into the incoming mode (the *incoming current*) and the flux of the quanta discarded in the outgoing mode (the *outgoing current*) should balance each other. The results of Fig. 25 support our conjecture. The incoming current $j_{\rm in}(t_p)$ is computed as the population of the incoming mode $\varphi_{\rm in}(p)$ at the end of stage b in Fig. 21 (after propagation under $\widehat{U}_p \ldots \widehat{U}_p^\dagger$

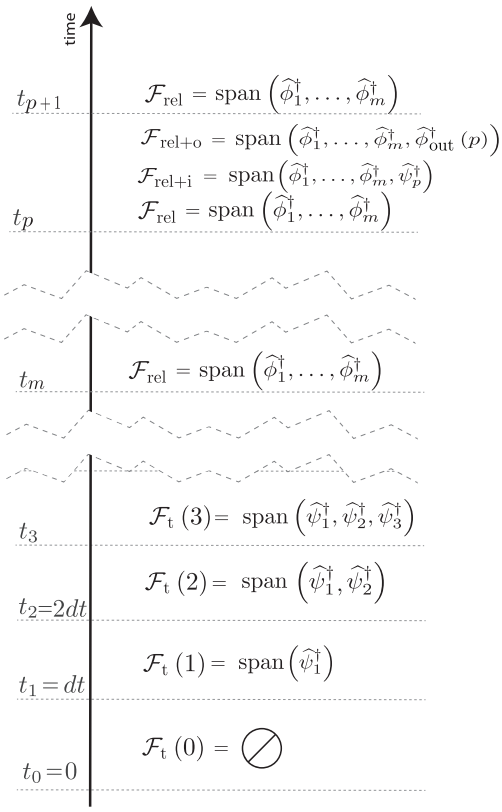

FIG. 22. The renormalization group for density matrices has two regimes: (1) Before time moment t_m, all the time cells are relevant and the tape Fock space continuously grows and (2) after time moment t_m, the Fock space stops growing and starts to oscillate between $\mathcal{F}_{\rm rel}$, $\mathcal{F}_{\rm rel+i}$, $\mathcal{F}_{\rm rel+o}$. Here span(…) designates the Fock space generated by applying creation operators inside the brackets to the vacuum state. In a numerical simulation, the Fock spaces are truncated in the maximal total occupation of the modes. Such a truncation is justified by the conjectured balance of complexity: see Sec. VI F. In a numerical simulation, the Fock spaces $\mathcal{F}_{\rm rel+i}$ and $\mathcal{F}_{\rm rel+o}$ are the same: it is our interpretation that the additional mode alternatively plays the role of the incoming and outgoing modes.

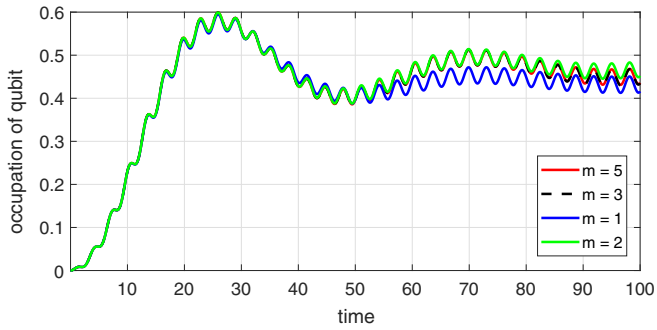

FIG. 23. For the system of a driven qubit in a highly non-Markovian waveguide, only three relevant modes at a maximal occupation of two quanta is enough to achieve the convergence of observable properties. The calculation is done by RG for density matrices.

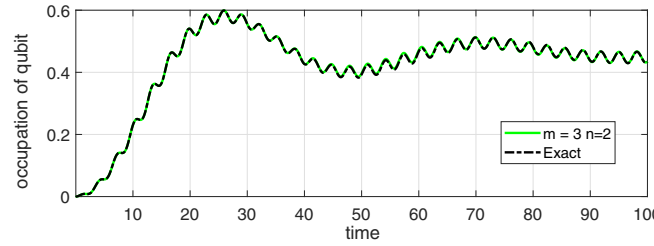

FIG. 24. For the same situation as in previous Fig. 23, we compare the converged RG for density matrices with the numerically exact solution of Schrodinger equation. The latter required us to keep 14 lattice sites in Eq. (11) and all states of maximum total occupation of seven quanta.

but before the pairing update):

$$j_{\rm in}(t_p) = \frac{1}{dt}\mathrm{Tr}\left\{\widehat{\rho}^{(1)}_{\rm rel+i}(t_{p+1})\widehat{\psi}_p^\dagger\widehat{\psi}_p\right\}. \tag{53}$$

The outgoing current $j_{\rm out}(t_p)$ is computed as the population of the outgoing mode $\phi_{\rm out}(p)$ at the end of stage d in Fig. 21 (after disentangling under $\widehat{W}_p \ldots \widehat{W}_p^\dagger$ but before the oblivion):

$$j_{\rm out}(t_p) = \frac{1}{dt}\mathrm{Tr}\left\{\widehat{\rho}^{(3)}_{\rm rel+o}(t_{p+1})\widehat{\phi}_{\rm out}^\dagger(p)\widehat{\phi}_{\rm out}(p)\right\}. \tag{54}$$

Finally, the total occupation of relevant modes is computed as

$$n_{\rm tot}(t_p) = \mathrm{Tr}\left\{\widehat{\rho}^{(1)}_{\rm rel+i}(t_{p+1})\left(\widehat{\psi}_p^\dagger\widehat{\psi}_p + \sum_{k=1}^{m}\widehat{\phi}_k^\dagger\widehat{\phi}_k\right)\right\}. \tag{55}$$

This balance of complexity has the following physical interpretation, Fig. 26. The incoming modes inject new quanta with the flux $j_{\rm in}(t_p)$ into the cavity which is formed by the relevant modes. The mirrors of the cavity are formed by the coupling to the future motion. These mirrors are imperfect: the outgoing modes are continuously leaking out and carry away with them a flux $j_{\rm out}(t_p)$ of quanta.

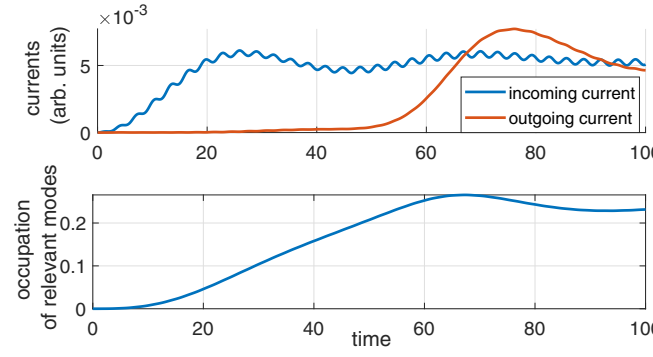

FIG. 25. The system of a driven qubit in a waveguide. The outgoing current of quanta which are discarded in the outgoing modes balances the incoming flux of quanta which are emitted into the incoming modes. The units for the currents are common but otherwise arbitrary. As a consequence, the total occupation of the relevant modes saturates.

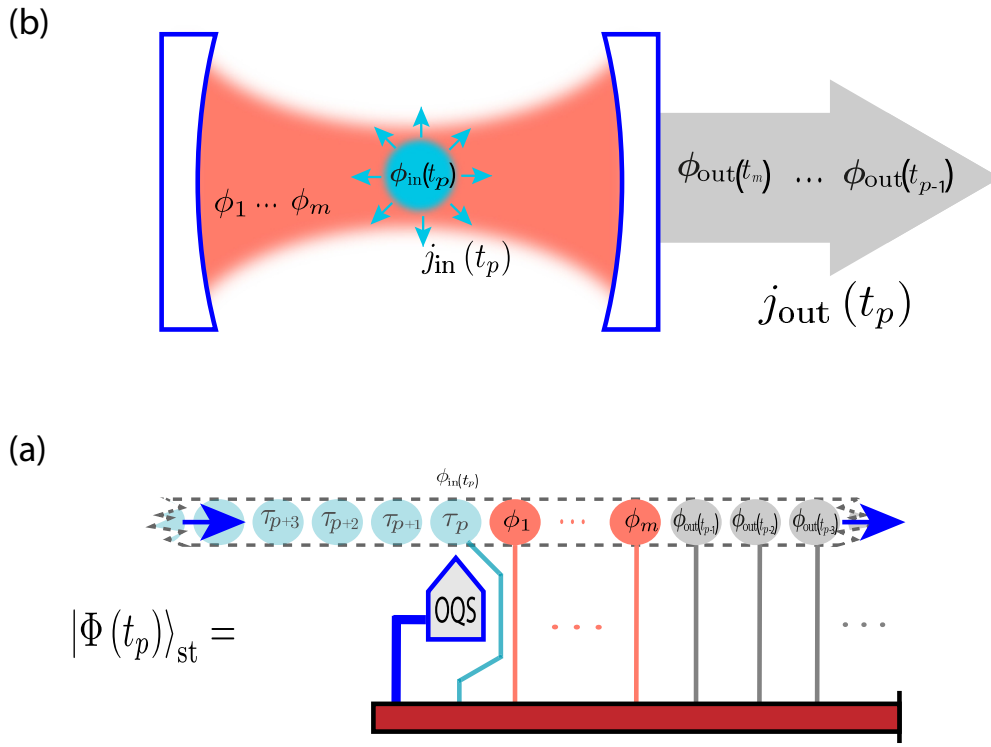

FIG. 26. We conjecture that the quantum complexity of the real-time motion of open quantum systems is asymptotically bounded. The interpretation is the following (a). Suppose we are given a joint quantum state $|\Phi(t_p)\rangle_{\rm st}$ for the open system and the time cells, in the frame of incoming/relevant/outgoing modes. (b). It can be interpreted that the relevant modes $\phi_1 \ldots \phi_m$ play the role of the "cavity" modes. The "mirrors" of the cavity are the coupling to the future evolution. New quanta are injected into the "cavity" with a flux $j_{\rm in}(t_p)$ via the incoming mode $\varphi_{\rm in}(p)$. However the "mirrors" are imperfect: the outgoing modes are continuously leaking out and carry away with them a flux $j_{\rm out}(t_p)$ of quanta. As a result, the total occupation $n_{\rm tot}(t_p)$ of the "cavity" modes is expected to be bounded due to the balance of the fluxes.

G. Analogies with the time-symmetric formulation of quantum mechanics

Observe that the general structure of the RG flow described above is time symmetric: If we apply the steps in Fig. 21 forward in time, then (i) one incoming mode in the vacuum gets entangled and (ii) one outgoing mode gets disentangled and projected to the vacuum. If we reverse this procedure in time, we get (i') one outgoing mode in the vacuum gets entangled and (ii') one incoming mode gets disentangled and projected to the vacuum. This has interesting analogies to the two-state vector formulation (TSVF) of quantum mechanics by Aharonov and Vaidman [67]. In TSVF, one considers the two measurements. The outcome of the first measurement at time t produces the state $\psi_{\rm in}(t)$. The outcome of the second measurement at $T > t$ produces the state $\psi_{\rm out}(T)$. Then, TSVF considers the quantum evolution inside the interval $[t, T]$ with the fixed initial and final boundary conditions $\psi_{\rm in}(t)$ and $\psi_{\rm out}(T)$, correspondingly, Fig. 27. This formalism is applied when analyzing the experiments with the postselection of measurement results [68]. This formalism also yields an interpretation of quantum mechanics: One may assume that there is a final boundary condition for the universe which singles out a definite outcome for all the measurements [69]. However the real-time entanglement structure suggests an interesting alternative: Instead of global initial and final states, one may consider the *streams* of initial and final states, so there is a continuous competition between the birth and death of the quantum reality in real time, see Fig. 27.

VII. MARKOVIAN LIMIT

In this section, we relate our RG procedure Fig. 21 to the Lindblad master equation which is applied in the Markovian regime [66,70]. This will help us to develop intuition about the steps of our RG procedure.

There are many ways to perform the Markovian limit. A good way should be based solely on the spectral decoupling mechanism represented in Sec. IV. A rough way is to apply the conventional formal arguments which lead to the Lindblad master equation. Here we choose the latter to connect the RG procedure to the conventional terms. Moreover, later it will help us to assess the additional insights provided by the spectral decoupling mechanism.

We choose the derivation of the Markovian limit via the quantum stochastic differential equations [66,70]. Essentially, this approach assumes that we are dealing with a small-coupling, near-resonant, and broadband setup. Then the time cells can be considered as local independent degrees of freedom, $[\widehat{b}(t), \widehat{b}^\dagger(t')] = \Gamma\delta(t - t')$. In terms of the stream of discrete time moments, this reads

$$[\widehat{b}(\tau_p), \widehat{b}^\dagger(\tau_q)] = dt^{-1}\Gamma\delta_{pq}. \tag{56}$$

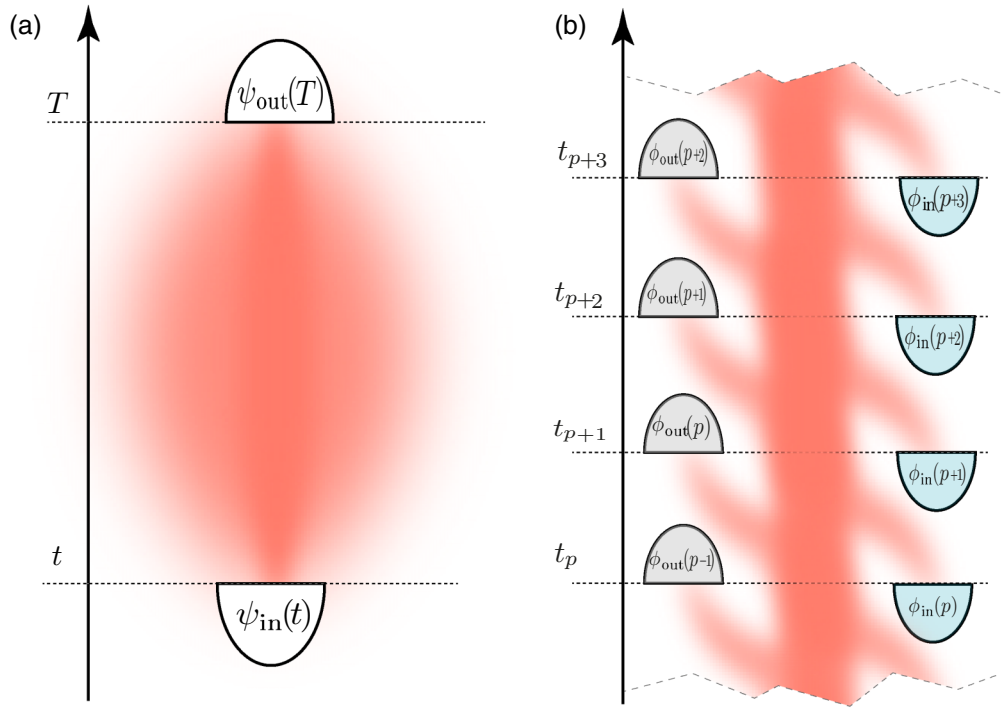

FIG. 27. (a) In the time-symmetric formulation of quantum mechanics (also called the two-state vector formalism, TSVF) of Aharonov and Vaidman [67], the quantum evolution is considered which starts from some initial state $\psi_{\rm in}(t)$. Then one assumes that there exists a final boundary condition in the future $\psi_{\rm out}(T)$. The conjecture is that this final boundary condition is fine-tuned to yield an effective collapse to definite outcomes of all the quantum measurements happening inside the interval $[0, T]$ [69]. (b) However, the real-time structure of entanglement suggests an interesting alternative: Instead of the speculated global future boundary condition, there are *streams* of initial $\varphi_{\rm in}(p)$ and final $\varphi_{\rm out}(p)$ states, so there is a continuous competition between the birth and death of the quantum reality during each infinitesimal time interval.

This means that we have $m = 0$ relevant modes: only the incoming mode appears in Fig. 21. The disentangler in Fig. 21(d) is the identity operator: $\phi_{\rm out}(p) = \phi_{\rm in}(p)$. The small-coupling assumption means that we can consider at most one quantum in the incoming mode.

Figure 21(a) considers the relevant density matrix $\widehat{\rho}_{\rm rel}(t_p)$ at a time moment t_p, which is simply

$$\widehat{\rho}_{\rm rel}(t_p) = \widehat{\rho}_{\rm s}(t_p), \tag{57}$$

where $\widehat{\rho}_{\rm s}(t_p)$ is a reduced density matrix of open system.

Let us assume for a moment that $\widehat{\rho}_{\rm rel}(t_p)$ is a pure state $|\phi\rangle_{\rm rel}$. After the entangling step, Fig. 21(b), this state becomes

$$\begin{aligned}|\phi^{(1)}\rangle_{\rm rel+i} = (1 - i\widehat{H}_{\rm s}dt)|\phi\rangle_{\rm rel} \otimes |0\rangle_{\varphi_{\rm in}(p)} \\ - i\widehat{s}|\phi\rangle_{\rm rel} \otimes |1\rangle_{\varphi_{\rm in}(p)}dt \\ - \tfrac{1}{2}\Gamma\widehat{s}^\dagger\widehat{s}|\phi\rangle_{\rm rel} \otimes |0\rangle_{\varphi_{\rm in}(p)}dt.\end{aligned} \tag{58}$$

Here we keep only $O(dt)$ terms in the midpoint propagation under Eq. (34). In the last line, we see the second-order virtual process because there is dt^{-1} in the memory function commutator Eq. (56). We observe that the first line yields the unitary free motion of open system $-i[\widehat{H}_{\rm s}, \widehat{\rho}_{\rm rel}]$ in the Lindblad equation and the last line yields the standard term $-\frac{1}{2}\Gamma\{\widehat{s}^\dagger\widehat{s}, \widehat{\rho}_{\rm rel}\}$, which describes the decay of probability of no-emission event.

After applying the pairing update, Fig. 21(c), to the state $|\phi^{(1)}\rangle_{\rm rel+i}$, we obtain the quantum jump term from the second line of Eq. (58):

$$\begin{aligned}\widehat{\rho}^{(2)}_{\rm rel+i}(t_p) = (\widehat{\rho}_{\rm rel} - i[\widehat{H}_{\rm s}, \widehat{\rho}_{\rm rel}]dt) \otimes |0\rangle_{\varphi_{\rm in}(p)\varphi_{\rm in}(p)}\langle 0| \\ - \tfrac{1}{2}\Gamma\{\widehat{s}^\dagger\widehat{s}, \widehat{\rho}_{\rm rel}\}dt \otimes |0\rangle_{\varphi_{\rm in}(p)\varphi_{\rm in}(p)}\langle 0| \\ + \Gamma\widehat{s}\widehat{\rho}_{\rm rel}\widehat{s}^\dagger dt \otimes |0\rangle_{\varphi_{\rm in}(p)\varphi_{\rm in}(p)}\langle 0| \\ + \{\text{terms containing either } |1\rangle_{\varphi_{\rm in}(p)} \text{ or } {}_{\varphi_{\rm in}(p)}\langle 1|\}.\end{aligned} \tag{59}$$

Finally, the oblivion step, Fig. 21(e) removes the emitted quanta and the incoming mode. We obtain the conventional Lindblad equation:

$$\begin{aligned}\widehat{\rho}_{\rm s}(t_{p+1}) = \widehat{\rho}_{\rm s}(t_p) - i[\widehat{H}_{\rm s}, \widehat{\rho}_{\rm s}]dt \\ - \tfrac{1}{2}\Gamma\{\widehat{s}^\dagger\widehat{s}, \widehat{\rho}_{\rm s}\}dt + \Gamma\widehat{s}\widehat{\rho}_{\rm s}\widehat{s}^\dagger dt.\end{aligned} \tag{60}$$

Therefore, we obtain the following rough picture of the Markovian mode. At each infinitesimal time interval, one incoming mode $\varphi_{\rm in}(p)$ is coupled to the open system, a quantum is emitted into $\varphi_{\rm in}(p)$ during the entangling step, and the quantum jump is taken into account via the pairing update. After that, the incoming mode (which is equal to the outgoing mode in this case) is irreversibly decoupled and the quantum is discarded.

In summary, our RG procedure can be considered an *entanglement-assisted* non-Markovian generalization of the Lindblad master equation [30].

VIII. STOCHASTIC UNRAVELLING: RENORMALIZATION GROUP ALONG A QUANTUM TRAJECTORY

Here we implement our intuition that the outgoing modes in Fig. 1 can be replaced by a classical stochastic signal. In other words, we explore the second alternative for the irrelevant degrees of freedom: Instead of tracing them out, we collapse them to a classical noise as soon as they emerge. This results in a stochastic variant of RG which we call the RG along a quantum trajectory. This way, we completely implement the intuitive picture of Introduction that the ultimate fate of the emitted field is not only to decouple but also to become observed.

A. Ensembles versus quantum trajectories

Let us recall that in the Markovian regime the motion of an open quantum system can be described in two alternative but equivalent ways [66]. The first way is the ensemble description. It is given in terms of a reduced density matrix and its evolution is governed by the Lindblad master equation. The second way is the description by the quantum trajectories. Here one takes into account the fact that every open system will exercise a random motion under the influence of the environment. The environment stores a classical record of the history of such motion. The quantum trajectory is the quantum evolution which is conditioned on a particular realization of the record. This results in a stochastic pure-state evolution which is known under various names in literature: quantum jumps, quantum state diffusion, stochastic wave function, etc. Then the description in terms of the reduced density matrix is recovered as an average over the ensemble of all possible records (hence the name ensemble description). In other words, the quantum trajectories provide a stochastic unravelling of the dissipative master equations.

The merit of quantum trajectories is twofold. First, they yield efficient Monte Carlo simulation methods for the dissipative dynamics. This is because the size of the density matrix scales as N^2 with the dimension N of the Hilbert space [30,71], while the size of a pure state of the quantum trajectory scales as N. Second, they provide the interpretation for the experiments on observing and manipulating a single quantum system under the Markovian conditions [66].

Our RG for density matrices can also be considered an ensemble description. Then the question arises: What is the corresponding quantum trajectory description? The merit of this is again twofold: We obtain (1) efficient Monte-Carlo simulations for pure states and (2) insights into how the classical records are stored in the non-Markovian environment.

B. Pairing function as average over the vacuum fluctuations of environment

In the Markovian regime, the sandwich term $\Gamma\widehat{s}\widehat{\rho}_{\rm s}\widehat{s}^\dagger$ arises as an average over the ensemble of quantum-jump histories [30,66,70]. In our RG, the pairing function plays the role of the non-Markovian sandwich term, see Eqs. (44) and (59). Therefore, we want to represent it as an ensemble of some observable events. Here we show that as such events, one can choose the vacuum fluctuations of the classical field in the environment, see Fig. 28.

The classical field z is carried by the coherent state

$$|z\rangle_{\rm b} = \mathcal{Q}_{\rm vac}(z)^{\frac{1}{2}} \exp\left(\int d\omega z^*(\omega)\widehat{a}^\dagger(\omega)\right)|0\rangle_{\rm b}, \tag{61}$$

where the normalization factor $\mathcal{Q}_{\rm vac}(z)$ is the probability to observe a vacuum fluctuation z of the field,

$$\mathcal{Q}_{\rm vac}(z) = |{}_{\rm b}\langle z|0\rangle_{\rm b}|^2 \propto \exp\left(-\int d\omega |z(\omega)|^2\right). \tag{62}$$

At the coupling site $\widehat{b}^\dagger(t)$, the vacuum fluctuation z appears as a colored (non-Markovian) noise $\xi^*(t)$:

$$\xi^*(t) = \int d\omega c^*(\omega) z^*(\omega) e^{i\omega t}. \tag{63}$$

This noise has the Gaussian statistics

$$\overline{\xi_r} = \overline{\xi_r^*} = 0, \ \overline{\xi_r \xi_s^*} = M_{rs}, \tag{64}$$

where we consider the noise ξ at the midpoint times: $\xi_r = \xi(\tau_r)$. Each realization of z leads to a single realization of the entire time trajectory of $\xi^*(t)$.

It turns out that the pairing function can be represented as an average over these vacuum fluctuations, Fig. 28,

$$\left\{e^{\sum_{rs=0}^{\infty}\widehat{\psi}_r^\dagger M_{rs}\widehat{\psi}_s}\right\}_A = \overline{\left[\left\{e^{\sum_{r=0}^{\infty}\xi_r\widehat{\psi}_r^\dagger} e^{\sum_{s=0}^{\infty}\xi_s^*\widehat{\psi}_s}\right\}_A\right]}_\xi, \tag{65}$$

where $\{\cdot\}_A$ is the antinormal averaging. Observe that in the pairing function we extend the summation range from $[0, p-1]$ [as in Eq. (43)] to $[0,\infty)$. This is possible since the incoming modes $\phi_{\rm in}(p), \phi_{\rm in}(p+1), \ldots$ are empty at a time moment t_p. Then the density matrix Eq. (43) is represented as an average over the ensemble of pure states, Fig. 29:

$$\widehat{\rho}_{\rm st}(t_p) = \overline{[|\Phi(\xi,t_p)\rangle_{\rm st\,st}\langle\Phi(\xi,t_p)|]}_\xi. \tag{66}$$

Here the joint pure state of the time cells and of the open system is

$$|\Phi(\xi,t_p)\rangle_{\rm st} = e^{\sum_{s=0}^{\infty}\xi_s^*\widehat{\psi}_s}|\Phi(t_p)\rangle_{\rm st}. \tag{67}$$

Observe the interpretation of the state $|\Phi(\xi,t_p)\rangle_{\rm st}$. The action of operator

$$\widehat{S}(\xi) = e^{\sum_{s=0}^{\infty}\xi_s^*\widehat{\psi}_s} \tag{68}$$

induces a nonunitary Bogoliubov transform of the creation/annihilation operators in $|\Phi(t_p)\rangle_{\rm st}$:

$$\widehat{S}(\xi)\widehat{\psi}_r\widehat{S}^{-1}(\xi) = \widehat{\psi}_r, \tag{69}$$

$$\widehat{S}(\xi)\widehat{\psi}_r^\dagger\widehat{S}^{-1}(\xi) = \widehat{\psi}_r^\dagger + \xi_r^*. \tag{70}$$

In other words, the operation $\widehat{S}(\xi)$ introduces a classical background ξ in state $|\Phi(t_p)\rangle_{\rm st}$, see Fig. 29. As a result, each emitted quantum $\widehat{\psi}_r^\dagger$ in $|\Phi(\xi,t_p)\rangle_{\rm st}$ becomes a superposition of the classical background ξ_r^* and of a purely quantum part:

$$\widehat{\psi}_r^\dagger \to \xi_r^* + \widehat{\psi}_r^\dagger. \tag{71}$$

We call $|\Phi(\xi,t_p)\rangle_{\rm st}$ the quantum state over a classical background ξ. When we perform the partial trace Eq. (42),

$$\widehat{\rho}_{\rm s}(t_p) = \overline{[{}_{\rm t}\langle 0|\Phi(\xi,t_p)\rangle_{\rm st\,t}\langle\Phi(\xi,t_p)|0\rangle_{\rm t}]}_\xi, \tag{72}$$

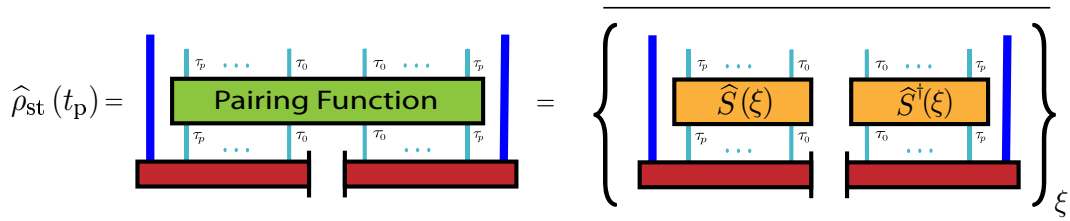

FIG. 28. The pairing function can be stochastically decoupled into the two separate displacement operators $\widehat{S}(\xi)$ and $\widehat{S}^{\dagger}(\xi)$ which act on the ket and the bra states, correspondingly. The averaging is over the displacement ξ which is a classical noise of vacuum fluctuations at coupling site $\widehat{b}^{\dagger}(t)$.

the purely quantum part gets discarded due to projection to the vacuum. In other words, all the quanta *collapse* to the classical background,

$$\widehat{\psi}_r^{\dagger} \to \xi_r^*, \tag{73}$$

and then we average over all the possible vacuum fluctuations.

C. Renormalization group along a quantum trajectory

Now we derive the evolution equations in which the irrelevant degrees are collapsed to a classical noise as soon as they emerge.

Below we follow the convention of the growing Fock space of Sec. VI A. Then the wave function $|\Phi(t_p)\rangle_{\rm st}$ belongs to space $\mathcal{H}_{\rm s}\otimes\mathcal{F}_{\rm t}(p)$, with the Fock space $\mathcal{F}_{\rm t}(p)$ being spanned by the time cells $\psi_{p-1}^{\dagger}\dots\psi_0^{\dagger}$.

Let us introduce the relevant wave function

$$|\Phi(\xi,t_p)\rangle_{\rm rel} = {}_{\rm out(p)}\langle 0|e^{\sum_{s=0}^{p-1}\xi_s^*\widehat{\psi}_s}|\Phi(t_p)\rangle_{\rm st}, \tag{74}$$

which means that we take the quantum state $|\Phi(\xi,t_p)\rangle_{\rm st}$ over the classical background ξ and collapse all the outgoing modes $\phi_{\rm out}(m),\dots,\phi_{\rm out}(p-1)$ which have emerged by time moment t_p, Fig. 30. As a result, the relevant wave function belongs to the space $\mathcal{H}_{\rm s}\otimes\mathcal{F}_{\rm rel}$.

Given an environment with a spectral density $J(\omega)$, one computes its memory function $M(t-t')$. Then the incoming/outgoing/relevant modes, and disentanglers W_p are found according to the algorithm of Sec. IV D. This needs to be done once for a given $J(\omega)$.

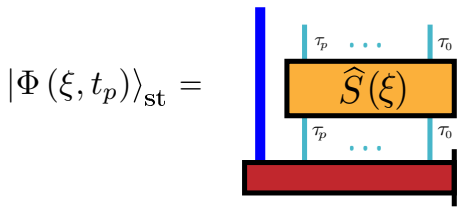

FIG. 29. The density matrix $\widehat{\rho}_{\rm st}(t_p)$ can be represented as the ensemble of displaced pure states $|\Phi(\xi,t_p)\rangle_{\rm st}$. This state is displaced by $\widehat{S}(\xi)$. The result is that the emitted quanta are "centered" on a classical signal ξ, see Eqs. (68)–(70).

Suppose we have a random noise sample ξ. The initial condition for evolution is $|\Phi(\xi,0)\rangle_{\rm rel}=|\phi_0\rangle_{\rm s}$, since there are no relevant modes at $t_0=0$.

The steps of how $|\Phi(\xi,t_p)\rangle_{\rm rel}$ is propagated in time closely mirror those of RG for density matrices of Sec. VI D, see Fig. 31. The first step, *the entangling step*, begins by enlarging the Hilbert space $\mathcal{H}_{\rm s}\otimes\mathcal{F}_{\rm rel}$ with the states of the incoming mode via the embedding $|\Phi(\xi,t_p)\rangle_{\rm rel}\to|\Phi(\xi,t_p)\rangle_{\rm rel+i}=|\Phi(\xi,t_p)\rangle_{\rm rel}\otimes|0\rangle_{\varphi_{\rm in}(p)}$. It is followed by the Hamiltonian propagation:

$$\begin{aligned}|\Phi^{(1)}(\xi,t_{p+1})\rangle_{\rm rel+i} &= |\Phi(\xi,t_p)\rangle_{\rm rel+i}\\ &\quad - idt\widehat{H}_{\rm st}(\xi,\tau_p)\tfrac{1}{2}\{|\Phi^{(1)}(\xi,t_{p+1})\rangle_{\rm rel+i}\\ &\quad + |\Phi(\xi,t_p)\rangle_{\rm rel}\},\end{aligned} \tag{75}$$

where the Hamiltonian

$$\begin{aligned}\widehat{H}_{\rm st}(\xi,\tau_p) &= \widehat{S}(\xi)\widehat{H}_{\rm st}(\tau_p)\widehat{S}^{-1}(\xi)\\ &= \widehat{H}_{\rm s}+\widehat{s}\{\widehat{\psi}_p^{\dagger}+\xi_p^*\}+\widehat{s}^{\dagger}M(0)\widehat{\psi}_p\\ &\quad +\widehat{s}^{\dagger}\sum_{i=1}^{\min(p,m)}M_i(p)\widehat{\phi}_i\end{aligned} \tag{76}$$

takes into account the classical noise of vacuum fluctuations. Here the subscript rel+i means that the Hilbert space is enlarged by an additional incoming mode $\phi_{\rm in}(p)$.

The second step, *the disentangling step,* identifies the new outgoing mode $\phi_{\rm out}(p)$ which has already decoupled:

$$|\Phi^{(2)}(\xi,t_{p+1})\rangle_{\rm rel+o}=\widehat{W}_p|\Phi^{(1)}(\xi,t_{p+1})\rangle_{\rm rel+i}. \tag{77}$$

Please note that since we apply the active change of frame $\widehat{W}_p$, the quantum content of the outgoing mode $\phi_{\rm out}(p)$ just replaces the content of $\phi_{\rm in}(p)$, so the Hilbert space rel+o is actually equal to rel+i.

Finally, in *the oblivion step,* the quantum content of the newly formed outgoing mode is discarded (it collapses to the classical noise):

$$|\Phi(\xi,t_{p+1})\rangle_{\rm rel}={}_{\phi_{\rm out}(t_p)}\langle 0\,|\Phi^{(2)}(\xi,t_{p+1})\rangle_{\rm rel+o}. \tag{78}$$

Observe that, as a result, we return to the Hilbert space $\mathcal{F}_{\rm rel}\otimes\mathcal{H}_{\rm s}$. Then the propagation procedure is repeated for the next time moment t_{p+1}.

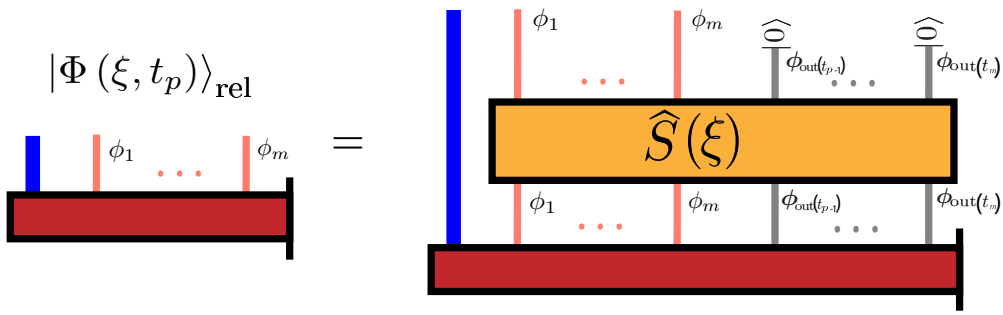

FIG. 30. The relevant wave function $|\Phi(\xi,t_p)\rangle_{\rm rel}$ is defined as a joint pure state of open system and relevant modes. All the outgoing modes $\phi_{\rm out}(m),\ldots,\phi_{\rm out}(p-1)$ which have emerged by time moment t_p are projected to vacuum (their quantum content is discarded).

D. Computing the observables

The observables $\widehat{o}$ for the open system are computed as

$$\langle\widehat{o}(t_p)\rangle \equiv {\rm Tr}\{\widehat{o}\widehat{\rho}_{\rm s}(t_p)\} = \overline{[{}_{\rm rel}\langle\Phi(\xi,t_p)|0\rangle_{\rm rel}\widehat{o}_{\rm rel}\langle 0|\Phi(\xi,t_p)\rangle_{\rm rel}]}_{\xi} Z^{-1}(t_p), \tag{79}$$

where $|0\rangle_{\rm rel}$ is the joint vacuum for the relevant modes $\widehat{\phi}_1^\dagger,\ldots,\widehat{\phi}_m^\dagger$; the state ${}_{\rm rel}\langle 0|\Phi(\xi,t_p)\rangle_{\rm rel}$ belongs to $\mathcal{H}_{\rm s}$; the normalization

$$Z(t_p) = \overline{\|{}_{\rm rel}\langle 0|\Phi(\xi,t_p)\rangle_{\rm rel}\|^2}_{\xi} \tag{80}$$

is equal to 1 in the exact simulation, but should be included in the approximate computation to keep the normalization of the probability. The observables for the environment can also be computed via the mappings Eqs. (24) and (25).

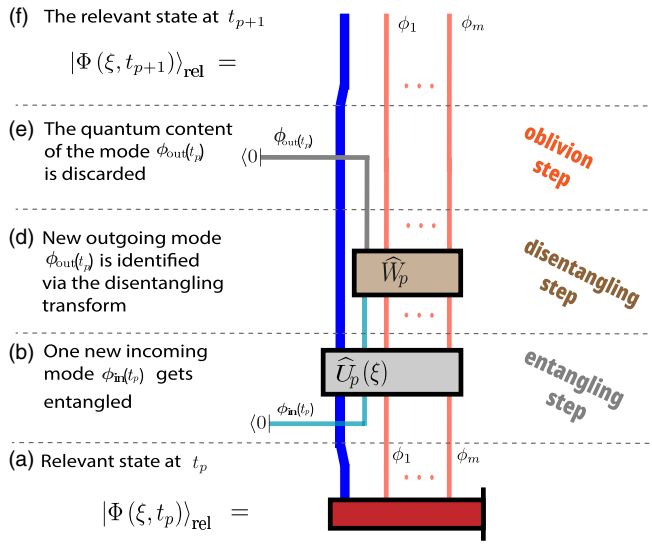

FIG. 31. The renormalization group along a quantum trajectory. For each realization (trajectory) of the classical noise ξ of vacuum fluctuations of the environment, the relevant wave function $|\Phi(\xi,t_p)\rangle_{\rm rel}$ is propagated in time. The full quantum dynamics is obtained as average over ξ. The realizations of ξ can be generated via Monte Carlo sampling. On a conceptual level, this structure shows the life cycle of the quantum complexity during the real-time evolution. First the complexity is generated at step (b). However, eventually the quantum complexity is destroyed in step (e). This is because the decoupled entanglement is equivalent to the stochastic ensemble of classical records.

E. Monte Carlo sampling of vacuum fluctuations

The realizations of the noise ξ can be sampled stochastically by

$$\xi_r = \sqrt{\Delta\omega}\sum_k c(\omega_k)e^{-i\omega_k\tau_r}z_k, \tag{81}$$

where we have introduced a discretization of the frequency axis ω_k. The coefficients $c(\omega_k)=\sqrt{J(\omega_k)/\pi}$, which follows from Eqs. (5) and (8). The complex random numbers z_k have the statistics

$$\overline{z_k} = \overline{z_k^*} = 0, \quad \overline{z_k z_l^*} = \delta_{kl}. \tag{82}$$

We generate a sample of M noise instances $\xi^1\ldots\xi^M$, and the averages Eqs. (79) and (80) are computed as the sample means.

The states $|\Phi(\xi,t_{p+1})\rangle_{\rm rel}$ are represented in the Hilbert space $\mathcal{H}_{\rm s}\otimes\mathcal{F}_{\rm rel}$ which is truncated in the maximal total occupation of the relevant modes. Such a truncation is expected to converge uniformly on wide timescales if we make the reasonable assumption that there is a balance between the flux of quanta $j_{\rm in}(t_p)$ being emitted by the open system and the flux of quanta $j_{\rm out}(t_p)$ which are eventually discarded in the outgoing modes, see Sec. VI F.

F. Importance sampling

Observe that the Hamiltonian $\widehat{H}_{\rm st}(\xi,\tau_p)$ is not Hermitian and does not conserve the norm. As a consequence, it may turn out that the ensemble of noise samples Eqs. (81) and (82) becomes nonrepresentative: the rarest noise realizations receive the highest weights. This can be fixed by applying an importance sampling technique. Any such technique will require shifting the noise sample, $\xi\to\xi+\Delta\xi$. In this paper, we employ the continuous shift of the noise with time. We refer the interested reader to Appendix D for the derivation. Here we present the resulting simulation procedure.

Given an environment with a spectral density $J(\omega)$, one computes its memory function $M(t-t')$. Then the incoming/outgoing/relevant modes and disentanglers W_p are found according to the algorithm of Sec. IV D. This needs to be done once for a given $J(\omega)$.

The initial condition for the simulation is $|\Phi(\xi,0)\rangle_{\rm rel} = |\phi_0\rangle_{\rm s}$. A noise sample ξ is generated as described in Sec. VIII E. Then the relevant wave function $|\Phi(\xi,t_p)\rangle_{\rm rel}$ is propagated for the noise sample ξ starting from the initial condition $|\Phi(\xi,0)\rangle_{\rm rel}$.

For a given noise sample ξ, the open system observable $\widehat{o}$ is averaged at a time t_p as

$$\overline{o}(t_p;\xi) = \frac{\mathrm{Tr}\{\widehat{o}\times {}_{\rm rel}\langle 0|\Phi(\xi,t_p)\rangle_{\rm rel\,rel}\langle\Phi(\xi,t_p)|0\rangle_{\rm rel}\}}{\|{}_{\rm rel}\langle 0|\Phi(\xi,t_p)\rangle_{\rm rel}\|^2}. \quad (83)$$

Then the full quantum average of $\widehat{o}$ is given by averaging over ξ:

$$\langle\widehat{o}(t)\rangle \equiv \mathrm{Tr}\{\widehat{o}\widehat{\rho}_{\rm s}(t)\} = \overline{[\overline{o}(t_p;\xi)]}_{\xi}, \quad (84)$$

which is implemented by generating a sample of M noise instances $\xi^1\ldots\xi^M$, and computing the sample mean of $\overline{o}(t_p;\xi^k)$, $k=1\ldots M$.

The propagation of $|\Phi(\xi,t_p)\rangle_{\rm rel}$ is done as follows. Suppose we know $|\Phi(\xi,t_p)\rangle_{\rm rel}$ at a time step t_p. The propagation to the next time moment begins with *the entangling step*: the embedding $|\Phi(\xi,t_p)\rangle_{\rm rel}\to|\Phi(\xi,t_p)\rangle_{\rm rel+i} = |\Phi(\xi,t_p)\rangle_{\rm rel}\otimes|0\rangle_{\varphi_{\rm in}(p)}$ and the Hamiltonian evolution

$$\begin{aligned}|\Phi^{(1)}(\xi,t_{p+1})\rangle_{\rm rel+i} &= |\Phi(\xi,t_p)\rangle_{\rm rel+i}\\ &\quad - idt\widehat{H}'_{\rm st}(\xi,\tau_p)\tfrac{1}{2}\{|\Phi^{(1)}(\xi,t_{p+1})\rangle_{\rm rel+i}\\ &\quad + |\Phi(\xi,t_p)\rangle_{\rm rel+i}\}. \end{aligned}\quad (85)$$

The Hamiltonian $\widehat{H}'_{\rm st}(\xi,\tau_p)$ takes into account the continuous noise shift f_p,

$$\begin{aligned}\widehat{H}'_{\rm st}(\xi,\tau_p) &= \widehat{H}_{\rm s} + \widehat{s}\{\widehat{\psi}_p^\dagger + \xi_p^* + f_p^*\}\\ &\quad + (\widehat{s}^\dagger - \overline{s}^*(\tau_p;\xi))\left\{M(0)\widehat{\psi}_p + \sum_{i=1}^{\min(p,m)} M_i(p)\widehat{\phi}_i\right\}. \end{aligned}\quad (86)$$

The shift f_p is computed as a convolution of averages $\overline{s}(\tau_p;\xi)$ of $\widehat{s}$ at all the previous midpoint times τ_p with the memory function:

$$\begin{aligned} f_p &= -i\frac{dt}{2}M\left(\frac{dt}{2}\right)\overline{s}(\tau_p;\xi)\\ &\quad - idt\sum_{l=0}^{p-1}M((p-l)dt)\overline{s}(\tau_l;\xi). \end{aligned}\quad (87)$$

Here one can approximate $\overline{s}(\tau_l;\xi)\approx\{\overline{s}(t_{l+1};\xi)+\overline{s}(t_l;\xi)\}/2$, and $\overline{s}(t_l;\xi)$ is the average of $\widehat{s}$ according to Eq. (83). Observe that when solving Eq. (85) by iteration, the shift f_p should also be recomputed for each iteration since it contains the midpoint term $\overline{s}(\tau_p;\xi)$ which changes from iteration to iteration.

The second step, *the disentangling step,* identifies the new outgoing mode $\phi_{\rm out}(p)$ which has already decoupled:

$$|\Phi^{(2)}(\xi,t_{p+1})\rangle_{\rm rel+o} = \widehat{W}_p|\Phi^{(1)}(\xi,t_{p+1})\rangle_{\rm rel+i}. \quad (88)$$

Finally, in *the oblivion step,* the quantum content of the newly formed outgoing mode is discarded (it collapses to the classical noise):

$$|\Phi(\xi,t_{p+1})\rangle_{\rm rel} = {}_{\phi_{\rm out}(t_p)}\langle 0|\Phi^{(2)}(\xi,t_{p+1})\rangle_{\rm rel+o}. \quad (89)$$

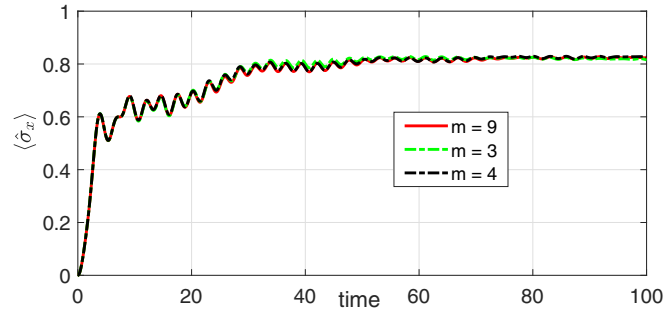

FIG. 32. For the system of a driven qubit with a non-RWA coupling to the subohmic environment, the good almost quantitative result is provided by $m=3$ relevant modes. The convergence is achieved for $m=4$ relevant modes. The computation is by RG along a quantum trajectory.

Then the propagation procedure is repeated for the next time moment t_{p+1}.

G. Example calculations

1. Driven qubit

Here we provide an example calculation for the model of the driven open quantum system

$$\widehat{H}_{\rm sb}(t) = -\frac{\Delta}{2}\widehat{\sigma}_x + \widehat{\sigma}_z f\cos\omega t + \widehat{\sigma}_z(\widehat{b}(t)+\widehat{b}^\dagger(t)), \quad (90)$$

with the Heaviside-regularized spectral density $J(\omega) = 2\pi\alpha\omega_{\rm c}^{1-s}\omega^s\theta(\omega-\omega_{\rm c})$ for $\alpha=0.1$, $s=0.5$, $\Delta=1$, $\omega_{\rm c}=1$, $f=0.1$, $\omega=1$. This leads to the memory function $M(\tau) = \frac{2\alpha\omega_{\rm c}^2}{s+1}\times\exp(-i\tau\omega_{\rm c})\times{}_1F_1(1,s+2,i\tau\omega_{\rm c})$. This situation corresponds to the non-RWA resonant driving and a highly non-Markovian behavior due to the subohmic spectrum at the origin and because the transition of the open system is at the sharp edge of the band. This is a good benchmark problem since we expect that the resulting dynamics is strongly determined by long-range memory effects. In Fig. 32, we demonstrate that only $m=3$ relevant modes are required to yield almost quantitative agreement. The complete convergence is achieved for $m=4$. In Fig. 33, we demonstrate the uniform convergence of RG with respect to the maximal

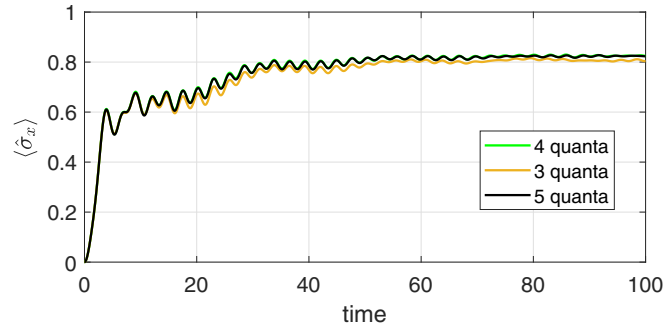

FIG. 33. The system of a driven qubit with a non-RWA coupling to the subohmic environment. Uniform convergence of the RG along a quantum trajectory with respect to the maximal number of quanta in the relevant modes.

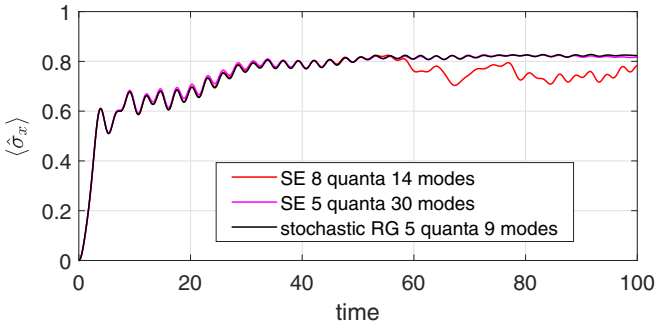

FIG. 34. The system of a driven qubit with a non-RWA coupling to the subohmic environment. Comparison of the RG along a quantum trajectory with the solution of Schrodinger equation (SE). In RG, the number of relevant modes is $m = 9$, the maximal occupation is truncated at $n = 5$ quanta. SE was computed for the two sets of parameters: To validate the large-time asymptotics, the Fock space was truncated at $n = 5$ quanta and $m = 30$ sites of the semi-infinite chain; to validate the midtime solution, $n = 8$ and $m = 14$ was used.

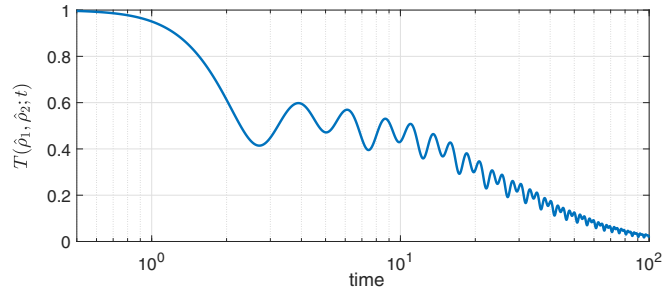

FIG. 35. Time dependence for the trace distance $T(\widehat{\rho}_1, \widehat{\rho}_2; t)$ Eq. (91) between the initial open system states $\widehat{\rho}_1(0) = |\uparrow\rangle\langle\uparrow|$ and $\widehat{\rho}_2(0) = |\downarrow\rangle\langle\downarrow|$ for the model Eq. (90) without driving ($f = 0$). The nonmonotonic behavior indicates that we are in the non-Markovian regime.

occupation of the relevant modes for the same system. Again, three quanta yield almost quantitative agreement, and the full convergence is provided by five quanta. To test our approach, we also solve the Schrodinger equation for this model represented in the semi-infinite chain form [72]. In Fig. 34, we compare the stochastic RG versus the numerical solution of the Schrodinger equation for $\alpha = 0.1$, $s = 0.5$, $\Delta = 1$, $\omega_c = 1$, $f = 0.1$, $\omega = 1$. It is seen that the RG simulation quantitatively reproduces the time dependence of observables up to the steady state.

2. Information backflow

When the dynamics of the open quantum system is non-Markovian, it is accompanied by such a phenomenon as information backflow [73–75]. This phenomenon refers to the special time behavior of the distinguishability of states of the open quantum system. The distiguishability of two quantum states $\widehat{\rho}_1(t)$ and $\widehat{\rho}_2(t)$ (reduced density matrices) of the open quantum system is measured by the trace distance [73]:

$$T(\widehat{\rho}_1, \widehat{\rho}_2; t) = \tfrac{1}{2}\mathrm{Tr}\sqrt{(\widehat{\rho}_1(t) - \widehat{\rho}_2(t))^2}. \tag{91}$$

In the Markovian regime, $T(\widehat{\rho}_1, \widehat{\rho}_2; t)$ should monotonically nonincrease with time for any pair of states [76]. On the contrary, in the non-Markovian mode, we can identify at least one pair of states for which $T(\widehat{\rho}_1, \widehat{\rho}_2; t)$ is increasing for some time interval. This is the information backflow and is one of the signatures of non-Markovian behavior.

The concept of relevant modes presented in this paper proposes a physical mechanism behind this phenomenon. As shown in Fig. 26, the relevant modes play the role of a finite imperfect cavity. Then the interaction between the open quantum system and these modes leads to the vacuum Rabi oscillations, i.e., oscillating exchange of energy between the open system and the cavity. These damped oscillations lead to the nonmonotonous behavior of the measures of information backflow. Roughly speaking, when the open quantum system loses its energy, the available phase space shrinks and the states get closer, becoming less distinguishable. However, when the energy flow is reversed, the available phase space of the open quantum system expands and the states move away from each other (becoming more distinguishable).

Here we present the calculation of the time dependence of trace distance Eq. (91) for the system Eq. (90). We take $\widehat{\rho}_1(0) = |\uparrow\rangle\langle\uparrow|$ and $\widehat{\rho}_2(0) = |\downarrow\rangle\langle\downarrow|$. In Fig. 35, we present the plot of $T(\widehat{\rho}_1, \widehat{\rho}_2; t)$ for the model Eq. (90) without driving ($f = 0$): We observe the periodic increase of distinguishability, so we are indeed in the non-Markovian regime.

3. Comparison with the tensor network methods

Here we provide a numerical comparison with the time-evolving matrix product operator (TEMPO) method [28]. TEMPO is a state-of-the-art approach for the computation of open quantum system dynamics. It was used in recent works, e.g., to calculate the quantum heat statistics [77]. We use the package provided by Ref. [78]. TEMPO represents the correlated state of the open system and the environment as a matrix product operator (MPO) state [28]. It depends on parameters dt, K, and ϵ. The evolution is discretized with a time step dt. The length K of the MPO corresponds to cutoff timescale $t_{\mathrm{cut}} = Kdt$. All the correlation effects of the environment at timescales larger than t_{cut} are neglected. Finally, ϵ defines the threshold below which the SVD components are discarded. In Fig. 36, we present the time dependence of $\langle\widehat{\sigma}_z\rangle/2$ computed by the RG along a quantum trajectory and compare it with the TEMPO computation. The system under consideration is again given by Eq. (90) without driving ($f = 0$). We start from $\widehat{\rho}_s(0) = |\uparrow\rangle\langle\uparrow|$. We observe that only $m = 4$ relevant modes at a finite occupation (five quanta) is enough to achieve the converged time dependence on large timescales. At the same time, the finite length K of the TEMPO corresponds to the finite revival time t_{cut} after which the computed evolution is corrupted. The longer we want to simulate the dynamics, the longer MPO should we employ. TEMPO cannot correctly capture the large-time asyptotics with a finite number of variables. Also, TEMPO requires a rather small SVD threshold $\epsilon = 10^{-9}$ to quantitatively reproduce the observable properties of the open quantum system. This leads to a rapid growth of the bond dimension, Fig. 37. The computational time per one time step ($dt = 0.03$) also increases. As a result of these two effects

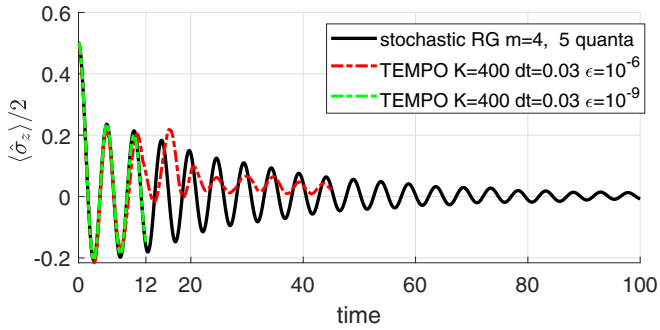

FIG. 36. Comparison of stochastic RG along trajectories and TEMPO. Time dependence of $\langle\widehat{\sigma}_z\rangle/2$ is computed for model Eq. (90) without driving ($f=0$). Initial state is $\widehat{\rho}_s(0)=|\uparrow\rangle\langle\uparrow|$. Stochastic RG (black line) is for $m=4$ relevant modes and is truncated at $n=5$ quanta. It yields the converged result on the presented timescales. The TEMPO (dashed green and red lines) employs a matrix product operator of length $K=400$ with bond dimensions up to 358. However, it can capture correctly the dynamics only up to the revival time $t_{\rm cut}=Kdt=12$, with $dt=0.03$. TEMPO with SVD threshold $\epsilon=10^{-9}$ (green dashed line) agrees with the stochastic RG results before the revival at $t_{\rm cut}$. However, each time step $dt=0.03$ becomes rather time consuming (≈ 40 min on a 40 CPU core cluster). TEMPO with larger SVD threshold $\epsilon=10^{-6}$ (red dashed line) starts to deviate even before $t_{\rm cut}$, but can be efficiently propagated to larger times, so we see clearly see the revival behavior.

(increasing length of MPO with the increasing bond dimensions), the large time asymptotics of nonstationary evolution is a computationally hard property for state-of-the-art tensor network methods. That is why the conjectured boundedness of complexity (as a function of simulation time) for the proposed RG methods is a nontrivial result.

IX. ENTANGLEMENT IN THE TIME DOMAIN

In the previous sections, we repeatedly refer to the entanglement as a *temporal* property. For example, we say that the outgoing mode $\phi_{\rm out}(t)$ is not entangled to the future (after t) in Fig. 1. We also introduce the entanglers and disentanglers in Figs. 15 and 17. However, the cautious reader may notice that the entanglement is usually considered as a spatial property and not a temporal one. The reason is that the entanglement is defined by dividing a quantum system into parts with strictly independent degrees of freedom. Due to the nonlocality of the time degrees of freedom, Fig. 14, it is impossible to perform such a strict partitioning in the time domain. Thus, the question arises, What is the exact content of our concept of temporal entanglement?

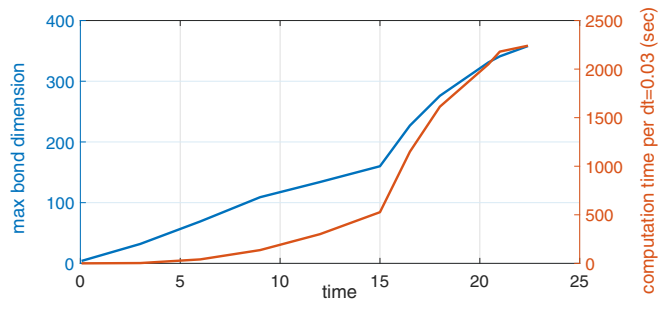

FIG. 37. For the same situation as in previous Fig. 36. The maximal bond dimension of TEMPO ($K=400$, $\epsilon=10^{-9}$, $dt=0.03$) is growing with the propagation time. This growth is accompanied with the increase in the computation time per one time step dt.

A. Absence of entanglement

We believe there are no doubts how one should define the absence of entanglement. Suppose we have a pure state $|\Phi(t_p)\rangle_{\rm st}$ which depends on the time cell degrees of freedom $\widehat{\psi}_0^\dagger,\ldots,\widehat{\psi}_{p-1}^\dagger$ and on the quantum numbers of the open system. Let us divide it into two subsystems. Subsystem A consists of the open quantum system and of the q most recent time cells $\widehat{\psi}_{p-q}^\dagger,\ldots,\widehat{\psi}_{p-1}^\dagger$. Subsystem B is chosen to contain the remaining time cells $\widehat{\psi}_0^\dagger,\ldots,\widehat{\psi}_{p-q-1}^\dagger$. There is no entanglement between A and B if after tracing out the B degrees of freedom the reduced state of A is still pure. Recalling the trace relation Eq. (31) for the tape model, we have for the reduced density matrix of A:

$$\widehat{\rho}_A={}_{\tau_{p-q-1}}\langle 0|\ldots{}_{\tau_0}\langle 0|\widehat{\rho}_{A|B}|0\rangle_{\tau_0}\ldots|0\rangle_{\tau_{p-q-1}}, \tag{92}$$

where $|0\rangle_{\tau_k}$ is the vacuum of mode $\widehat{\psi}_k^\dagger$ and

$$\widehat{\rho}_{A|B}=\Big\{e^{\sum_{r=0}^{p-q-1}\sum_{s=p-q}^{p-1}(\widehat{\psi}_r^\dagger M_{rs}\widehat{\psi}_s+\text{c.c.})}e^{\sum_{rs=0}^{p-q-1}\widehat{\psi}_r^\dagger M_{rs}\widehat{\psi}_s} : |\Phi(t_p)\rangle_{\rm st\,st}\langle\Phi(t_p)| : \Big\}_A \tag{93}$$

takes into account the pairings between the time cells of B and the cross pairings between the time cells of A and B. Observe that there is no pairing between the time cells of A in $\widehat{\rho}_{A|B}$: otherwise $\widehat{\rho}_A$ could be mixed irrespectively of its entanglement to B. We say that there is no entanglement between A and B if $\widehat{\rho}_A$ is pure, $\widehat{\rho}_A=\text{const}\times|f\rangle_{AA}\langle f|$. In other words, after tracing out B we still can consider that A is defined by a pure state $|f\rangle_A$.

One example situation when A and B are not entangled is the state of the form

$$|\Phi(t_p)\rangle_{\rm st}=|f\rangle_A\otimes|f_{\rm out}(t_{p-q-1})\rangle_B, \tag{94}$$

where in state $|f_{\rm out}(t_{p-q-1})\rangle_B$ only the outgoing modes $\phi_{\rm out}(m),\ldots,\phi_{\rm out}(p-q-1)$ are populated by quanta. Then the cross pairings in Eq. (93) are negligible by construction of the incoming and outgoing streams in Sec. IV D and $\widehat{\rho}_A\propto|f\rangle_{A\,A}\langle f|$ is pure. This is the exact meaning of saying that the outgoing modes at time t_{p-q-1} are not entangled to the future incoming modes.

B. Measure of temporal entanglement

There are situations when we need to measure the amount of entanglement between the subsystems. For example, one usually wants to know whether the entanglement is short range or long range. If the entanglement is long range, then it is interesting to know its asymptotical scaling. Therefore, here we propose a measure of temporal entanglement.

The entanglement is measured by the entropy of distribution of nonzero eigenvalues over the ensemble of eigenvectors. If $\widehat{\rho}_A$ [from Eq. (92)] is pure, then this distribution is localized on a single eigenvector: the entropy is

zero and there is no entanglement. In the opposite case of a maximally mixed $\widehat{\rho}_A$, the distribution is evenly smeared over the eigenvectors: the entropy is maximal and so is the entanglement.

Therefore, we define the entanglement entropy as

$$S_{A|B} = -\ln \mathrm{Tr}_A\{|\widehat{\rho}_A|/\mathrm{Tr}_A|\widehat{\rho}_A|\}^2 = 2\ln \mathrm{Tr}_A|\widehat{\rho}_A| - \ln \mathrm{Tr}_A|\widehat{\rho}_A|^2. \quad (95)$$

Here we base our definition on the Renyi entropy of the second order. The absolute value $|\widehat{\rho}_A|$ is employed because $\widehat{\rho}_A$ may have negative eigenvalues. This is due to the restriction of the set of pairings, see Sec. VI B. Also we normalize the density matrix by $\mathrm{Tr}|\widehat{\rho}_A|$ because $\widehat{\rho}_A$ is in general not normalized, $\mathrm{Tr}_A\widehat{\rho}_A \neq 1$. Here, Tr_A is the trace in the conventional sense, over some basis in the Fock space of the time cells $\mathcal{F}_\mathrm{t}$.

Our definition of the entanglement entropy reduces to the conventional Renyi entropy in the limit of infinite-band environment with $M(t-t') = \delta(t-t')$. It is reasonable because in this limit the time cells are local independent degrees of freedom, and the conventional partitioning into the independent subsystems is possible.

C. Entanglement is long range in time

Let us consider as a simple example the pure state created by the two emission events: one at τ_p and the other at τ_q, with $\tau_p > \tau_q$:

$$|\Phi\rangle_\mathrm{t} = \widehat{\psi}_p^\dagger \widehat{\psi}_q^\dagger |0\rangle_\mathrm{t}. \quad (96)$$

Let us compute the entanglement entropy $S_{p|q}$ between these two time moments. Applying Eqs. (92), (93), and (95), we find

$$S_{p|q} = 2\ln(p_1+p_2) - \ln\left(p_1^2+p_2^2\right), \quad (97)$$

where $p_1 = M(0)/(M(0)+|M_{pq}|^2)$, $p_2 = |M_{pq}|^2/(M(0)+|M_{pq}|^2)$. At a large time interval between the emission times, the memory function decays as an inverse power law, $|M_{pq}|^2 \propto (\tau_p-\tau_q)^{-s}$, and the entanglement entropy also decays according to the inverse power law $S_{p|q} \propto |M_{pq}|^2 \propto (\tau_p-\tau_q)^{-s}$. In Fig. 38, we present the plot of $S_{p|q}$ vs $\tau_p-\tau_q$ for the ohmic memory function Eq. (10) with $\alpha = 1$, $\omega_\mathrm{c} = 1$, $s = 1$.

D. Entanglement is finite range in the frame of incoming/relevant/outgoing modes

Now let us consider the pure state $|\Phi\rangle_\mathrm{t} = \widehat{\psi}_p^\dagger \widehat{\phi}_k^\dagger |0\rangle_\mathrm{t}$ when one quantum is emitted at a time moment τ_p, and the other is in the fastest decoupling basis state ϕ_k, computed for the time moment t_p, see Sec. IV B. The formula Eq. (97) for the entanglement entropy still holds, with the substitution $S_{p|q} \to S_{p|k}$ and $M_{pq} \to (p|M|\phi_k)$. In Fig. 39, we plot the dependence of $S_{p|k}$ with respect to the fastest decoupling basis element number k. We see that in the frame of incoming/relevant/outgoing modes the entanglement becomes effectively finite-ranged.

X. CONCLUSION

A. Structure of entanglement

In this paper, we proposed a constructive way of how to characterize the structure of entanglement. By tracking the degrees of freedom (the bricks) which couple to the evolution and decouple (irreversibly) from the evolution, we obtained a useful and *intrinsic* (free from *ad hoc* assumptions) characterization. The entanglement starts to look like a Lego built from these bricks. Here the evolution can be understood in a generalized sense, e.g., as an RG flow parameter.

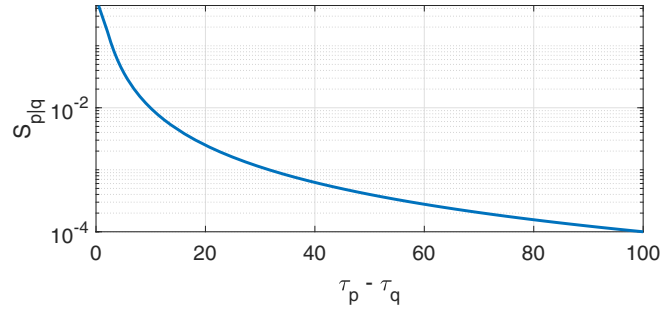

FIG. 38. The entanglement entropy $S_{p|q}$ of the state $\widehat{\psi}_p^\dagger \widehat{\psi}_q^\dagger |0\rangle_\mathrm{t}$ with two quanta emitted at τ_p and τ_p, $\tau_p > \tau_q$. It is a long-range function of the time distance $\tau_p - \tau_q$: $S_{p|q} \propto |M_{pq}|^2 \propto (\tau_p-\tau_q)^{-s}$. The plot is for the case of ohmic bath with the memory function $\frac{1}{2}(1+it)^{-2}$. Observe that although the state $\widehat{\psi}_p^\dagger \widehat{\psi}_q^\dagger |0\rangle_\mathrm{t}$ seems to be factorized, actually the states of emitted quanta are nonlocal in time, see Fig. 14. That is why when we trace out one of the time cells, the reduced state of the other time cell becomes mixed: the quanta are distributed nonlocally between both time cells

B. Real-time motion of open quantum systems

In this paper, we described the entire life cycle of the entanglement, from its generation through the entanglement of incoming modes to its death in the oblivion of outgoing modes. This sheds light on a number of questions. First, this shows that the true quantum complexity [3,4,46,79,80] of the real-time motion survives only in the modes of the environment which are non-negligibly coupled to the future quantum motion. If there is a balance between the flux of emitted quanta and the flux of quanta which are forgotten in

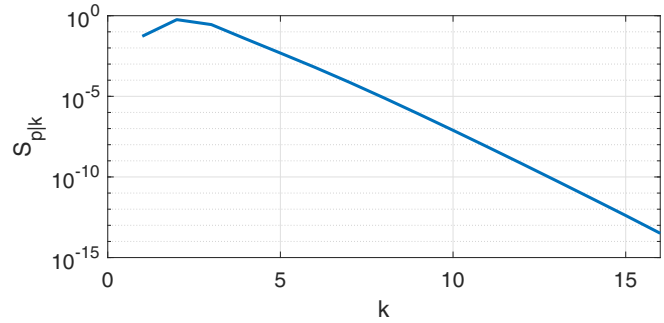

FIG. 39. The entanglement entropy $S_{p|k}$ of state $\widehat{\psi}_p^\dagger \widehat{\phi}_k^\dagger |0\rangle_\mathrm{t}$ with one quantum emitted at τ_p and the other quantum in the fastest decoupling basis state ϕ_k, computed for the time moment t_p, see Sec. IV B. The case of ohmic bath with the memory function $\frac{1}{2}(1+it)^{-2}$. The plot is for $S_{p|k}$ with respect to the fastest decoupling basis element number k. It is seen that the entanglement entropy decays exponentially fast with k. Therefore, in the frame of incoming/relevant/outgoing modes, the entanglement becomes effectively finite ranged.

the outgoing modes, then this complexity is asymptotically bounded on large times. Then the real-time motion of open quantum system becomes efficiently computable on a classical computer. Second, we find how the decoherence happens continuously in the non-Markovian regime. We find how tiny parts of quantum information decouple and disappear each infinitesimal time moment. An interesting future direction would be to study the distributed open quantum systems when there is a number r of coupling sites $\widehat{b}^\dagger_\alpha(t)$, $\alpha = 1 \ldots r$, to the environment. We expect that the presented approach should be straightforwardly extended to this case. The main modification is that the memory function Eq. (8), the matrix $K(p)$ Eq. (18), and the relevant modes will acquire additional indices $\alpha, \alpha' = 1 \ldots r$. The important question is whether it is possible to construct low-dimensional relevant modes inside the distributed open system so as to escape the growth of its Hilbert space dimension.

C. Few-mode approximations of non-Markovian environments

It turns out that for each moment of time, only a finite number m of degrees of freedom of the environment are significantly coupled to the future motion. Moreover, the significance of the neglected degrees of freedom decreases exponentially fast. This opens an interesting perspective on the few-mode approximations of the environments with memory.

D. RG methods

We also obtained a persepective on RG methods. Traditionally, these methods are based on the iterative application of the scale and coarse-graining transformations. Here we went beyond this paradigm. Any evolution can be considered as a certain RG flow provided it is accompanied by the continuous emergence of degrees of freedom which are not entangled to the future evolution. These degrees of freedom are irrelevant and can be iteratively traced out. Then the relevant subspace of such an RG procedure is not the conventional infrared limit, but the subspace of degrees of freedom which are significantly coupled to the future evolution. We illustrated this point (down to the resulting numerical schemes) for the case of real-time flow for open systems. To extend this idea to other many-body problems is a subject of future research.

E. Emergence of classical records

There is a interesting interrelationship between the entanglement, RG, and the models of continuous measurement [81]. The irrelevant degrees of freedom (which are not entangled to the future) can be collapsed [82,83] to a classical measurement signal as soon as they emerge. Computationally, this leads to a stochastic RG along a quantum trajectory. The numerical benefit over the deterministic RG for density matrices is that the latter scales as N^2 for N being the dimension of the relevant Fock subspace, whereas the former scales as N.

F. Quantum trajectories

In this paper, we promoted a constructive viewpoint on quantum trajectories [84–89]: We proposed to define the quantum trajectory as a model of how the quantum complexity decays into the classical complexity of a stochastic ensemble.

These results were illustrated with a number of calculations for the model of a two-level system (qubit), with and without driving, which was coupled to the environments with subohmic/ohmic/superohmic and semicircle spectral densities. In particular, in the cases considered, only three to four relevant modes were enough to achieve the numerical convergence.

Of course, we illustrated these ideas on a single specific model: the spin in the bosonic bath. However, we believe the picture presented in the Introduction and the concept of irreversible decoupling as a negligible average intensity of future interactions (sec. IV) are rather physically transparent and general. They can be applied to a variety of other models and situations, although specific formal implementation may differ.

ACKNOWLEDGMENT

The work was carried out in the framework of the Roadmap for Quantum computing in Russia

APPENDIX A: SOLVING EQUATIONS IN THE TRUNCATED FOCK SPACE

The total Hilbert space for the procedure in Sec. VI D has the basis elements

$$|q\rangle_{\rm s} \otimes |n_1\rangle_1 \otimes |n_2\rangle_2 \otimes \ldots |n_{m+1}\rangle_{m+1}, \tag{A1}$$

where $|q\rangle_{\rm s}$ is some basis in the Hilbert space $\mathcal{H}_{\rm s}$ of the open system and $|n_i\rangle_i$ is the state of n_i quanta in mode i. The modes $i = 1 \ldots m$ are our relevant modes. The mode $m+1$ becomes coupled only after $t = t_m$ and alternatively plays the role of incoming and outgoing modes.

We truncate the Hilbert space at a certain number n of quanta: only the basis states with $\sum_i n_i \leqslant n$ are being kept. Let us assume that N is the total number of remaining basis elements. All the basis elements Eq. (A1) are numbered

$$|k\rangle = |q^{(k)}\rangle_{\rm s} \otimes \left|n_1^{(k)}\right\rangle_1 \otimes \left|n_2^{(k)}\right\rangle_2 \otimes \ldots \left|n_{m+1}^{(k)}\right\rangle_{m+1} \tag{A2}$$

for $k = 1 \ldots N$. Then the joint many-particle wave function $|\Psi\rangle$ of the open system and the modes is represented as $|\Psi\rangle = \sum_{k=1}^N \Psi_k |k\rangle$, with Ψ_k being the $1 \times N$ array of complex numbers. The density matrix is represented as $\widehat{\rho} = \sum_{kl=1}^N \rho_{kl} |k\rangle\langle l|$, with ρ_{kl} being the $N \times N$ Hermitian matrix of complex numbers.

The operators of the open system, the creation/annihilation operators for modes are represented as sparse matrices in the basis of $|k\rangle$. Therefore, all the operations Eqs. (49)–(52) are implemented in terms of space matrix multiplications.

Please observe that at time t_p, mode $\min(m+1, p)$ plays the role of the incoming mode before the disentangling step Eq. (51). After the disentangling step, mode $\min(m+1, p)$ plays the role of the outgoing mode. The oblivion step Eq. (52) is implemented by setting to zero all elements of ρ_{kl} which correspond to non-zero occupation of mode $\min(m+1, p)$. After the oblivion step, at the next time moment, $p \to p+1$, the mode $\min(m+1, p)$ again becomes the incoming mode.

APPENDIX B: COMPUTING THE PAIRING UPDATE

Our propagation procedure is permitted to have a local error $O(dt^3)$. Then it is sufficient to compute the pairing update Eq. (50) up to the error $O(dt^3)$. Observe how the pairing update Eq. (50) is acting: If we consider the Taylor series of the pairing function, then at order n it annihilates at least n quanta in the incoming mode, either from the left (via $\widehat{\psi}_p$) or the right (via $\widehat{\psi}_p^\dagger$) of the density matrix $\widehat{\rho}^{(1)}_{\text{rel+i}}(t_{p+1})$. However, the amplitude to find n quanta in the incoming mode scales as dt^n. Indeed, looking at the propagation Eq. (49) and the Hamiltonian $\widehat{H}_{\text{st}}(\tau_p)$, Eq. (34), we see that the new quanta are created via $\propto dt\,\widehat{\psi}_p^\dagger$. Therefore, with second-order accuracy we compute the pairing update Eq. (50) as

$$\widehat{\rho}^{(2)}_{\text{rel+i}}(t_{p+1}) = \widehat{\rho}_0 + \widehat{\rho}_1 + \tfrac{1}{2}\widehat{\rho}_2, \tag{B1}$$

where

$$\widehat{\rho}_0 = \widehat{\rho}^{(1)}_{\text{rel+i}}(t_{p+1}), \tag{B2}$$

and the recurrent relation between $\widehat{\rho}_i$ and $\widehat{\rho}_{i-1}$,

$$\widehat{\rho}_i = M(0)\widehat{\psi}_p\widehat{\rho}_{i-1}\widehat{\psi}_p^\dagger + \sum_i M_i(p)\widehat{\phi}_i\widehat{\rho}_{i-1}\widehat{\psi}_p^\dagger + \sum_i M_i^*(p)\widehat{\psi}_p\widehat{\rho}_{i-1}\widehat{\phi}_i^\dagger, \tag{B3}$$

for $i = 1, 2$.

APPENDIX C: COMPUTING THE DISENTANGLER TRANSFOM

Here we present the algorithm we use to apply the disentangler transforms Eqs. (51) and (77). The latter are defined as a unitary transformation, Eq. (36). The unitary transform has the general form

$$\widehat{W} = \exp\left(i\sum_{kl}\widehat{\psi}_k^\dagger h_{kl}\widehat{\psi}_l\right) \equiv \exp(i\widehat{H}_W), \tag{C1}$$

with suitably defined $\widehat{\psi}_l$, $\widehat{\psi}_l^\dagger$ and a Hermitian matrix h_{kl}. Here we introduce the effective Hamiltonian $\widehat{H}_W$ which generates $\widehat{W}$. We need to apply $\widehat{W}$ to some wave function $|\Psi\rangle$:

$$|\Psi_W\rangle = \widehat{W}|\Psi\rangle. \tag{C2}$$

In general, h_{kl} is a dense matrix [as it turns out to be in Eq. (36)]. Therefore, each application of $\widehat{H}_W$ is expensive if $|\Psi\rangle$ is many-particle. We need to devise an algorithm which minimizes the number of applications of$\widehat{H}_W$.

Suppose that our budget is M applications of $\widehat{H}_W$. Then we construct the orthonormal basis $|\Phi_0\rangle \ldots |\Phi_M\rangle$ from $M+1$ vectors $|\Psi\rangle, \widehat{H}_W|\Psi\rangle, \ldots, \widehat{H}_W^M|\Psi\rangle$. The basis is constructed recurrently. We begin as

$$|\Phi_0\rangle = |\Psi\rangle/\|\Psi\|, \tag{C3}$$

where we normalize $|\Psi\rangle$ since it is normalized differently in the tape model, see Eq. (45). Now suppose we know $|\Phi_k\rangle$. We apply $\widehat{H}_W$ and find a new unnormalized basis element $|\widetilde{\Phi}_{k+1}\rangle$:

$$\begin{aligned} |\Phi_k^H\rangle &= \widehat{H}_W|\Phi_k\rangle,\ \ \beta_k = \langle\Phi_k|\Phi_k^H\rangle, \\ |\widetilde{\Phi}_{k+1}\rangle &= |\Phi_k^H\rangle - \beta_k|\Phi_k\rangle - \alpha_{k-1}|\Phi_{k-1}\rangle, \\ \alpha_k &= \|\widetilde{\Phi}_k\|, \end{aligned} \tag{C4}$$

where we set $\alpha_{-1} = 0$, $|\Phi_{-1}\rangle = 0$. Starting from $k = 1$, we additionally orthogonalize $|\widetilde{\Phi}_{k+1}\rangle$ to all the previous basis elements:

$$|\Phi^\perp{}_{k+1}\rangle = (1 - |\Phi_k\rangle\langle\Phi_k|)\ldots(1 - |\Phi_0\rangle\langle\Phi_0|)|\widetilde{\Phi}_{k+1}\rangle. \tag{C5}$$

Otherwise, the procedure will be numerically unstable. Finally, we normalize the basis element:

$$|\Phi_{k+1}\rangle = |\Phi^\perp{}_{k+1}\rangle/\||\Phi^\perp{}_{k+1}\rangle\|. \tag{C6}$$

As a result, $\widehat{H}_W$ is represented as a tridiagonal matrix:

$$H_{\text{ch}} = \begin{bmatrix} \beta_0 & \alpha_0 & 0 & 0 \\ \alpha_0 & \beta_1 & \alpha_1 & 0 \\ 0 & \alpha_1 & \ddots & \vdots \\ \vdots & \ddots & \ddots & \alpha_{M-1} \\ 0 & 0 & \alpha_{M-1} & \beta_M \end{bmatrix}. \tag{C7}$$

We see from this form that the Hamiltonian $\widehat{H}_W$ is represented as a semiinfinite chain attached to $|\Phi_0\rangle$. The hopping between the sites of the chain is given by α_k. Therefore, we obtain the first criterion for truncation: If α_k^2 is below some threshold, e.g., 10^{-5}, then the remaining sites are effectively decoupled and we can stop at k applications of $\widehat{H}_W$ and set $M = k$. The second criterion is the norm $\||\Phi^\perp{}_{k+1}\rangle\|^2$: If it is below some threshold, e.g., 10^{-4}, then the new basis elements are essentially linearly dependent, so we stop at k applications of $\widehat{H}_W$ and set $M = k$.

Finally, the $M \times M$ tridiagonal matrix H_{ch}, Eq. (C7), is diagonalized,

$$H_{\text{ch}} = U\begin{bmatrix} \omega_1 & \ldots & 0 \\ \vdots & \ddots & \vdots \\ 0 & \ldots & \omega_M \end{bmatrix}U^\dagger, \tag{C8}$$

and the approximation $|\Psi_W^M\rangle$ to $|\Psi_W\rangle$ is computed as

$$|\Psi_W^M\rangle = \sum_{k,l,l'=1}^{M} \exp(-i\omega_k)U_{lk}|\Phi_l\rangle U^*_{l'k}\langle\Phi_{l'}|\Psi\rangle. \tag{C9}$$

If α_k^2 and $\||\Phi^\perp{}_{k+1}\rangle\|^2$ are still above their thresholds, then the last, fourth criterion, is that we stop adding basis elements when $\||\Psi_W^M\rangle - |\Psi_W^{M+1}\rangle\|^2$ is below some threshold, e.g., 10^{-3}. Then we set $|\Psi_W\rangle \approx |\Psi_W^M\rangle$. For the numerical computations in the paper, we obtain that M lies in the range $3 \ldots 16$.

APPENDIX D: IMPORTANCE SAMPLING

The noise shift leads to an additional Bogoliubov transform in the state vector Eq. (74):

$$S(\Delta\xi) = e^{\sum_{s=0}^{\infty}\Delta\xi_s^*\widehat{\psi}_s}. \tag{D1}$$

Then the restriction on $\Delta\xi$ is that $S(\Delta\xi)$ should not couple to the outgoing modes which have appeared by the time moment

t_p. Otherwise, the entanglement structure will be spoiled and the oblivion step Eq. (78) will become invalid. This restricts the shifts to

$$\Delta\xi_r = \begin{cases} \text{arbitrary} & \text{for } r \geqslant p \\ \text{const} \times M_{pr} & \text{for } r < p. \end{cases} \tag{D2}$$

Apart from this, there is no restriction on the choice of importance sampling technique.

In this paper, we derive the importance sampling technique from the evolution of the probability distribution $Q(\xi, t_p)$ of the classical noise trajectories ξ at a time t_p. At $t_0 = 0$, this distribution coincides with the probability distribution of the vacuum fluctuations:

$$Q(\xi, 0) \propto \exp\left(-\sum_{rs=0}^{\infty} \xi_r^* [M^{-1}]_{rs} \xi_s\right). \tag{D3}$$

However, at later time moments it becomes weighted,

$$Q(\xi, t_p) = \|{}_{\rm t}\langle 0|\Phi(\xi, t_p)\rangle_{\rm st}\|^2 Q(\xi, 0), \tag{D4}$$

which follows from the partial trace relation Eq. (72). This probability distribution is properly normalized in the sense that

$$\overline{\left[\frac{Q(\xi, t_p)}{Q(\xi, 0)}\right]}_{\xi} = 1, \tag{D5}$$

which follows from Eq. (72) and $\mathrm{Tr}\widehat{\rho}_{\rm s}(t_p) = 1$. The importance sampling is required when the ratio on the left of Eq. (D5) starts to fluctuate violently.

Let us find the master equation for $Q(\xi, t_p)$ [27]. From the tape model Hamiltonian Eq. (27), we find

$$\begin{aligned} \partial_t Q(\xi, t_p) &= -i\mathrm{Tr}_{\rm s}\{|\xi\rangle_{\rm t\,t}\langle\xi|[\widehat{H}_{\rm st}(\tau_p)|\Phi(t_p)\rangle_{\rm st\,st}\langle\Phi(t_p)| - \text{c.c.}]\} \\ &= -i\mathrm{Tr}_{\rm s}\left\{\left[|\xi\rangle_{\rm t\,t}\langle\xi|\left(\widehat{s}\widehat{\psi}_p^\dagger + \widehat{s}^\dagger \sum_{r=0}^{\infty} M_{pr}\widehat{\psi}_r\right) - \text{c.c.}\right]\right. \\ &\quad \left.\times|\Phi(t_p)\rangle_{\rm st\,st}\langle\Phi(t_p)|\right\}, \end{aligned} \tag{D6}$$

where we introduce the time-cell coherent states:

$$|\xi\rangle_{\rm t} = Q^{\frac{1}{2}}(\xi, 0) e^{\sum_{s=0}^{\infty}\xi_s\widehat{\psi}_s^\dagger}|0\rangle_{\rm t}. \tag{D7}$$

In the second line of Eq. (D6), we have employed the cyclic trace property and the fact that $\widehat{H}_{\rm s}$ commutes with the time-cell coherent state projections. Observe that we extend the summation to infinity in the annihilation term on the second line of Eq. (D6). This is possible since the incoming modes are in vacuum. It turns out that Eq. (D6) can be reduced to the convection (drift) form:

$$\begin{aligned} \partial_t Q(\xi, t_p) = &\sum_r \partial_{\xi_r}\{\mathcal{A}_r(t_p) Q(\xi, t_p)\} \\ &+ \sum_r \partial_{\xi_r^*}\{\mathcal{A}_r^*(t_p) Q(\xi, t_p)\}. \end{aligned} \tag{D8}$$

To demonstrate this, we employ the fact that the creation $\widehat{\psi}_s^\dagger$ and annihilation $\widehat{\psi}_s$ operators act as differential operators on the coherent state projections:

$$|\xi\rangle_{\rm t\,t}\langle\xi|\widehat{\psi}_p^\dagger = \xi_p^*|\xi\rangle_{\rm t\,t}\langle\xi|, \tag{D9}$$

$$\widehat{\psi}_p|\xi\rangle_{\rm t\,t}\langle\xi| = \xi_p|\xi\rangle_{\rm t\,t}\langle\xi|, \tag{D10}$$

$$|\xi\rangle_{\rm t\,t}\langle\xi|\sum_{r=0}^{\infty} M_{pr}\widehat{\psi}_r = \left\{\sum_{r=0}^{\infty} M_{pr}\partial_{\xi_r^*} + \xi_p\right\}|\xi\rangle_{\rm t\,t}\langle\xi|, \tag{D11}$$

$$\sum_{r=0}^{\infty} M_{pr}^*\widehat{\psi}_r^\dagger|\xi\rangle_{\rm t\,t}\langle\xi| = \left\{\sum_{r=0}^{\infty} M_{pr}^*\partial_{\xi_r} + \xi_p^*\right\}|\xi\rangle_{\rm t\,t}\langle\xi|. \tag{D12}$$

Substituting these into Eq. (D6), we find

$$\mathcal{A}_r(t_p) = i\bar{s}(t_p; \xi)\sum_{r=0}^{\infty} M_{pr}^*, \tag{D13}$$

where the conditional average $\bar{s}(t_p; \xi)$ of the coupling operator $\widehat{s}$ is defined as

$$\bar{s}(t_p; \xi) = \frac{\mathrm{Tr}\{\widehat{s} \times {}_{\rm t}\langle 0|\Phi(\xi, t_p)\rangle_{\rm st\,st}\langle\Phi(\xi, t_p)|0\rangle_{\rm t}\}}{\|{}_{\rm t}\langle 0|\Phi(\xi, t_p)\rangle_{\rm st}\|^2}. \tag{D14}$$

Switching to the frame of incoming/relevant/outgoing modes and employing the relevant wave function, we reexpress this equation as

$$\bar{s}(t_p; \xi) = \frac{\mathrm{Tr}\{\widehat{s} \times {}_{\rm rel}\langle 0|\Phi(\xi, t_p)\rangle_{\rm rel\,rel}\langle\Phi(\xi, t_p)|0\rangle_{\rm rel}\}}{\|{}_{\rm rel}\langle 0|\Phi(\xi, t_p)\rangle_{\rm rel}\|^2}, \tag{D15}$$

which is Eq. (83). The velocity Eq. (D13) means that the noise trajectory ξ is shifted with time as

$$\xi(\tau; t_p) = \xi(\tau) - i\int_0^{t_p} dt\bar{s}(t; \xi)M^*(t - \tau). \tag{D16}$$

Observe that here we switch back and forth between the continuous and the discrete-time relations. This is permissible because we have chosen the discrete propagator in Sec. V B so it converges to the continuous evolution with the global error $O(dt^2)$.

The importance sampling procedure is to shift the noise ξ continuously in time according to the relation Eq. (D16). As mentioned in Eq. (D1), the infinitesimal shift of noise

$$\xi_r(t_{p+1}) = \xi_r(t_p) - idtM_{pr}^*\bar{s}(\tau_p; \xi) \tag{D17}$$

will generate the infinitesimal Bogoliubov transform

$$S(d\xi) = 1 + idt\bar{s}^*(\tau_p;\xi)\sum_{r=0}^{p-1} M_{pr}\hat{\psi}_r, \tag{D18}$$

which should be incorporated into the Hamiltonian. The latter for the continuously shifting noise becomes

$$\hat{H}'_{\rm st}(\xi,\tau_p) = \hat{H}_{\rm s} + \hat{s}\{\hat{\psi}_p^\dagger + \xi_p^* + f_p^*\} + (\hat{s}^\dagger - \bar{s}^*(\tau_p;\xi))\left\{M(0)\hat{\psi}_p + \sum_{i=1}^{\min(p,m)} M_i(p)\hat{\phi}_i\right\}, \tag{D19}$$

which is Eq. (86). Here ξ_p^* are sampled from the vacuum probability distribution and the self-consistent displacement is

$$f_p = -i\int_0^{t_p} dt\bar{s}(t;\xi)M(\tau_p - t). \tag{D20}$$

The consistent midpoint discretization of f_p leads to Eq. (87). The Hamiltonian $\hat{H}'_{\rm st}(\xi,\tau_p)$ should be employed in the entangling step Eq. (75). The rest of the RG procedure is the same except that the average of any system observable $\hat{o}$ should be computed as

$$\langle\hat{o}(t_p)\rangle = \left[\frac{\mathrm{Tr}\{\hat{o}\times {}_{\rm rel}\langle 0|\Phi(\xi,t_p)\rangle_{\rm rel\,rel}\langle\Phi(\xi,t_p)|0\rangle_{\rm rel}\}}{\|{}_{\rm rel}\langle 0|\Phi(\xi,t_p)\rangle_{\rm rel}\|^2}\right]_\xi. \tag{D21}$$

The reason is that now we directly sample the probability distribution Eq. (D4), hence the denominator.

[1] R. P. Feynman, A. R. Hibbs, and D. F. Styer, *Quantum Mechanics and Path Integrals: Emended Edition* (Dover Publications, Mineola, New York, 2010).

[2] P. A. M. Dirac, *The Principles of Quantum Mechanics* (Clarendon Press, Oxford, 1982).

[3] D. Poulin, A. Qarry, R. Somma, and F. Verstraete, Quantum Simulation of Time-Dependent Hamiltonians and the Convenient Illusion of Hilbert Space, Phys. Rev. Lett. **106**, 170501 (2011).

[4] F. G. Brandao, W. Chemissany, N. Hunter-Jones, R. Kueng, and J. Preskill, Models of quantum complexity growth, PRX Quantum **2**, 030316 (2021).

[5] S.-H. Lin, R. Dilip, A. G. Green, A. Smith, and F. Pollmann, Real- and imaginary-time evolution with compressed quantum circuits, PRX Quantum **2**, 010342 (2021).

[6] Y. Zhou, E. M. Stoudenmire, and X. Waintal, What Limits the Simulation of Quantum Computers? Phys. Rev. X **10**, 041038 (2020).

[7] D. S. Franca and R. Garcia-Patron, Limitations of optimization algorithms on noisy quantum devices, Nat. Phys. **17**, 1221 (2021).

[8] G. Vidal, Entanglement Renormalizatiom, Phys. Rev. Lett. **99**, 220405 (2007).

[9] G. Vidal, Class of Quantum Many-Body States that can be Efficiently Simulated, Phys. Rev. Lett. **101**, 110501 (2008).

[10] K. Van Acoleyen, A. Hallam, M. Bal, M. Hauru, J. Haegeman, and F. Verstraete, Entanglement compression in scale space: From the multiscale entanglement renormalization ansatz to matrix product operators, Phys. Rev. B **102**, 165131 (2020).

[11] J. Haegeman, T. J. Osborne, H. Verschelde, and F. Verstraete, Entanglement Renormalization for Quantum Fields in Real Space, Phys. Rev. Lett. **110**, 100402 (2013).

[12] S. R. White, Density Matrix Formulation for Quantum Renormalization Groups, Phys. Rev. Lett. **69**, 2863 (1992).

[13] U. Schollwock, The density-matrix renormalization group in the age of matrix product states, Ann. Phys. **326**, 96 (2011).

[14] I. de Vega and D. Alonso, Dynamics of non-Markovian open quantum systems, Rev. Mod. Phys. **89**, 015001 (2017).

[15] T. Brandes, Feedback Control of Quantum Transport, Phys. Rev. Lett. **105**, 060602 (2010).

[16] G. Kiesslich, C. Emary, G. Schaller, and T. Brandes, Reverse quantum state engineering using electronic feedback loops, New J. Phys. **14**, 123036 (2012).

[17] J. Gough, Feedback network models for quantum transport, Phys. Rev. E **90**, 062109 (2014).

[18] T. Brandes and C. Emary, Feedback control of waiting times, Phys. Rev. E **93**, 042103 (2016).

[19] J. Y. Luo, J. Jin, S.-K. Wang, J. Hu, Y. Huang, and X.-L. He, Unraveling of a detailed-balance-preserved quantum master equation and continuous feedback control of a measured qubit, Phys. Rev. B **93**, 125122 (2016).

[20] T. Wagner, P. Strasberg, J. C. Bayer, E. P. Rugeramigabo, T. Brandes, and R. J. Haug, Strong suppression of shot noise in a feedback-controlled single-electron transistor, Nat. Nanotechnol. **12**, 218 (2017).

[21] J. Kondo, Diffusion of light interstitials in metals, Physica B+C **125**, 279 (1984).

[22] K. G. Wilson, The renormalization group: Critical phenomena and the Kondo problem, Rev. Mod. Phys. **47**, 773 (1975).

[23] L. Bulla and M. Vojta, Quantum phase transitions in models of magnetic impurities, in *Concepts in Electron Correlations. NATO Science Series,* Series II: Mathematics, Physics and Chemistry, Vol. 110, edited by A. C. Hewson and V. Zlatic (Springer, Dordrecht, 2003), pp. 209–217.

[24] R. Bulla, T. A. Costi, and T. Pruschke, Numerical renormalization group method for quantum impurity systems, Rev. Mod. Phys. **80**, 395 (2008).

[25] C. Lazarou, K. Luoma, S. Maniscalco, J. Piilo, and B. M. Garraway, Entanglement trapping in a nonstationary structured reservoir, Phys. Rev. A **86**, 012331 (2012).

[26] M. M. Rams and M. Zwolak, Breaking the Entanglement Barrier: Tensor Network Simulation of Quantum Transport, Phys. Rev. Lett. **124**, 137701 (2020).

[27] E. A. Polyakov and A. N. Rubtsov, Dressed quantum trajectories: novel approach to the non-Markovian dynamics of open

quantum systems on a wide time scale, New J. Phys. **21**, 063004 (2019).

[28] A. Strathearn, P. Kirton, D. Kilda, J. Keeling, and B. W. Lovett, Efficient non-Markovian quantum dynamics using time-evolving matrix product operators, Nat. Commun. **9**, 3322 (2018).

[29] J. Eisert, M. Cramer, and M. B. Plenio, Colloquium: Area laws for the entanglement entropy, Rev. Mod. Phys. **82**, 277 (2010).

[30] H.-P. Breuer and F. Petruccione, *The Theory of Open Quantum Systems* (Oxford University Press, Oxford, 2007).

[31] I. Percival, *Quantum State Diffusion* (Cambridge University Press, Cambridge, 1999).

[32] H. M. Wiseman, Quantum trajectories and quantum measurement theory, Quantum Semiclass. Opt. **8**, 205 (1996).

[33] H. M. Wiseman and G. J. Milburn, Quantum theory of field-quadrature measurements, Phys. Rev. A **47**, 642 (1993).

[34] A. J. Daley, Quantum trajectories and open many-body quantum systems, Adv. Phys. **63**, 77 (2014).

[35] D. Segal, A. J. Millis, and D. R. Reichman, Numerically exact path-integral simulation of nonequilibrium quantum transport and dissipation, Phys. Rev. B **82**, 205323 (2010).

[36] N. Makri, Numerical path integral techniques for long time dynamics of quantum dissipative systems, J. Math. Phys. **36**, 2430 (1995).

[37] N. Makri and D. E. Makarov, Tensor propagator for iterative quantum time evolution of reduced density matrices. I. Theory, J. Chem. Phys. **102**, 4600 (1995).

[38] N. Makri, E. Sim, D. E. Makarov, and M. Topaler, Long-time quantum simulation of the primary charge separation in bacterial photosynthesis, Proc. Natl. Acad. Sci. **93**, 3926 (1996).

[39] D. E. Makarov and N. Makri, Path integrals for dissipative systems by tensor multiplication. condensed phase quantum dynamics for arbitrarily long time, Chem. Phys. Lett. **221**, 482 (1994).

[40] M. Richter and B. P. Fingerhut, Coarse-grained representation of the quasi-adiabatic propagator path integral for the treatment of non-Markovian long-time bath memory, J. Chem. Phys. **146**, 214101 (2017).

[41] M. P. Woods, R. Groux, A. W. Chin, S. F. Huelga, and M. B. Plenio, Mappings of open quantum systems onto chain representations and Markovian embeddings, J. Math. Phys. **55**, 032101 (2014).

[42] L. Mazzola, S. Maniscalco, J. Piilo, K.-A. Suominen, and B. M. Garraway, Pseudomodes as an effective description of memory: Non-Markovian dynamics of two-state systems in structured reservoirs, Phys. Rev. A **80**, 012104 (2009).

[43] N. Lambert, S. Ahmed, M. Cirio, and F. Nori, Modelling the ultra-strongly coupled spin-boson model with unphysical modes, Nat. Commun. **10**, 3721 (2019).

[44] D. Tamascelli, A. Smirne, S. F. Huelga, and M. B. Plenio, Nonperturbative Treatment of Non-Markovian Dynamics of Open Quantum Systems, Phys. Rev. Lett. **120**, 030402 (2018).

[45] M. R. Jorgensen and F. A. Pollock, Exploiting the Causal Tensor Network Structure of Quantum Processes to Efficiently Simulate Non-Markovian Path Integrals, Phys. Rev. Lett. **123**, 240602 (2019).

[46] I. A. Luchnikov, S. V. Vintskevich, H. Ouerdane, and S. N. Filippov, Simulation Complexity of Open Quantum Dynamics: Connection with Tensor Networks, Phys. Rev. Lett. **122**, 160401 (2019).

[47] A. D. Somoza, O. Marty, J. Lim, S. F. Huelga, and M. B. Plenio, Dissipation-Assisted Matrix Product Factorization, Phys. Rev. Lett. **123**, 100502 (2019).

[48] W. Zhu, Z. Huang, Y.-C. He, and X. Wen, Entanglement Hamiltonian of Many-Body Dynamics in Strongly Correlated Systems, Phys. Rev. Lett. **124**, 100605 (2020).

[49] L. Diosi, N. Gisin, and W. T. Strunz, Non-Markovian quantum state diffusion, Phys. Rev. A **58**, 1699 (1998).

[50] L. Diosi and W. T. Strunz, The non-Markovian stochastic Schrodinger equation for open systems, Phys. Lett. A **235**, 569 (1997).

[51] Y. Zhou and J. Shao, Solving the spin-boson model of strong dissipation with flexible random-deterministic scheme, J. Chem. Phys. **128**, 034106 (2008).

[52] Y.-A. Yan and J. Shao, Stochastic description of quantum Brownian dynamics, Front. Phys. **11**, 110309 (2016).

[53] J. Shao, Decoupling quantum dissipation via stochastic fields, J. Chem. Phys. **120**, 5053 (2004).

[54] L. Han, V. Chemyak, Y.-A. Yan, X. Zheng, and Y. J. Yan, Stochastic Representation of Non-Markovian Fermionic Quantum Dissipation, Phys. Rev. Lett. **123**, 050601 (2019).

[55] D. Suess, A. Eisfeld, and W. T. Strunz, Hierarchy of Stochastic Pure States for Open Quantum System Dynamics, Phys. Rev. Lett. **113**, 150403 (2014).

[56] R. Hartmann and W. T. Strunz, Exact open quantum system dynamics using the hierarchy of pure states (HOPS), J. Chem. Theory Comput. **13**, 5834 (2017).

[57] J. M. Moix and J. Cao, A hybrid stochastic hierarchy equations of motion approach to treat the low temperature dynamics of non-Markovian open quantum systems, J. Chem. Phys. **139**, 134106 (2013).

[58] J. Strümpfer and K. Schulten, Open quantum dynamics calculations with the hierarchy equations of motion on parallel computers, J. Chem. Theory Comput. **8**, 2808 (2012).

[59] A. Ishizaki and G. R. Fleming, Unified treatment of quantum coherent and incoherent hopping dynamics in electronic energy transfer: Reduced hierarchy equation approach, J. Chem. Phys. **130**, 234111 (2009).

[60] C. Duan, Z. Tang, J. Cao, and J. Wu, Zero-temperature localization in a sub-ohmic spin-boson model investigated by an extended hierarchy equation of motion, Phys. Rev. B **95**, 214308 (2017).

[61] H. Rahman and U. Kleinekathofer, Chebyshev hierarchical equations of motion for systems with arbitrary spectral densities and temperatures, J. Chem. Phys. **150**, 244104 (2019).

[62] E. A. Polyakov and A. N. Rubtsov, Stochastic wave-function simulation of irreversible emission processes for open quantum systems in a non-Markovian environment, AIP Conf. Proc. **1936**, 020028 (2018).

[63] E. A. Polyakov and A. N. Rubtsov, Information loss pathways in a numerically exact simulation of a non-Markovian open quantum system (unpublished).

[64] L. Diosi, Non-Markovian open quantum systems: Input-output fields, memory, and monitoring, Phys. Rev. A **85**, 034101 (2012).

[65] A. Atland and B. D. Simons, *Condensed Matter Field Theory* (Cambridge University Press, New York, 2010).

[66] M. B. Plenio and P. L. Knight, The quantum-jump approach to dissipative dynamics in quantum optics, Rev. Mod. Phys. **70**, 101 (1998).

[67] Y. Aharonov and L. Vaidman, The two-state vector formalism: An updated review, in *Time in Quantum Mechanics*, Lecture Notes in Physics, Vol. 734, edited by J. Muga, R. S. Mayato, and I. Egusquiza (Springer, Berlin, 2008), Chap. 13, pp. 399–447.

[68] *Quantum Theory: A Two-Time Success Story* (Springer, Milano, 2014).

[69] Y. Aharonov, E. Cohen, and T. Landsberger, The two-time interpretation and macroscopic time-reversibility, Entropy **19**, 111 (2017).

[70] C. W. Gardiner and P. Zoller, *Quantum Noise*, 3rd ed. (Springer-Verlag, Berlin, 2004).

[71] M. B. Plenio and S. Virmani, An introduction to the entanglement measures, Quantum Inf. Comput. **7**, 1 (2007).

[72] A. W. Chin, A. Rivas, S. F. Huelga, and M. B. Plenio, Exact mapping between system-reservoir quantum models and semi-infinite discrete chains using orthogonal polynomials, J. Math. Phys. **51**, 092109 (2010).

[73] H.-P. Breuer, E.-M. Laine, and J. Piilo, Measure for the Degree of Non-Markovian Behavior in Open Quantum Systems, Phys. Rev. Lett. **103**, 210401 (2009).

[74] B. Bylicka, M. Johansson, and A. Acin, Constructive Method for Detecting the Information Backflow of Non-Markovian Dynamics, Phys. Rev. Lett. **118**, 120501 (2017).

[75] F. Buscemi and N. Datta, Equivalence between divisibility and monotonic decrease of information in classical and quantum stochastic processes, Phys. Rev. A **93**, 012101 (2016).

[76] M. B. Ruskai, Beyond strong subadditivity? Improved bounds on the contraction of generalized relative entropy, Rev. Math. Phys. **6**, 1147 (2009).

[77] M. Popovic, M. T. Mitchison, A. Strathearn, B. W. Lovett, J. Goold, and P. R. Eastham, Quantum heat statistics with time-evolving matrix product operators, PRX Quantum **2**, 020338 (2021).

[78] Peter Kirton and Jonathan Keeling (2018), Software package for the time-evolving matrix product operator (TEMPO) method (v1.0.0), Zenodo, https://doi.org/10.5281/zenodo.1322407.

[79] T. Ali, A. Bhattacharyya, S. S. Haque, E. H. Kim, and N. Moynihan, Time evolution of complexity: A critique of three methods, J. High Energy Phys. 04 (2019) 087.

[80] A. Bhattacharyya, P. Nandy, and A. Sinha, Renormalized Circuit Complexity, Phys. Rev. Lett. **124**, 101602 (2020).

[81] N. Megier, W. N. Strunz, and K. Luoma, Continuous quantum measurement for general Gaussian unravelings can exist, Phys. Rev. Research **2**, 043376 (2020).

[82] S. L. Adler and A. Bassi, Collapse models with non-white noises, J. Phys. A: Math. Theor. **40**, 15083 (2007).

[83] M. Carlesso, L. Ferialdi, and A. Bassi, Colored collapse models from the non-interferometric perspective, Eur. Phys. J. D **72**, 159 (2018).

[84] W. T. Strunz, L. Diosi, N. Gisin, and T. Yu, Quantum Trajectories for Brownian Motion, Phys. Rev. Lett. **83**, 4909 (1999).

[85] W. T. Strunz, L. Diosi, and N. Gisin, Open system dynamics with non-Markovian quantum trajectories, Phys. Rev. Lett. **82**, 1801 (1999).

[86] J. Gambetta, T. Askerud, and H. M. Wiseman, Jumplike unravelings for non-Markovian open quantum systems, Phys. Rev. A **69**, 052104 (2004).

[87] H.-P. Breuer, Genuine quantum trajectories for non-Markovian processes, Phys. Rev. A **70**, 012106 (2004).

[88] K. Luoma, K.-A. Suominen, and J. Piilo, Connecting two jump-like unravelings for non-Markovian open quantum systems, Phys. Rev. A **84**, 032113 (2011).

[89] D. Durr, S. Goldstein, R. Tumulka, and N. Zanghi, Bohmian Mechanics and Quantum Field Theory, Phys. Rev. Lett. **93**, 090402 (2004).